Theoretical and practical investigations in non LTE phenomena in an ICP

Raaijmakers, I.J.M.M.

Award date:
1982

THEORETICAL AND PRACTICAL INVESTIGATIONS IN NON LTE PHENOMENA IN AN ICP

I.J.M.M. Raaijmakers

September 1982

A report on the graduate work of the author, performed in the Spectrochemical Department of the Philips Research Laboratories during the period Oct. '81 to Oct. '82.

VDF/NT 82-21(a)

Supervision

Dr. P.W.J.M. Boumans	(Nat.Lab.)
Prof.Dr.Ir. D.C. Schram	(University of Technology,
Dr.Ir. B. v.d. Sijde	plasma-physical Dept., Eindhoven).

ERRATUM.

Page	is:	should be:
106	46. P.W.J.M. Boumans....	46. J.C. de Vos, Physica 20, 690,(1954).
110	$\beta = 2.6 \times 10^7$	$\beta = -2.6 \times 10^7$
Fig. C1.	k_{1+}	k_{0+}
Fig. C2.	- lineair....	----- lineair....
	- Vriens....	- - - Vriens....
	-Drawin....	-.-.- Drawin....
Fig. C3.	R_{12}	R_{01}
	R_{13}	R_{02}
	R_{14}	R_{03}

N.B. Page 77 is not present.

General Introduction.

Structure of this report.

The purpose of this report is to summarize the theoretical and experimental work on (I) fundamental research in some plasma physical aspects of inductively coupled plasmas (IC85) and (II) "torch miniaturisation" performed in the Philips Research Laboratories ("Nat.Lab.") during the past year as the graduate work (University of Technology, Physics Dept., Eindhoven) of the author.

Although the two subjects I and II concern the same object (ICP) they have no interrelation. Therefore this report is split up into two independent parts, each provided with its own abstract, introduction, and list of references.

Part I deals with the fundamental research, part II deals with the design of a new micro ICP (ICuP) system ("torch miniaturisation"). The latter part has been previously available as Nat.Lab. Technical Note Nr. 132/82 (ref. [56]).

The present general introduction deals with the basic principles and definitions in ICP atomic emission spectroscopy (AES). This general introduction is immediately followed by Part I of the report. Part II is added separately as Nat.Lab. Technical Note Nr. 132/82.

Because of the large target group for which this report is written (both plasma physical and spectrochemical disciplinaries) some items are treated rather extensive in order to provide acessability for both disciplinaries. Plasma physicists should be able to skip the sections marked "o", while spectrochemicists should be able to skip sections marked "+".

Historical aspects of ICP-AES +

Reviews including a discussion of the history of ICP-AES [17,70-75] give credit to Babat [76-77] as the individual who first succeeded to sustain induction heated plasmas at atmospheric pressure. Babat generated his plasmas in a closed system and used power inputs as high as 30-50 kW, having in mind industrial applications of RF discharges.

Stabilization of an inductively heated plasma operated at atmospheric pressure in gases flowing through an open-ended tube was achieved in the early 1960s. Reed [64,78,79] was the first to describe such a discharge, which he designed with the primary aim of crystal growing and not for spectrochemical analysis, although he made reference to the possibility.

Fassel [74,75] and Greenfield [73] recount their independent starting of analytical studies of ICPs in 1962, the first results of which were communicated in 1964 [80] and 1965 [81]. Both authors had recognized that Reed's "plasma torch" offered, in principle, unique potentials as a high-temperature atomization-excitation source, free of contamination from electrode vapours. Major efforts by the groups of Fassel [81-84] and Greenfield during the 1960s established the viability of the principle as a useful basis of spectroanalytical measurements. This work and that of other authors exploring the potentialities of ICPs for spectrochemical analysis in the initial period [11] is discussed in various reviews [17,70 ,75,83].

One criterion of the progress in the early years is the improvement in the detection limits. From Barnes' tabular survey of the various results [17] it is evident that the paper of Dickinson and Fassel [82], published in 1969, heralded a new era in ICP-AES. Those authors succeeded in bringing down the detection limits to the 0.1-10 ng/ml range for many elements, which meant an improvement by two or more orders of magnitude compared to the results achieved previously. Therefore this report stands as a major landmark paper in ICP progress [91].

Dickinson and Fassel had recognized the concept of Reed [64,78] and Greenfield [86] to exploit the skin effect of high-frequency currents and to also configure their ICP arrangement in such a way that a toroidal instead of an ellipsoidal ("tear drop") discharge was formed. Thus the sample could be effectively introduced through the central channel of the toroid.

Since the aerosol was generated with an ultrasonic nebulizer and desolvated prior to its introduction into the plasma, the high efficiency of ultrasonic nebulization further contributed to the success of the efforts.

By 1971 the major advantages of ICPs as excitation sources for AES had been documented and were summarized by Fassel [83] as follows "(a) effective injection of the sample into the hot portion of the plasma; (b) relatively long residence time of the sample in the plasma: (c) higher temperature than combustion flames; (d) continuous temperature gradient from 9000 K to room temperature, allowing greater latitude in selecting optimal temperature; (e) free atoms may be generated in the hottest zones of the plasma and then observed in lower temperature zones where background emission is lower; (f) chemical environment may be manipulated, within limits; and (g) no electrode contamination".

The results reported by Dickinson and Fassel were verified independently in 1972 by Souilliart and Robin [92] and Boumans and de Boer [65] using different ICP instruments and operating conditions. The potentials of low-power argon ICPs as excitation sources for simultaneous multielement analysis using "compromise operating conditions" were recognized and firmly established [65,66,93,94], the exceptionally high sensitivity of ionic lines in the spectra emitted from argon ICPs was noted and exploited [92,66,67] and such performance characteristics as low interference levels under judiciously chosen operating conditions, large dynamic range and fair stability were further documented by various groups of authors who followed Fassel's line of exploring and developing low-power argon ICPs. Although a variety of experimental facilities was used, the results obtained in different laboratories showed a marked degree of congruence. These results, along with those of the early efforts, form the basis of present-day ICP-AES.

Greenfield and his co-workers followed a different line and became the champions of the high-power nitrogen-argon ("nitrogen-cooled") ICPs, of which higher sensitivity, smaller liability to interferences and better precision were postulated to be major advantages in comparison to low-power argon ICPs [69,71]. The past has seen many - often confusing - arguments in favour of either low-power argon or high-power nitrogen-argon ICPs, but it is only since rather recently that unambiguous experimental data are beginning to clear up the complex picture.

The confusion about the advantages and disadvantages of the categories of ICPs should not detract from the fact that Greenfield et al. [69] could state in 1975 that they had been using their high-power nitrogen-argon ICP system on a daily routine basis for practical analysis of a large variety of samples during the past four years. Although various applications of low-power argon ICPs had been reported by 1975 [93-97] the era of wide-spread use of these ICPs for practical applications was just beginning with the advent of commercial instruments.

Instrument manufacturers had become gradually aware of the potentialities of ICP-AES and thus 1974 saw the first modern commercial ICP instrument [98,99] . Rather explosive developments were to follow, as may be deduced from the tabular surveys of commercial equipment in the Annual Reports on Analytical Atomic Spectroscopy (A.R.A.A.S.) [109] .

Barnes [100] concluded that ICP instruments have developed from laboratory curiosities into something usable by non-specialists, while the introduction of new ICP systems bears witness of the continuation of the development phase.

It is predicted that with the resources at present available, the ICP will probably become one of the best characterized excitation sources of emission spectroscopy, while the ever-widening range of applications, extending toward standardized procedures, indicates the maturing of the technique as an accepted approach in competition and co-operation with other methods. According to Barnes, ICP-AES will probably not reach in the 1980s the stage in which it will be gradually

replaced by other methods with greater speed, economy, convenience, sensitivity, and selectivity.

PRINCIPLES OF ICP GENERATION

Basic set-up[+]

Figure A is a schematic drawing of an assembly of three concentric tubes, most frequently made of silica, used for operating an ICP. The assembly of tubes, called "torch", is set up in a water-cooled coil of a radio frequency (RF) generator. The torch consists of three tubes here designated unambiguously "outer tube", "intermediate tube" and "carrier gas tube". Flowing gases are introduced into the torch, the RF field is switched on and the gas in the coil region is made electrically conductive by Tesla sparks. Then a plasma will be formed provided the magnetic field strength is high enough and the gas streams follow a particular, rotationally symmetrical pattern.
This inductively coupled plasma thus formed, the ICP, is maintained by inductive heating of the flowing gas in a way similar to the inductive heating of a metallic cylinder placed in the induction coil, i.e. the radio frequency current flowing in the coil generated oscillating magnetic fields with lines of force axially oriented inside the coil. These induced magnetic fields generate in turn high-frequency, annular electric currents in the conductor, which is then heated as a result of its ohmic resistance. If the conductor is a flowing gas, an insulating confinement tube must surround the gas to prevent it from extending to the coil, which would lead to shortcircuiting. On the other hand, the gas flow should be made so that a thin sheath of cold gas separates the plasma from the outer confinement tube in order to prevent the latter from melting. The thermal isolation of the plasma can be achieved by Reed's vortex stabilization technique [64,78] using a tangentially introduced gas flow, as shown in Fig. A. For that reason, this outer gas flow was originally termed "coolant gas flow", as it was thought that the plasma itself was sustained by the "plasma gas", introduced through the space between the outer and intermediate tubes.

Using argon for both the outer and intermediate gas, it was found, however, that an ICP could be sustained with the outer gas only, which thus showed to play various roles, namely those of maintaining the plasma, stabilizing its position and thermally isolating the plasma from the outer confinement tube. Therefore a change in terminology has been proposed: "coolant gas" would become "plasma gas" and "plasma gas" would become "auxiliary gas". Although these terms are rational, a more confusing proposal could not have been made to bring historical developments into line with new insights. To avoid this confusion in the present text we shall use the unambiguous terms: "outer gas" and "intermediate gas". It should be noted that in ICPs with nitrogen or air as outer gas and argon as intermediate and inner gas, the nitrogen or air serves primarily as a coolant so the form "nitrogen-cooled ICP" still appears appropriate.

For the gas flowing through the carrier gas tube the terms "carrier gas" or "aerosol carrier gas" have become common, because this gas is used to carry the sample to the plasma.

In spectrochemical applications of ICPs argon is the most frequently used as carrier and intermediate gas, while either argon or nitrogen (sometimes oxygen or air) is used as outer gas. More recently, ICPs with nitrogen as carrier gas or ICPs running completely on nitrogen or air have been investigated. The majority of the samples at present analyzed by ICP-AES are offered to the ICP instrument in the form of liquids, which are converted into an aerosol by pneumatic or ultrasonic nebulization. A fraction of the aerosol is eventually carried to the ICP.

ICP configuration and appearance +

The torch dictates the flow patterns of the two or three gas streams in the ICP and is the most critical component of the ICP assembly. The various considerations that underlie the design of the present torches used for analytical ICPs have been gradually developed from Reed's original concepts [64,78] and the early work of Greenfield and Fassel. Reed introduced the

intermediate gas tangentially to produce a low pressure area at the centre of the torch and to cause recirculation of the plasma giving a continuous supply of ions in the coil region. The outer gas flow too was introduced tangentially to provide axial stabilization. This technique still is widely used in present day torch design.

Greenfield et al. [86] had initially recognized the necessity to form a toroidal discharge. This toroidal configuration, which was more or less evident from Reed's work was explicitly featured in a patent of Greenfield et al. [86] as being essential to the effective introduction of aerosols into an ICP for spectrochemical analysis. A toroidal shape implies that the axial zones of the plasma are relatively cool compared to the surrounding zones. This phenomenon is related to the skin effect of the RF current and to aerodynamic factors. RF inductive heating provides the possibility to generate a plasma into which a stream of gas with a relatively small cross section can "bore" a hole without disturbing the stability of the plasma. Thus a major problem of introducing an aerosol effectively into a high-temperature plasma, with its inherent high viscosity [101,102] , is elegantly overcome. The aerosol is injected via a "weak spot" in the bottom of the plasma and subsequently carried through a tunnel to the plasmas zones located above the coil. Under the conditions normally used in analysis, the temperature in the tunnel of the ICP is sufficiently high (i.e. 4000-5000 K) and the transit time of aerosol particles sufficiently long (i.e. of the order of a few milliseconds) for the sample to become volatilized and atomized during its passage through the coil region of the ICP, so atomic spectra can be produced in the regions above the coil. Whether complete atomization is achieved depends in part on the power input to the ICP and on the flow rate of the carrier gas.

The appearance of an ICP (Fig.8) is that of an intensely luminous, non-transparent core and a flamelike, less luminous tail. The core fills the region inside the coil and usually extends a few millimetres below and above the coil. It emits an intense continuum and the spectrum of hydrogen and neutral argon, and various band spectra (in particular if aerosols are

introduced). Above the coil, the core becomes conical and fades into a still bright but slightly transparent zone. In argon ICPs the transition region between the core and this second zone is the best region for analytical observations, since it yields the highest signal-to-background ratios (SBR) combined with low background noise; so this region, which is located between 10 and 20 mm above the coil in low-power argon ICPs, yields the best detection limits. The precise value of the optimum observation height must be established empirically in combination with the optimization of the two other principal ICP parameters, power input to the plasma and carrier gas flow rate.

The third region of an ICP is the tail flame, which is hardly visible when pure water is nebulized, but assumes typical colours as observed in flames when aerosols of metals are injected into the plasma. Such colours are also seen in the tunnel of the toroid when the metal concentration in the solution is made sufficiently high. The colouring of the tunnel can be seen by both side-on and end-on observations. The latter way of observing reveals an ICP as a luminous ring (Fig. 3) with a dark hole when pure water is nebulized. Side-on observation is the commonest in ICP-AES, although some work with end-on observation has been reported [103-107].

During the period between 1964 and 1975, ICP research was explorative and involved the use of a variety of RF generators, designed for other purposes. The primary aim of this research was to establish the effects of essential parameters, including the torch configuration, on the analytical characteristics of the ICP to optimize the analytical performance. The relevant literature reflects the explorative nature of this research and covers a diversity of torch configurations and operating conditions. This literature is summarized in the reviews of Greenfield et al. [71] and Barnes [17], which include tabular surveys of the RF generator characteristics, torch configurations and operating parameters. For popular arrangements also see [108].

The various developments have led to a few standardized torches of the "conventional type", at present used in commercial equipment. These torches, in turn, serve as starting-points in the development of a second generation of ICPs that are being

developed with the primary goal of reducting the operating cost (lower argon consumption or replacement of argon by nitrogen or air) and the generator cost (lower power) without loosing the excellent analytical performance achieved with the classical torches.

Abstract

The main fundamental problem in inductively coupled plasma emission spectroscopy (ICP AES) is the understanding of a) high ionic line sensitivity and b) the absence of significant matrix effects.

This report chiefly deals with the first of these items.

For an adequate understanding of the mentioned "mysteries" an accurate characterisation of the discharge is indispensable. Some models developed to this aim,and measurements concerning the argon system served this purpose.

Opposed to the abundancy of former research with a Local Thermal Equilibrium (LTE) as the starting-point,we indicated the possibilities of describing argon and analyte level densities in a partial LTE regime. Former investigations by other authors characterized the discharge by means of an "excitation temperature", which was derived from e.g. relative intensity measurements. We showed this approach to be fundamentally inappropriate because the principal parameter appeared to be the electron density.

Furthermore we proved many temperature measurements to be basically incorrect, although agreement with reality may be satisfactory.

From absolute intensity and electron density measurements we concluded that for high argon levels with an excitation energy above the 4d level excitation energy, there existed Saha equilibrium with the argon ionic ground level. The 4p levels and presumably the 4s levels could be described in the recombining saturation regime. The ground level was found to be under populated by a factor of 10^2-10^4 in the observation zone commonly used in ICP-AES.

The argon system in an ICP thus behaves as a strongly recombining plasma with virtually completely decoupled ionic and neutral ground state densities.

Therefore we could state that the ground level density is ruled by diffusion and convection only.

The clue to an understanding of argon level densities in an ICP lies in (a) gaseous dynamics describing ionic and neutral ground state densities and (b) the saturation and pLTE phase models describing argon excited states coupled to the argon ion density.

Former investigations by other authors considered penning ionisation to be a possible excitation channel for analyte ions with the appropriate energy. We showed the charge transfer process to be much more probable. A rate model accounting for this charge transfer processes could explain over populations of ionic excited states with respect to atomic excited analyte states up to a factor of 10^3 for Mg.

From absolute and relative intensity measurements in the Mg system it appeared that the Boltzmann plot of excited level densities yielded two different temperatures. One of these temperatures (T_{exc}^{MgI}) described the ionisation and excitation between the MgI excited levels and the MgII ground state. The other (T_{exc}^{MgII}) described the excitation equilibrium in the MgII system including the ground state.

It was found that $T_{exc}^{MgI} < T_{exc}^{MgII}$. These two excitation temperatures approached each other more and more as the observation height above the load coil increases.

The only possible explanation for this behaviour is that ions are created and observed at different radial positions in the flame. This is in accordance with literature. In this so called "ion creation zône" ions must be excited in a direct process. The most probable process for this ionic level population is charge transfer.

Another important conclusion is that practically all Mg neutral excited atoms are created by a recombination process from the ions after diffusion to the central (cooler!) regions of the analyte channel.

The neutral Mg ground state was found to be over populated with respect to excited states.
It is concluded that this must be due to inhomogenities in the neutral groundstate density

Owing to the large inhomogenities in the discharge, future research must be aimed at detailed absolute radial level density measurements. The key to the further understanding of ICP excitation mechanisms must be sought in these radial density profiles.

Table of Contents

Page

1. Introduction

As mentioned in the general introduction ICP AES shows exceptionally high sensitivity for ionic spectral lines and rather low interference effects from alkali matrices compared to eg. classical flames and DC arcs.

Since the first days of ICP-AES, investigators have been interested in the mechanisms that can explain this analytically favourable behaviour.

It is generally accepted that the extreme sensitivity of ionic levels and the absence of significant matrix effects is caused by a non local thermal equilibrium (LTE) situation at least in some spatial regions of the discharge [12,13,16,19,23].

This non-LTE situation in the discharge has frequently led to completely erroneous temperature measurements and, in turn, a wrong characterisation of the discharge.

In this work we shall take partial LTE (pLTE) as the starting point instead of the LTE situation so often used in the past. The main parameter describing the discharge in this work is considered to be the electron density, and not the electron temperature as is commonly done in previous publications. This electron density can be measured accurately with the aid of Stark H_β linewidths.

To establish the validity of pLTE we shall solve a balance equation for argon excited levels for a nearly equilibrium plasma (chapter 2).

As a second possible approach we shall assume the plasma to behave as a predominantly ionizing or recombining plasma in the sense proposed by Fujimoto [7-10].

Boumans [13] considered the recombining mode to be applicable to ICP discharges. The distinction between the ionizing and recombining mode opens the possibility to adopt Fujimoto's plasma models [7-10] . In the ICP electron density regime the saturation phase is most likely to occur. The proof of the existence of such a phase in atmospheric argon discharges is also of general

interest in plasma physics disciplinaries [11], (chapter 2).

Absolute density measurements of many excited argon levels and the electron density (chapter 5) will deliver the necessary information to trial the pLTE and/or saturation phase model (chapter 6).

In the light of analyte ionic level overpopulations Boumans and de Boer distinguish between "hard" and "soft" lines. According to their proposal soft lines will have their emission maxima in the "thermal" region of the discharge while hard lines peak in the "nonthermal" region, thus violating the norm temperature concept and LTE considerations. Generally ionic lines show hard line behaviour and atomic lines of elements with low to medium ionisation potentials ($E_i \lesssim 7eV$) show soft line behaviour. This means that a non-LTE mechanism must account for the non-LTE population of excited analyte ionic levels.

It will be discussed that this non-LTE overpopulation can be in part explained by a temperature correction; however, depending on the analyte in question,part of the over populations remain to be explained (chapter 2).

Following Mermets suggestion [57], Blades and Horlick [58] propose as the principal mechanism supplying the excess of ionic excited states a penning ionisation process by argon metastable atoms.

In this and other treatments the rôle of the metastable argon atoms generally is overestimated since equilibration times between the radiating 4s levels and the metastable 4s levels are very short compared to the radiative decay process. In contrast, Blades and Hieftje, [59] argue that absorption of resonance radiation may contribute essentially to the 4s level population, thus prolonging the life time of the entire 4s group. Lifetimes are shown to be large enough to carry 4s argon atoms into the ICP observation zône where penning reactions would create the excited ion level over population.

Boumans and de Boer [19] calculate that for a significant contribution of the Penning reaction the rate coefficient for penning ionisation should be at least 70 times larger than the electron ionisation rate-coefficient but they did not consider the reverse penning process. This would require a larger penning rate coefficient.

In this paper penning ionisation is considered to be an unimportant process compared to the very similar charge transfer proces:

$$Ar^{+} + X \longrightarrow X^{+*} + Ar^{o} + \Delta E$$

since the argon ion density exceeds the argon excited level density by orders of magnitude and furthermore, cross sections for the latter reaction are known to be large even when the energy fit is not accurate.

The not detailed balanced charge transfer reaction will be taken as a startingpoint to calculate overpopulations of the analyte ion system with respect to the atom system. Again pLTE in the analyte system is assumed.

Absolute density measurements in the analyte (chapter 5) ion and atom system (MgI + II) will be performed.

These measurements should confirm the relevance of the charge transfer process, at least qualitatively (chapter 6). The present investigation is a first effort in this laboratory to tackle the problem along these lines. Therefore we cannot expect the models for analyte and argon to give an accurate quantitative description of the ICP discharge. Qualitative conclusions, however, and the formulation of some more precisely specified objectives for further research can certainly be considered as a useful contribution to the clarification of some intriging fundamental problems of ICP AES.

2. Modelling the argon system in pLTE and saturation phase regimes.

2.0. Introduction

If a plasma is in Thermal Equilibrium (TE), then, in addition to the pressure (or the total number of atoms) only one parameter e.g. n_e or Te is needed to describe the system completely. Any deviation from TE will require additional parameters.

In the subsequent text we shall assume atmospheric pressure ($p = 10^5$ N/m^2). This pressure will be considered as a parameter with a constant value.

A special form of TE is Local Thermal Equilibrium (LTE). This means that every volume element of the plasma can be described in terms of a thermal equilibrium, thus requiring one space dependent parameter to describe the plasma. Of course there must be limits to the gradients of this parameters [1-4]. This means that spatial inhomogenities should not exceed certain well definite maxima in order to neglect the transport contributions.

In TE or LTE (further referred to as LTE) all level populations, including the neutral groundstate population can be calculated using the Saha and Boltzmann equations together with Dalton's law and the quasi neutrality condition.

$$\sum_q n_q q_q = 0 \qquad (2.0.0)$$

$$\frac{n_e n^+}{n_i} = \frac{2g^+}{g_i}\left(\frac{2\pi m kT_e}{h^2}\right)^{3/2} \exp\left[-\frac{E^+ - E_i}{kT_e}\right] \qquad (2.0.1)$$

$$= S(T_e, E_i)$$

$$n_i/n_j = g_i/g_j \exp\left[-\frac{E_i - E_j}{kT_e}\right] \qquad (2.0.2)$$

$$p = kT_e \sum_q n_q \qquad (2.0.3)$$

where n_e = the electron density

n^+ = the ion groundstate density

n_i, n_j = the density of excited states i, j

g_i, g_j = the statistical weights of excited states i and j

E_i, E_j = the excitation energy of excited states i and j

n_∞ level density of a fictitious level just below the ionisation limit

E^+ the ionisation energy of the atoms in question

g^+ the statistical weight of the ion ground level

p the total pressure

$\sum_q$ denotes a sum over all particle species and levels

T_e the electron temperature

q_q the charge of particle q.

From this four equations principally the population densities of all excited levels and ground levels of ion and neutral atom can be computed (see Fig. 2.0.1a).Characterizing such a system only requires measurement of one parameter (besides the pressure). Commonly used is e.g. the method of the two line temperature measurement [1,3,5,6]. By measuring the relative densities of two levels one determines the slope in the Boltzmann plot and thus the electron temperature. Another method is to measure Stark widths in order to obtain the electron density (frequently used for this method is the Balmer H_β line).

If any departure from the LTE situation occurs, e.g. by energy losses of a volume element of the plasma to the surrounding areas, as said extra parameters are needed to describe the system.

A frequently occurring deviation from LTE can be described by the partial LTE (pLTE) (see Fig. 2.0,1.b). In pLTE systems all excited levels are in Saha equilibrium with the ion ground state, only the neutral groundstate is not in equilibrium with this levels. Note that the temperature T_o of groundstate atoms may differ from T_e.

In this simple case only one extra parameter is needed to describe the system. The following possibilities are frequently used.

i) (Frequently used in the AES disciplinaries). Defining two different temperatures from which one (T_{exc}) describes the Boltzmann equilibrium between excited states and the other (T_{ion})describes the Saha ionisation equilibrium between the groundstate of the ion and the atom.

ii) (Frequently used in plasmaphysics disciplinaries). Defining an over population b_o of the neutral groundstate with respect to the Saha population of the neutral groundstate viz.:

$$b_o = \frac{n_o}{n_{o,s}} \tag{2.04}$$

$$n_{o,s} = n_e\, n^+ \frac{1}{S(T_e,o)} \tag{2.05}$$

Generally for an ionizing plasma the ground level is over-populated ($b_o > 1$), for a recombining plasma the ground level is under populated ($b_o < 1$).

Further deviations fromthe LTE regime have resulted in a wide scala of different temperatures or, more logically,a set of over populations b_i of levels, with respect to the Saha population of this levels.

If deviations from the LTE regime (see Fig. 2.0.1.c) are very large it is easier to drop the description with Saha-Boltzmann equations. This results in collisional radiative models such as Corona or Saturation models (see sections 2.2 and 2.3). In the intermediate region, the saturation phase [3, 7-10, 11] can be used as a description (see section 2.3).

It is generally accepted that an ICP shows more or less drastic deviations from LTE [12-20].
This deviations frequently led to erroneous temperature measurements (see section 2.1.2).

In this attempt to describe the equilibrium in an ICP two different approaches can be distinguished.

i) We shall assume that the deviations of LTE are not too large. The measured over populations of excited levels with respect to the LTE populations are assumed to be partly due to erroneous temperature measurements.
After a discussion on the relevance of temperature in the ICP we shall calculate a collisional radiative model for a simplified argon system consisting of four levels in an ICP [21]. (section 2.1 and 2.2). In this paper.
this model will be called the "4 level model."

We shall calculate the deviations from the first excited levels as a consequence of an over population of the ground level, to check the validity of pLTE. It is assumed that all levels which are sufficiently close to the ionisation limit are in Saha equilibrium with the ion ground level.

ii) We shall accept appreciable deviations from LTE. A description of the plasma as elaborately treated by Fujimoto [7-10] and proposed to be an explanation for ICP population densities by Boumans [13] will be adopted. In this model many levels are used in calculations. We shall make a distinction between predominantly ionizing and predominantly recombining plasmas. This model will be called the "Fujimoto model".

The aim of both models is ofcOurse to describe the population densities of excited states of the argon system, thereby opening a possibility to explain the analyte excitation. In this paper the analyte and argon system are still treated completely seperately except for the change transfer proces (see chapter 3).

From the calculations on the proposed models useful conclusions can be drawn. These are listed in section (2.4).

2.1. The relevance of the temperature in an ICP

2.1.1. Modified Saha and Boltzmann equations for a simple description of pLTE

As is noted in the introduction of this chapter we shall treat this subject in the pLTE regime, over or under populations are expected to be small (e.g. limited by a factor 10).

If we take LTE as a starting point at a given pressure a relation between n_e and T_e can be predicted from the Saha equation and the Boltzmann equation. If we use the Saha equation and neglect the pressure component of excited states, ions and electrons with respect to the pressure component of the neutral groundstate atoms (justified if $n_o \gg n_e$ which is the case since Te $<$ 1 eV) one obtains

$$n_e^2 = \frac{p}{kT_e} S(T_e, 0) \qquad (2.1.1)$$

for a pure LTE population density.
This relation is shown in Fig. 2.1.1 by the solid curve.

If one accounts for an over or under population b_o of the ground level with respect to the Saha population of the excited levels one obtains a modified Saha equation and pressure relation

$$b_o n_e^2 = n_o S(T_e, 0) \qquad (2.1.2)$$

$$\frac{p}{kT_o} = n_o \qquad (2.13)$$

where $b_o > 1$ indicates an over population, and $b_o < 1$ an under population of the ground level with respect to excited levels.

T_o may be different from Te. (Generally $0{,}5\ T_e < T_o < T_e$).
Combination of those two relations results in a relation similar to eq. 2.1.1

$$n_e^2 = \frac{p}{kT_o} \frac{1}{b_o} S(T_e, 0) \qquad (2.1.4)$$

In ref. [21] measurements of b_o in an atmospheric argon arc indicate for $T_e \approx 0{,}50$ eV (approximately ICP electron temperature [12,14,16,18,19,23,36-39,58,60-62] the value of b_o may be well below 10.

Fig. 2.1.2 shows the dashed curves for these extreme over or under populations.

From this approach it thus becomes clear that if one parameter, namely n_e, is measured reasonable accurately, the two dashed curves define a maximum ($b_o = 10$) and a minimum ($b_o = 1/10$) temperature. Since the curves are fairly steep in the n_e region of interest ($10^{19} < n_e < 10^{21}$) the temperature will not vary very much with a variation of b_o of one order of magnitude.

For our ICP, $n_e \approx 2.10^{20}$ m^{-3} in the observation zone (see section (6.1.1)).
This results in the following temperature clenching (neglecting the difference between T_o and T_e).

$$0,54 < T_e < 0,64 \qquad (2.1.5)$$

This range (20%) approaches the accuracy of temperature measurements using e.g. a two line method for Argon lines (10 à 20%) [1,12,14,16,59].

The accuracy can even be improved by measuring the density of one excited level (e.g. the 4p level). This is clear from Fig. 2.1.2.

If one succeeds in measuring the absolute density of one of the 4p levels ($E_i \approx 13,2$ eV) with an overall accuracy of $\approx$ 10%, one can improve the temperature determination to an accuracy of $\approx$ 6%. Though this requires very precise calibration techniques, to measure the absolute intensity from a transition with a 4p upper level, this method is more accurate than the argon two line method if pLTE applies.

Another important consequence of the foregoing discussion is, that not n_e and T_e determine the characteristics of the discharge but n_e and b_o (assuming $T_o = T_e$) of course an exact measurement of b_o is not possible, however, the absolute density of an excited level will also serve as an independent second parameter. Fortunately n_e can be measured very accurately, e.g. by Stark broadening of the Balmer H_β line [1,22].

Note that this approach is basically different from the approach adopted by other authors. No electron temperature is needed to describe the population density of excited states with reasonable accuracy. (This electron temperature however determines the intersection of the Saha curve with the axis $E = E^+$. This is a minor influence compared to the exponential factor in the Saha equation and does not affect the validity of the above).

Much to often authors assume a constant electron density (e.g. taken from literature and adopted to their ICP), and characterize the discharge by means of a varying electron tempe-

rature. From the above discussion it appears that this is basically not correct because n_e appears to be the parameter of major importance.

Finally, even the neutral ground state density is often not needed for the clarification of many excitation processes involving analyte atoms (see chapter 3), thus, this proposed characterisation appears to be sufficient to explain analyte and argon excitation.

2.1.2. The underestimated electron temperature

The electron temperature measured by various authors seems to be underestimated. This conclusion can be derived from the facts that:

i) electron densities do not agree with calculated electron densities from the measured temperature, measured electron densities are orders of magnitude to high [12,16,18,19,23].

ii) the huge over population of analyte excited levels compared to the LTE values [14,19,58].

iii) ionic/atomic analyte line emission intensity ratios exceed the LTE values by orders of magnitude [14,19,58].

i) This point of view has been elaborately treated in the foregoing section. One finds $\hat{T}_e$ = 0,58 eV. This yields T_e = 6700 K. This is rather high compared to the reported values which scatter between as low as 4000 K and as high as 6000 K [12,14,16,18,19,23,37, 58,60-62]. Since the calculated electron density is rather sensitive to temperature variations (as ionic/atomic line intensities and level populations are too!), the disagreement is not surprising.

ii) For the line intensities resulting from two transitions in the same ionisation stage one writes [1]

$$\left(\frac{I_n}{I_m}\right)_{T_e} = \frac{g_n A_n \lambda_m}{g_m A_m \lambda_n} \exp\left[-\frac{E_n - E_m}{kT_e}\right] \qquad (2.1.5)$$

where g_i, A_i = the statistical weight of the upper level of the transition and the transition probability.

I_n/I_m = the ratio of calculated line intensities.

T_e = the "real" electron temperature.

Suppose one assumes the temperature is T_e^* instead of T_e with $T_e = T_e^* (1+\beta)$. Then one calculates for the quotient α of the real line intensity ratio $(I_n/I_m)_{T_e}$ and the assumed line intensity ratio $(I_n/I_m)_{T_e^*}$

$$\alpha \propto \exp\left[\beta \frac{\Delta E}{kT_e^*}\right] \qquad (2.1.6)$$

where $\Delta E = E_n - E_m$.

So if we plot the logarithme of α as a function of ΔE we can derive the systematic error β from the slope of this line. Note that at $\Delta E = 0$, α equals unity. Boumans [19] measures relative over populations α of various MgII lines assuming an electron temperature (derived from a two line method with Zn) $\hat{T}_e^* =$ 0,50 eV. From the plot in Fig. 2.1.3a one finds for β : $\beta = 0{,}34$. This would yield a true electron temperature $\hat{T}_e = 0{,}67$ eV. Note over and under populations of a factor 1-3 in the MgII system remain. This could be due to experimental errors.

iii) For the line intensities resulting from two transitions in different ionisation stages one writes [1]

$$\left(\frac{I_n^+}{I_m}\right)_{T_e} = \frac{g_n A_n \lambda_m}{g_m A_m \lambda_n} \frac{2}{n_e}\left(\frac{2\pi m kT_e}{h^2}\right)^{3/2} \exp\left[\frac{-\Delta E}{kT_e}\right] \qquad (2.1.7)$$

where ΔE is the energy difference including the ionisation energy viz.: $E = (E_m + E^+) - E_n$.

I_n^+ spectral line intensity from an ion line.

Again we suppose the temperature to be T_e^* with $T_e = T_e^*(1+\beta)$. One calculates for the ratio of true line intensity ratio and assumed line intensity ratio

$$\alpha = (1+\beta)^{3/2} \exp\left[\beta \frac{\Delta E}{kT_e^*}\right] \qquad (2.1.8)$$

If we neglect $(1+\beta)^{3/2}$ variations with respect to the variations in the exponent, one finds in a similar way as described under ii) the systematic error in the temperature.
Fig. 2.1.3.b shows line intensity ratios as measured by Boumans et al. [19] and Furuta et al. [14]. The points show quite a large scattering. There seems to be a dependence as scetched by the dotted curve. Physically we have no reasonable explanation for this. Furthermore Mn, Ca Ba and Pd seem to agree with line ①, β = 0,56, however Be Mg V and Cd do not fit this sceme.
If we draw line ②, β = 0,34, through the point for Mg, we conclude this value fits with the value found for lines in the same ionisationstage (ii). This means that both Mg excitation and ionisation can be described with the same temperature.
Note that the values from ref. [14] are generally somewhat lower, despite the fact that they used a lower temperature (T_e^* = 5300 K). From their values one would calculate a "true" electron temperature T_e = 6600 K. For the electron density they [14] assumed (10^{21} m^{-3}) one would find (Fig. 2.1.1) T_{eLTE} = 7700 K. The difference in electron density can explain the difference in results between ref. [14] (10^{21} m^{-3}) and ref. [19] (5.10^{21} m^{-3}). The ratios found in ref. [19] would become lower if one recalculates them at $n_e = 10^{21}$ m^{-3}. However, both these electron densities are assumed to high. We measured the electron density to be 2.10^{20} m^{-3} in the observation zone of the plasma. This results in an equilibrium temperature T_{eLTE} = 6700 K. If one corrects the results for the high n_e of ref. [14] by a factor 5 and of ref. [19] by a factor 25, one would obtain for the systematic temperature error β = 0,18 for both references (with lines ② and ③ giving the initial systematic error), thus the "true" electron temperatures would be: 6300 K and 6800 K respectively, which are very close to the equilibrium value (6700 K) with $n_e = 2.10^{20}$ m^{-3}. Note that, despite the temperature correction, over and under populations of one or two orders of magnitude remain to be explained. This can not be due to experimental errors. The next chapter will deal with a possible mechanism which could explain this non LTE behaviour.

2.2. The four level model

2.2.1. General

If we permit the first excited levels of the 4p and 4s group of argon to be slightly over or under populated besides the non LTE population of the neutral groundstate, then the appraoch described in section 2.1 is not sufficient for the description of the population densities of this levels.

We will use a collisional radiative model as proposed by Rosado [21].

The starting point of this model is, that because the energy exchange between sublevels in a group (eg. 4p (10 levels) or 4s (4 levels)) is much more intense than the exchange between groups (in the subsequent called (effective) levels), the argon energy level diagram can be simplified to contain a set of effective levels.

One may calculate effective energies, transition probabilities and collisional-radiative transition rates between those levels. Appendix C will deal with this subject.

In the approach of Rosado the argon energy level diagram is simplified to contain 4 effective levels and the ion ground level (see Fig. 2.2.1). The balance equations account for: electron excitation-deexcitation, radiative decay, radiative recombination, 3 body recombination, electron ionisation and radiation trapping.

The escape factors for line radiation are calculated in appendix A, for the recombination radiation we have taken an extrapolated value to this low temperatures from Rosado [21].

Rosado accounts for diffusion of neutral groundstate atoms. We shall also account for convection as this is believed to play also a major rôle in an ICP discharge [24].
Rosado [21] derives the balance equation accounting for all this effects which results in:

$$\frac{1}{n_{q,s}}\frac{dn_q}{dt} = n_e \sum_{i\neq q}^{3}\left[(b_i - b_q)\,k_{qi}\right] - k_{q+}(b_q - 1) \qquad (2.2.1)$$
$$+ R_{q+}\,k_{+q}\,\Lambda^{(2)}_{+q} - \sum_{p=0}^{q-1} b_q A_{qp}\Lambda_{qp} + \sum_{r=q+1}^{3} b_r R_{rq} A_{rq}\Lambda_{rq}$$

for meaning of symbols refer to equation (2.2.3-5).

In this equation the assumption $b_i = 1$ $(i > 4)$ is made. This means all excited levels with an excitation energy above the excitation energy of the $^{6S}/_{3d}$ level are in Saha equilibrium with the ion ground level. This assumption may lead to wrong conclusions for the level over populations as the non LTE contribution of all these higher excited levels possibly may not be neglected. As Rosado finds good agreement with experiments in his argon arc discharge we expect the model to be valid in the ICP discharge too.
In this section the results of the four level model are summarized and recalculated for an electron density of 2.10^{20} $1/m^3$ and an electron temperature of 0,56 eV.

2.2.2. Application of the CRM to an ICP discharge

The various rate coefficients and other properties occurring in the balance equation are listed in table 2.2.1.

Rosado finds as the solution of the rate equations for the levels 1 and 2

$$\delta b_1 = \frac{k_{10}k_2 + k_{20}\left[k_{12} + \alpha/n_e\right]}{D}\,\delta b_0 + \frac{\left[k_2\,\alpha/n_e + \left[k_{12} + \alpha/n_e\right]\beta/n_e\right]}{D} \qquad (2.2.3)$$

$$\delta b_2 = \frac{k_{12}k_{10} + k_{20}\left(K_1 + \frac{A_{10}\Lambda_{10}}{n_e}\right)}{D}\,\delta b_0 + \frac{k_{21}\,\alpha/n_e + \left(K_1 + \frac{A_{10}\Lambda_{10}}{n_e}\right)\beta/n_e}{D} \qquad (2.2.4)$$

$$D = \left(K_1 + \frac{A_{10}\Lambda_{10}}{n_e}\right) K_2 - k_{21}\left(k_{12} + \frac{\gamma}{n_e}\right)$$

$$\alpha = R_{1+}\, k^{(2)}_{+1} - A_{10}\Lambda_{10} + R_{21} A_{21} \Lambda_{21}$$

$$\beta = R_{2+}\, k^{(2)}_{+2} - A_{21}\Lambda_{21} + R_{32} A_{32} \qquad (2.2.5)$$

$$\gamma = R_{21} A_{21} \Lambda_{21}$$

$$K_i = \sum_{j \neq i} k_{ij} + k_{i+}$$

where k_{ij} collisional excitation rate $i \rightarrow j$

k_{i+} electron ionization rate from level i

$K^{(2)}_{+i}$ radiative recombination rate

$\Lambda^{(2)}_{+i}$ escape factor for recombination radiation

A_{ij} effective transition probability $i \rightarrow j$

Λ_{ij} escape factor for line radiation $i \rightarrow j$

b_i $n_i/n_{i,s}$ reduced density of level i (= over population)

$n_{i,s}$ Saha population of level i (see eq. 1.0.1)

R_{ij} $n_{i,s}/n_{j,s}$ (see appendix C, Figure C.3)

R_{i+} $S(Te, E_i) = n_e n^+/n_{i,s}$ (see appendix C, Figure C.3)

α, β total radiative contribution to levels 1, and 2 respectively

$\delta b_i = b_i - 1.$

The following approximations have been made:

$\Lambda_{32} = 1$: no trapping for (5d+3s) - 4p radiation (see appendix A).

$\Lambda^{(2)}_{+1} = \Lambda^{(2)}_{+2} = 1$: only recombination radiation to the ground state is partially trapped.

If we neglect γ/n_e compared to k_{12} (valid if $n_e > 10^{20}$) then eqs. (2.2.3-5) can easy be calculated with the values for rate coefficients from table 2.2.1.
One finds

$$\delta b_1 = 5*10^{-3}\delta b_0 + \frac{0,52}{\hat{n}_e} \qquad (2.2.6)$$

$$\delta b_2 = 7.7*10^{-4}\delta b_0 - \frac{0,053}{\hat{n}_e} \qquad (2.2.7)$$

where $\hat{n}_e$ the electron density in units of 10^{20} m^{-3}. If we substitute $n_e = \infty$ in this equations one obtains: $\delta b_1 = 5.10^{-3}\,\delta b_0$ and $\delta b_2 = 7,7.10^{-4}\,\delta b_0$, with $\delta b_0 = 0$ one obtains of course the LTE situation. If δb_0 gets appreciable values ($\delta b_0 \approx 100$) then one concludes that levels 1 and 2 are over populated. This is due to the competition between collisional excitation and collisional deexcitation which are not detailed balanced.

If we calculate the limits of δb_0 demanding the over population of the second level (δb_1) not to exceed 10% then we obtain

$$-1 < \delta b_0 < 120 \qquad (2.2.8)$$

So even if the ground level is over populated by a factor 120 then still the pLTE assumption is valid, since the second level does not deviate more than 10% from the pLTE value. This result indicates the validity of pLTE assumption in an ICP. Unfortunately this model does not predict correct values if the ground level is strongly under populated ($\delta b_0 \to -1$, $b_0 \to \frac{1}{\infty}$). This is only caused by a mathematical complication. One should try to solve eq. 2.2 1 with the substitution $\delta b_q = n_{q,s}/n_q - 1$ instead of $\delta b_q = \frac{n_q}{n_{q,s}} - 1$.

2.2.3. The source term in the balance equation

We will evaluate the source term by giving a rough estimate. We will suppose stationarity of the discharge. One writes for the left hand side of eq. (2.2.1)

$$\frac{1}{n_{o,s}} \frac{dn_o}{dt} = \frac{1}{n_{o,s}} \left(\frac{\partial n_o}{\partial t} + \mathrm{div}\,(n_o \underline{v}_d) + \mathrm{div}\,(n_o \underline{v}_c) \right) \quad (2.2.11)$$

where $\underline{v}_d$ diffusion velocity
$\underline{v}_c$ convection velocity.

If one uses Fick's law, and with the assumption of stationarity viz.:

$$\underline{v}_d = - \frac{D_a}{n_o} \mathrm{grad}\, n_o \; ; \; \frac{\partial}{\partial t} = 0 \quad (2.2.12)$$

where D_A is the ambipolar diffusion coefficient, one obtains for eq. (2 2.11):

$$\frac{1}{n_{o,s}} \frac{dn_o}{dt} = \frac{1}{n_{o,s}} \left[-D\, \mathrm{div}\, \mathrm{grad}\, n_o + \underline{v}_c \mathrm{grad}\, n_o + n_o \mathrm{div}\, \underline{v}_c \right] \quad (2.2.13)$$

The following assumptions can be made (cylindrical coordinates r, θ, z)

i) $\underline{v}_c = (0,0,v_c)$.
The convective velocity has only a z component (z is the coordinate along the axis of the discharge). Convection in other directions can be neglected. [24]

ii) $\underline{v}_d = (v_d, 0,0)$.
The main contribution to diffusion results from the radial component of the diffusion velocity. [24]

With these assumptions one can write for eq. (2.2.13)

$$\frac{1}{n_{o,s}} \frac{dn_o}{dt} = -\frac{1}{n_{o,s}} \left[D \frac{\partial^2 n_o}{\partial r^2} + \frac{D}{r} \frac{\partial n_o}{\partial r} - v_c \frac{\partial n_o}{\partial z} \right] \quad (2.2.14)$$

With the substitutions $\delta n_o = - \delta n_e$ and $R_{o+} = n_e^2/n_{0,s}$ one finds

$$\frac{1}{n_{0,s}} \frac{dn_o}{dt} = \frac{R_{o+}}{n_e}\left[D \frac{1}{n_e} \frac{\delta^2 n_e}{\delta z^2} + \frac{D}{r} \frac{1}{n_e} \frac{\delta n_e}{\delta z} - v_c \frac{1}{n_e} \frac{\delta n_e}{\delta z}\right] \quad (2.2.15)$$

Various authors [e.g. 12,16] measured radial and axial electron densit profiles. We consider the radial profiles of Jarosz et al. [12] the most reliable because he used starkwidths, while Kornblum et al. [16] used continuum intensities. One finds:

$$\frac{1}{n_e} \frac{\delta n_e}{\delta r} \approx -180 \ 1/m \quad (2.2.16a)$$

$$1/n_e \frac{\delta^2 n_e}{\delta r^2} \approx -2.10^4 \ 1/m^2 \quad (2.2.16b)$$

Axial electron density profiles have been measured in our laboratory (see section 6.1.1). Using the results one finds

$$\frac{1}{n_e} \frac{\delta n_e}{\delta z} \approx -30 \ 1/m \quad (2.2.16c)$$

The ambipolar diffusion coefficient can be calculated from [21,25]:

$$D_A = 2. \frac{2.76 * 10^{18}}{n_o + n_e} T_e^{0,64} \left(\frac{s}{m\ K^{0,64}}\right) \quad (2.2.17)$$

With $\hat{T}_e$ = 0,56 eV, $n_o = 10^{24}$ 1/m^3 and $n_e \ll n_o$ one finds

$$D_A = 1.5 * 10^{-3} \ m^2/s$$

Substitution of the numerical values given by eqs. (2.2.16-2.2.17) $v_c \approx 1$ m/s (outer flow/area-outer tube), $r = 6$ mm,

yields: $$\frac{1}{n_{0,s}} \frac{dn_o}{dt} = -\frac{1}{\tau_d} + \frac{1}{\tau_c} = \frac{1}{n_e}\left(-4.3 * 10^{17} + 1.9 * 10^{17}\right) \left(\frac{1}{m^3 s}\right)$$

(2.2.18)

where τ_d and τ_c are the characteristic diffusion and convection times

$$\tau_D = 2.3 * 10^{-18} n_e^* (m^3.s)$$
$$\tau_c = 5.3 * 10^{-18} n_e^* (m^3.s) \qquad (2.2.19)$$

This diffusion/convection times have to be compared with the radiative decay time and collisional excitation-deexcitation times in order to estimate their importance.

The major uncertainties in the source term are the differential quotients defined in eq. (2.2.16 a/b). Especially the radial diffusion contribution is very uncertain because the radial electron density gradients are very steep. Especially at the boundaries of the aerosol channel steep electron density and temperature gradients exist. To solve this problem detailed spatially resolved temperature and electron density data are required. Furthermore the flow divergence (see eq. 2.2.11) is assumed to be zero. This may also not be the case, especially far above the load coil.

However, in a first approximation it can be concluded that these diffusion and convection terms are competitive to the radiative terms in the balance equation. (see next section) In this stage of research we do not expect very accurate quantitative results.

If one assumes the diffusion time to be equal for excited states, then the assumption that diffusion can be neglected is confirmed. One must compare the diffusion/convection time constant ($\tau \approx 10^{-3}$ s) with the collision time constant $\tau_{coll} \approx 1/n_e K_i \approx 10^{-8}$ s. Thus $\tau_{coll} \ll \tau_c$ and diffusion (or convection) plays a minor role in excited states. This is, besides the results of section 2.2.2, another necessity in order to consider pLTE to be valid.

Note that convection and diffusion are phenomena with an opposite effect on the ground state over population (see next section).

2.2.4. The solution of the balance equation for the neutral ground level

As is said before, diffusion of the ground state is not neglected and we have to solve the full equation, including the source term. Rosado [21] gives for this solution: ($b_1 \approx b_2 \propto 1$)

$$\delta b_o = \frac{\delta - \frac{1}{n_{o,s}} \frac{dn_o}{dt}}{n_e K_o} \qquad (2.2.19)$$

$$\delta = R_{o+} K^{(2)}_{+o} \Lambda^{(2)}_{+o} + R_{1o} A_{1o} \Lambda_{1o} + R_{3o} A_{3o} \Lambda_{3o} \qquad (2.2.20)$$

where $1/n_{o,s}\ dn_o/dt$ the source term

δ radiative contribution to the ground state population density (see also eq. 2.2.5).

Substituting the diffusion term determined in the preceeding section and the other values found in table 1.2.1 yields

$$\delta b_o = \frac{73}{\hat{n}_e} + \frac{11}{\hat{n}_e^2} \qquad (2.2.30)$$

For $\hat{n}_e = 2$ eq. 2.2.30 can be calculated to yield

$$\delta b_o \approx 40 + 3 \qquad (2.2.31)$$

40 — radiative contribution

3 — diffusion/convection

From this result it is clear that the major non LTE mechanism is radiation escape. However diffusion seems to play a minor role, this could be not at all the case in or just above the load coil, or in the upper tail of the flame and the boundaries of the analyte channel. Furthermore the absorption of resonance radiation increases as the number of neutral ground state atoms increases. This number is a function of the neutral temperature. As we assumed this to be equal to the electron temperature in practical calculations, n_o will be generally to low. Then the effect will be that

i) b_o decreases (since the escape factor decreases)

ii) diffusion and convection start to overrule the radiative losses.

Especially at the boundaries of the discharge T_o will be orders of magnitude lower than T_e (caused by the sheath of cool argon outer gas around the discharge).

Note that the results of eq. 2.2.30 are too uncertain to predict any quantitative results. Only the order of magnitude will be correct.

Note that diffusion accounts for an increase in over population, and convection accounts for a decrease in over population. Even an under population of the ground state may result if convection becomes faster compared to diffusion. From the results (section 6.1.1) this appears to be the case. Unfortunately the four level model in this form does not yield accurate solutions for an under populated ground level.

2.3. The Fujimoto model

2.3.1. General

With a fixed electron temperature T_e one may distinguish between different plasma states as related to different electron densities in the plasma. This electron density determines what population and depopulation processes to and from excited and ground levels plan an important role.

One usually makes a distinction between the regimes: [7-11].

i) Corona (ionizing) or Capture Radiative Cascade (recombining)
$n_e < 10^{18}$ m^{-3}.
A complete radiation dominated plasma (apart from the excitation from the ground state).

ii) Saturation and pLTE.
$10^{18} < n_e < 10^{23}$ m^{-3}.
The transition from radiation dominated to collision dominated plasma's takes place gradually, starting at higher levels while radiation terms still remain significant in balancing the lower levels. Both saturation and pLTE regimes are collisionally dominated. The difference between these two different states will become clear from the following sections.

iii) LTE.
$n_e > 10^{23}$ m^{-3}.
A complete collision dominated plasma (see section 1.0).

Generally one writes for the population density n_i of an excited level in a plasma.

$$n_i = r_i^{o} n_o + r_i^{+} n^{+} \qquad (2.3.1)$$

where r_i^{o}, r_i^{+} the collisional radiative ionisation resp. recombination coefficients.

n_o the neutral ground state density

n^{+} the ion ground state density.

If one of the populationdensities n_o or n^{+} is zero one speaks of an ionizing plasma ($n^{+} = 0$) or a recombining plasma ($n_o = 0$). If we exclude any instationarity of the plasma and we look at a small volume in particular an ionizing plasma requires a net influx of neutral state atoms (e.g. by diffusion) and thus the result is an over population of the ground state of neutral atoms with respect to the saha population (calculated from n_e and T_e).

For the predominantly recombining plasma the situation is just opposite.

If the plasma can be thought of as a superposition of an ionizing and recombining plasma both of the population densities and CR coefficients are important.

One rewrites eq. (2.3.1) as follows:

$$n_i = \frac{r_i^{o}}{B(T_e, E_i)} n_{i,B} + \frac{r_i^{+} S(T_e, E_i)}{n_e} n_{i,S} \qquad (2.3.2)$$

$$= f_i^{o} n_{i,B} + f_i^{+} n_{i,S} \qquad (2.3.3)$$

where $$n_{i,B} = n_o \frac{g_i}{g_0} \exp \frac{-E_i}{kT_e} = n_o \cdot B(T_e, E_i)$$

(the density related to the Boltzmann relation)

$$n_{i,S} = n^{+} n_e / S(T_e, E_i)$$

(the density related to the Saha equation.)

and $S(T_e, E_i)$ as defined by eq. (2.0.1).

We can rewrite the reduced Saha density b_i (see eq. (2.0.4)) in the form

$$b_i = f_i^+ + f_i^o \frac{n_{i,\beta}}{n_{i,s}} \qquad (2.3.4)$$

$$b_i = f_i^+ + f_i^o b_o \qquad (2.3.5)$$

This relation can be clarified with the aid of Fig. 2.3.1. The Saha-Boltzmann coefficients f_i^+, f_i^o will generally depend on i, the species, temperature and electron density.

In a recombining plasma one obtains for Capture Radiative Cascade and saturation

$$b_i = f_i^+ \qquad (2.3.6)$$

In a ionizing plasma one obtains for corona and saturation

$$b_i = f_i^o b_o \qquad (2.3.7)$$

In a pLTE plasma both coefficients have to be evaluated. Then equilibrium between ionisation-recombination exists. Following the treatment of Fujimoto [7-10] we will describe the various states ((i)-(iii)) of the plasma with increasing n_e. We shall distinguish between ionizing and recombining plasmas.

Of course in an ICP neither of the statements $n^+ = 0$ or $n_o = 0$ is correct. This implies that for sufficiently high lying levels always recombination-ionisation equilibrium exists. For sufficiently high lying levels this will always cause a thermal distribution of excited states. For a clear treatment we will however distinguish between the purely ionizing and the purely recombining case.

In practice an ICP is a low temperature plasma in the sense of Fujimoto's definition [7-10] so we shall only treat this case. As the ICP electron density is 10^{20}-10^{21} m^{-3} the discharge is most likely to be in the saturation regime.

The boundaries between the various phases are shown in fig. 2.3.2.

Fujimoto uses hydrogen values for transition rates and neglects diffusion and absorption of radiation. Thus we shall not expect the model to predict the over or under population of the ground state (see also section 2.2.3-4 and appendix C).

2.3.2. The different states of an ionizing plasma

(i)The Corona phase

At very low electron densities, limited by the criterium of Griem

$$n_e = \frac{6.7 \times 10^{23}\, m^{-3}}{p^{8,5}} \left(\frac{k T_e}{z^2 \chi_H}\right)^{1/2} \qquad (2.3.8)$$

where p the effective quantum number

$$\left(p = \left[E_H/(E^+ - E_i)\right]^{1/2}\right) \qquad (2.3.9)$$

χ_H ionisation energy of hydrogen

z the charge of the ions in the plasma.

the corona phase applies.

The major population process of an excited level p is direct excitation from the ground state with a possible minor contribution from cascade radiation from higher lying levels. The major depopulation proces is radiative decay.

For levels in the corona phase the following balance equation results (neglecting cascade)

$$\sum_{q<p} A_{pq} n_p = n_o C_{op} n_e \qquad (2.3.10)$$

where C_{op} collisional excitation rate $0 \longrightarrow p$

and the other symbols have the usual meaning.

Fujimoto finds for the p dependence, substituting hydrogen values for the parameters A and C in an optically thin plasma

$$n_p/g_p \propto p^{-0.5} \qquad (2.3.11)$$

(ii)Saturation phase

With an increase in n_e the Griem criterium(eq. (2.3.8)) is affected, first for the higher excited levels (see fig. 2.3.2). Then the population process for such a level,entering the saturation phase,changes from direct excitation from the ground state to excitation from the lower lying level. The depopulation process changes from radiative decay to collisional excitation to the adjacent higher level.

The following balance equation results

$$n_{p-1} C_{p-1,p} n_e = n_p C_{p,p+1} n_e \qquad (2.3.12)$$

The mechanism described by this balance equation is called the ladder like excitation mechanism, the lower end of the ladder given by eq. (2.3.8)

The p dependence of the population density becomes

$$n_p/g_p \propto p^{-6} \qquad (2.3.13)$$

Essential for all levels to be in saturation is the absence of recombination. As is argued in section 2.3.1 this will not be the case for very high lying levels. If recombination-ionisation equilibrium exists for very high lying levels a thermal distribution applies.

(iii)Saturation (TE)

With a further increase in n_e the lower end of the ladder gradually comes down until a change in deexcitation processes occurs from collisional excitation to the next higher level to collisional deexcitation to the next lower level. This results in the balance equation:

$$C_{p,p+1} n_p n_e = F_{p+1,p} n_{p+1} n_p \qquad (2.3.14)$$

This is nothing more then detailed belancing between levels p and p+1, thus resulting in a thermal distribution (eq. 2.0.2)

The change in depopulation process occurs for levels p below the so called Byron limit

$$p_B = \left(\frac{z^2 \chi_H}{3kT_e}\right)^{1/2} \qquad (2.3.15)$$

2.3.3. The different states of recombining plasma

(i)Capture Radiative Cascade

This is the analogon of the Corona phase in the ionizing plasma. Both phases are radiation dominated.

Again the criterium of Griem(eq. (2.3.8))determines the maximum n_e for this phase at a certain level.

The major population process is direct radiative recombination with a minor cascade contribution. The major depopulation process is, as in the corona phase, radiative decay to lower lying levels.

The balance equation for levels in this phase yields:

$$n^+ n_e \beta(p) = n_p \sum_{p<q} A_{pq} \qquad (2.3.16)$$

where $\beta(p)$ is the radiative recombination coefficient to level p

Fujimoto calculates for the p dependence

$$n_p/g_p \propto p^{1.5} \qquad (2.3.17)$$

For high lying levels the population density will approach a thermal population density (caused by the ionisation, which will certainly play a role in high lying levels).

(ii)Saturation (TE)

An increase in n_e changes the population process from radiative recombination to collisional deexcitation from the next higher level. The depopulation process changes from radiative

decay to collisional excitation to the next higher level. This yields a balance equation similar to eq. (2.3.14)

$$n_{p+1}\, n_e\, F_{p+1,p} = n_p\, n_e\, C_{p,p+1} \qquad (2.3.18)$$

Thus, as in the ionizing analogon the population distribution is thermal, but now for the higher lying levels ($p > p_B$).
In the recombining mode the higher levels enter directly the "pLTE"phase, in the ionizing mode these levels enter first the saturation phase. Note that even with the absence of ionisation still a thermal distribution is reached for high lying levels,opposed to the ionizing mode level densities.

(iii)Saturation phase

With a further increase in n_e the "pLTE"limit gradually comes down until the depopulating process changes from collisional excitation to collisional deexcitation to the next lower level. Then a balance equation similar to eq. (2.3.13) is obtained for the lower lying levels

$$n_{p+1}\, n_e\, F_{p+1,p} = n_p\, F_{p,p-1}\, n_e \qquad (2.3.19)$$

This yields of course for the population densities

$$n_p/g_p \propto p^{-6} \qquad (2.3.20)$$

And, consequently a ladderlike deexcitation flow is established. This transition again takes place at the Byron boundary defined by eq. (2.3.15).

2.3.3. Application of the Fujimoto model to an ICP

We will calculate the Saha-Boltzmannconstants as derived in section 2.3.1 in the purely ionizing and recombining limit according to Fujimoto. For the argon system in an ICP we shall assume an electron temperature of 0,56 eV and electron densities of 10^{19}-10^{21} m^{-3}.

The model will not predict any relation between the 4s level and the ground level. In order to overcome this difficulty we put $b_o f_{4s}^{\circ} = f_{4s}^{+} = 1$. This will only have influence as a constant factor in equations 2.3.4-7, thus the shape of the curves is not affected.
In the ionizing limit, theoretically the ion ground state density should be zero. As is remarked already in practical discharges this will never occur, as for higher lying levels a thermal distribution will be the case due to the ionisation-recombination equilibrium.

The results of the calculations are shown in fig. 2.3.3.a) and b).

This figures immediately clarify many erroneous temperature measurements from former authors. Even using a least square fit of many level densities, errors are very likely to be the case. Temperature definition losses its validity in these two limiting modes. Only in (partial) ionisation-recombination equilibrium (pLTE or LTE) or for the higher levels in the recombining mode, the temperature concept is useful.

2.4. Conclusions

From the preceeding sections some conclusions can be drawn concerning the validity of the described models. Some are mentioned in the relevant text but will be listed here again for convenience. Subsequently the three sections 2.1-2.3 of this chapter are treated.

(Section 2.1)

The relevance of temperature in an ICP.

(i) the electron density is the parameter with the major importance. It can be measured accurately by Stark broadening of e.g. the Balmer H_β line.

(ii) Temperature clenching, which permits the ground level to be over or under populated by a factor 10 results in a 20% accurate value of T_e.

(iii) Even more accurate values can be obtained by measuring one absolute level density.
Measuring a 4p level density with an overall accuracy of $\approx$10% would improve the T_e accuracy to $\approx$ 6%.

(iv) These two parameters (n_e and n_{4p}) characterize the system very accurately.

(v) The unknown parameter still is b_o, the over or under population of the ground state. This is caused by the huge extrapolation we must make to determine this parameter from T_e and n_e. However, this is not a difficulty as we do not need the ground state density to describe many analytical excitation phenomena in an ICP (e.g. charge transfer, see chapter 3).

(vi) By several authors [14,16,19] electron temperature has been under estimated, thus resulting in a huge over population of analyte excited levels. This systematic error is shown to be $\approx$ 18% resulting in "true" electron temperatures very close to the equilibrium temperature.

(vii) Both MgII line intensity ratios and MgI/MgII intensity ratio yield the same temperature correction. This would indicate no substantial difference in MgI or MgII excitation. However line intensity ratios of other elements still are one or two orders of magnitude over or under populated. This is unlikely to be due to experimental errors and must be due to some non LTE phenomena in the discharge.

(viii) A basic different approach is adopted to characterize the plasma and to determine an accurate value of T_e.
Many authors [14,16,19] make the basic error to take n_e values from literature and measure T_e values. One should however measure n_e and calculate T_e.

Section 2.2

The four level model.

i) A non LTE population is found for level 0 (ground level). Over populations of the neutral ground level are found to be mainly due to radiative decay and convection in the axial direction.

ii) No exact calculation of the non LTE population of the ground level can be given, because then detailed radial information about neutral densities, n_e, T_e and gas velocity are required. With the proposed model for diffusion it is however possible to determine the magnitude of this effects by an elaborate calculation.

iii) In the present calculation radial diffusion is large with respect to axial convection. When one takes into consideration point (ii) this may not be valid anymore. Furthermore, convection and diffusion may exceed radiative losses by orders of magnitude if a more accurate treatment is used.
It is argued that an increase in the convection term would yield a decrease in ground state over population. Even an under population could be the result (see conclusion (vii)).

iv) Level 1 (4s group) is found to be slightly over populated if the ground level is over populated by a factor 40.
This is due to the lack of detailed balancing of the collisional excitation-deexcitation processes between the over populated ground state and level 4s.

v) It is justified to neglect diffusion of excited levels in a wide range of conditions. Even with greater inhomogenities in the discharge by a factor 100 this assumption remains valid.

vi) It is found that even with over populations b_o of the ground level up to 100 and down to 0. The levels 1 and 2 are less then 10% non LTE populated at an electron density of 2.10^{20} m^{-3}. This justifies the pLTE assumption in an ICP.

vii) The four level model does not predict accurate values for under populations of the ground level. This, only mathematical, complication could be solved by another approach of solving the set of balance equations.

Section 2.3

The saturation phase.

i) Application of Fujimoto's model [7-10] to an ICP discharge shows over or under populations of excited levels with respect to the Saha equation are possible in both the ionizing and recombining limit. Relative over populations of levels in the ionizing limit are possible up to a factor 10 at $n_e = 10^{20}$ m^{-3} with respect to the Saha population. Relative over populations of levels in the recombining limit are possible up to a factor 10 with respect to the Saha equation.

ii) The results from this model clarify the wide scattering range in measurements of argon excitation temperatures by a two line method.

iii) Especially in the ionizing limit the definition of temperature is very difficult, because it is difficult to determine what levels are in TE. A least square fit to all excited levels would yield erroneous temperatures up to 50%!!

vi) In the recombining limit, temperature can be defined in relation with the population densities of higher lying levels. These are in Saha equilibrium with the ion ground state.

3. The excitation model of the analyte atoms.

3.0. Introduction

In this chapter we shall assume charge transfer to be the non-LTE excitation channel from which overpopulations of the ionic system with respect to the atomic system can be explained.

A simplification has to be made in the analyte system to faciliate the calculations. It is therefore assumed that pLTE exists between analyte excited states and the ground level of the next ionisation stage.

The rate equation for the ionic system of the analyte, accounting for electron excitation-deexcitation, radiative decay and charge transfer, results in an estimate for the over-population of excited ionic levels with respect to the LTE population.

With rough assumptions for the maximum overpopulation of the analyte atomic system the ratio of ionic/atomic level population densities with respect to its LTE value can be obtained.

3.1. The proces of charge transfer.

3.1.0. Introduction

Generally one uses the term charge transfer for a reaction in which the charge of the colliding particle is transferred to the target particle,viz.

$$A^+ + B \longrightarrow A + B^+ + \Delta E$$

where ΔE denotes the energy defect.of the reaction.

It is possible that one or both of the reactionproducts formed are in an excited state.

It is convenient to make a distinction between two main types of charge transfer.

i) Symmetrical charge transfer

$$A^+ + A \longrightarrow A + A^+$$

The energy defect in this reaction is practically zero. The process is well known, and theoretically calculated cross sections match the observed cross sections [25-26] . The cross sections are known to be large, eg. for the reaction $Ar^+ + Ar \longrightarrow Ar + Ar^+$: $\sigma_c \approx 6.10^{-19}$ m^2 for ions with an energy of 0.56 eV [26].

ii) Non resonant or asymmetrical charge transfer

$$A + B^+ \longrightarrow A^+ + B + \Delta E$$

For this reaction the energy defect is generally not equal to zero. Generally the exothermic reaction ($\Delta E > 0$) is preferred over the endothermic reaction ($\Delta E < 0$). In contrast to the symmetrical reaction this reaction is not yet well understood. Substantial disagreements between observed and theoretically predicted cross sections are reported [27, 34].
Generally, observed cross sections exceed the predicted ones by several orders of magnitude.

In the next section some observed cross sections are listed, and some general theory is presented in order to obtain a first approximation for the range of values of charge transfer cross sections.

3.1.1. Non resonant charge transfer

In particular the following reaction is considered as a possible excitation channel for analytes in an ICP and comparable discharges

$$Ar_o^+ + M_o \longrightarrow M_q^+ + Ar_o + \Delta E$$

where M_o groundstate analyte atom
M_q^+ analyte ion in an excited state q
ΔE the energy defect
Ar_o^+ Groundstate argon ion
Ar_o Groundstate argon atom

The energy defect for this reaction can be written as

$$\Delta E = +E_{Ar}^+ - (E_M^+ + E_{M+}^q) \qquad (3.1.0)$$

where E_{Ar}^+ ionisation potential of argon

E_M^+ " " of analyte

E_{M+}^q excitation potential of level q in the analyte ion system.

Generally ΔE ranges from 0-2 eV. The cross section functions are known to increase rapidly at very low impact energy, to rise to a maximum, and then decrease rapidly [34]. The maximum cross section is located at an energy of the colliding particle which is determined by the adiabatic criterion proposed by Massey [33]

$$\frac{1}{\tau_{coll}} = \frac{v}{a} = \frac{(2E/m)^{1/2}}{a} = \frac{\Delta E}{h} \qquad (3.1.1)$$

where τ_{coll} the collision time

a the "adiabatic" parameter, an atomic parameter which describes the "length" over which the exchange takes place. Generally one can state: $a \approx 7\text{Å}$ [34]

E the energy of the colliding particle

m the mass of the colliding particle

v the relative velocity of approach

Note that the form of equation 3.1.1 is equal to that of the uncertainty principle of Heisenberg ($h = E.\tau_{coll}$).
One may split the entire energy region in two regimes.

i) The adiabatic region

$$\tau_{coll} \gg \frac{h}{\Delta E} \qquad (3.1.2)$$

In this region it is not likely for a reaction to occur. At this impact energy's one may approximate the charge transfer cross sections with [34]

$$\sigma = A \exp\left(\frac{-a \Delta E}{4 h v}\right) \qquad (3.1.3)$$

where A is a constant.

ii) The non adiabatic region

$$\tau_{coll} \ll \frac{h}{\Delta E} \qquad (3.1.4)$$

In this regime the charge transfer cross section of the non resonant reaction can be approximated by the cross section of the resonant reaction.
For intermediate velocities ($\tau_{coll} \approx h/\Delta E$) the cross section may be written as [35]

$$\sqrt{\sigma_c} = k_2 - k_1 \ln E \qquad (3.1.5)$$

Where E the energy of the colliding particle and k_1, k_2 constants for a given reaction.

3.1.2. Values of cross sections for non resonant charge transfer

In an ICP with an electron temperature $\hat{T}_e$ = 0,56 eV, the average thermal velocity of an Ar ion with the assumption of a Maxwellian velocity distribution and Te ≈ Ti, is

$$\bar{v}_{Ar} = \left(\frac{8kT_i}{m_{Ar}}\right)^{1/2} = 3.2 * 10^3 \ m/s \qquad (3.1.7)$$

For a charge transfer reaction with a positive energy defect of 1 eV one calculates from the adiabatic criterium (eq. 3.1.1):

$$\hat{v} = 1{,}7.10^5 \text{ m/s}$$

So evidently, practically all colliding particles are in the adiabatic energy region and formula 3.1.3 would give the cross sections. Figure 3.1.1 shows the theoretical and observed cross sections (extracted from various papers). This plot clearly shows the deviations between theoretical and observed cross sections, especially at high energies.
As a first, very rough approximation for the cross sections for small energy defects one can use (dotted line in Figure 3.1.1 for $\hat{T}_e = 2{,}6.10^{-2}$ eV)

$$\sigma_c \approx 2 * 10^{-18} \exp\left[\frac{-0.5\,\Delta E}{\sqrt{\hat{T}_e}}\right] \qquad (3.1.8)$$

Note this is not an exact formula. It is only given to show the temperature dependence and order of magnitude of the adiabatic charge transfer cross section. One must bear in mind that deviations of this formula by two orders of magnitude, dependent on the type of reaction, and on the energy defect are possible. Further, more elaborate, literature research has to be performed on this subject.
For magnesium the charge transfer reaction will preferably take place to the levels $3^2P_{5/2-3/2}$ and/or $4^2S_{1/2}$ of the Mg II

system (see Fig. 3.2.3).
If one defines the mean energy of those levels:

$$\bar{E} = \frac{\sum_i q_i E_i}{\sum_i q_i} \qquad (3.1.9)$$

one finds for ΔE, the energy defect

$$\Delta E = 0{,}7 \text{ eV}$$

A very rough approximation of the cross section can be calculated from eq. (3.1.7) as a function of the electron temperature T_e. For the rate coefficient for charge transfer k_c one can use:

$$k_c \approx \bar{v}_{Ar} \cdot \sigma_c \qquad (3.1.10)$$

The rate coefficient for the reaction $Ar_o^+ + Mg_o \longrightarrow Ar_o + Mg^+ + \Delta E$ is given in Fig. 3.1.2 as a function of the electron temperature.

3.2. The simplified level systems of argon and the analyte

3.2.1. Approximations in the level system, general assumptions

In order to make the calculations on the population of analyte excited states possible we will make some simplifications in the level system of the analyte.

In the following text we will use the term "system z" for the complete set of levels of ionisation stage z (so, for neutral atoms z = 0, for singly charged ions z = 1, etc.). With "subsystem p" we refer to the excited levels of system z = p-1 together with the ground state of system z = p (see Fig. 3.2.1).

For simplification of the level system and the charge transfer model the following approximations will be made. This assumptions will be more general then necessary for the applied model. This will be usefull for future calculations on a more extensive description of the excitation process.

(i) Each subsystem p is in Saha equilibrium.
(ii) The number of particles in subsystem p can be approximated by the number of particles in the groundstate of system p.

(iii) The charge transfer process to a subsystem p is much slower than the process for depopulation from that sub system to the next lower subsystem by radiative decay or the not detailed balanced part of the electron excitation-deexcitat

(iv) The radiative contributions resulting from photo ionisation and absorption of line radiation can be neglected.

assumption (i)

This means that all excited levels of the system z are in Saha equilibrium with the groundstate of the system z + 1.
One may use the Saha equation to calculate the population n_q^z of excited states in the system z if the population n_o^{z+1} of the groundstate in the system z+1 is known viz.:

$$\frac{n_e\, n_o^{z+1}}{n_q^z} = S(T_e, E_q^z) \qquad (3.2.1)$$

where $S(T_e, E_i)$ is the Saha function (see eq. 2.0.1)

$$S(T_e, E_q^z) = \frac{2g_o^{z+1}}{g_q^z}\left(\frac{2\pi m kT_e}{h^2}\right)^{3/2} \exp\left[-\frac{E_o^{z+1} - E_q^z}{kT_e}\right] \qquad (3.2.2)$$

where g_o^{z+1}, E_o^{z+1} the statistical weight and exc. energy of the groundlevel of system z+1

g_q^z the statistical weight and exc. energy of the excited state q in the system z.

The lowering of the ionisation energy can be neglected.

assumption (ii)

The validity of this assumption can be verified by calculating the ratio of the density of the level n_∞^z of system z just below the ionisation limit and the density of atoms in the groundstate level of the system z+1. One finds for this ratio from (3.2.1):

$$\frac{n_o^{z+1}}{n_\infty^z} = \frac{1}{n_e} S(T_e, E_o^{z+1})$$

$$= \frac{1}{n_e} \frac{2g_o^{z+1}}{g_\infty^z}\left(\frac{2\pi m kT_e}{h^2}\right)^{3/2} \qquad (3.2.3)$$

Commonly this quantity is called to as the "Saha jump" (see Fig. 2.0.1). With an electron temperature of $\hat{T}_e$ = 0,56 eV, and $n_e = 2.10^{20}$ m^{-3} one obtains:

$$\frac{n_o^{z+1}}{n_\infty^z} = 1.2 * 10^7 \gg 1 \qquad (3.2.4)$$

Since condition (i) and (ii) are fulfilled we shall express the rate coefficients for excitation-deexcitation from subsystem p to subsystems p $\pm$ 1 in a net excitation-deexcitation rate. Also the transition probabilities for radiative decay to the next lower subsystem can easily be expressed in a net transition probability. The next section will deal with these items). The level densities all will be expressed in groundstate level densities.

assumption (iii)

In terms of rate coefficients for the various processes one writes (neglecting higher subsystems)

$$(n\,k^{ij} - n\,k^{ji})\,n_e + n\,A^{ij} \gg n_{Ar^+}\,n\,k_c \qquad (3.2.5)$$

where k_c the rate coefficient for charge **transfer**

K^{ji} the net rate coefficient for deexcitation of subsystem i to subsystem j

K^{ij} the net rate coefficient for excitation of subsystem j to subsystem i

A^{ij} the net transition probability for radiative decay from subsystem i to subsystem j

n_{Ar^+} density of Argon ions

$n^{(o)}$ density of groundstate analyte atoms

$n^{(i)}$ density of analyte atoms in subsystem i

This condition implies that the charge transfer process is not detailed balanced. Before the atom in subsystem i decays to subsystem j a reverse charge exchange process is very unlikely to occur. Thus the charge transfer mechanism indeed will supplie a non LTE population in subsystem i, and will cause an excess of atoms in this system compared to the LTE situation.

Even if eq. (3.2.5) is not completely fulfilled if e.g. $n_i A^{ij} \approx \frac{1}{10} n \cdot n_{Ar^+} k_c$, then still a net charge transfer rate in the direction of subsystem i of the analyte is present. Roughly speaking $1/10$ of the atoms decays to system j before the reverse process can occur, thus still resulting in a net charge transfer rate of $1/10$ of the original one.

assumption (iv)

This assumption is valid if the discharge is optically thin for both continuum and line radiation.

a) line emission.

The absorption coefficient for line emission, if one assumes a purely Doppler broadened line, can be written as (see Appendix A)

$$k_g(\lambda_0) = \frac{\lambda_0^4}{\Delta\lambda_{FWHM}} \frac{2\sqrt{\ln 2}}{8\pi c} A_{mn} N_m \left[1 - \exp\left(-\frac{hc}{kTe}\right)\right] \quad (3.2.6)$$

For symbols refer to Appendix A.

The optical depth for analyte line emission can be defined as:

$$\tau_{analyte} = k_g(\lambda) \cdot a \quad (3.2.7)$$

where a is the radius of the analyte channel (see section 5.1).

The major contribution in the absorption results from resonance radiation. If one assumes a Doppler width of 0,03 Å, a 50% ionisation degree, $\hat{T}e$ = 0,56 eV and an initial analyte concentration n_t of $10^{19} m^{-3}$ (1000 ppm solution) then one obtains for the resonance lines of Mg I and Mg II (see section 3.2):

$$\tau_{analyte} \gtrsim 1$$

According to [21] the escape factor Λ will be 0.63. Kornblum and de Galan [16] measured a total absorption of 48% for the Mg I resonance transition in a 16 mm ICP at $n_t = 7.10^{18}\ m^{-3}$. This is in fair agreement with this calculation. Thus a correction for absorption is necessary at this high analyte concentrations. This correction is effectuated by substituting for the transition probabilities $A^{ij}\Lambda^{ij}$ instead of A^{ij}.

b) Continuum radiation.

In [21] the escape factor of continuum radiation for a ø 5 mm arc at atmospheric pressure is reported. At an electron temperature $\hat{T}_e$ = 0,56 eV the escape factor is ≈ 0,10 for Argon. As the analyte channel of an ICP is smaller (ø 2,8) and regarding the much smaller concentration of analyte atoms (≈ factor 10^5), the absorption of continuum radiation will be neglected. This implies that photo ionisation can be neglected in the Mg system.

3.2.2. The net rate coefficients for transitions between subsystems of the analyte°

General

Since we assume that the analyte levelsystems are in PLTE we do not need to know all collisional and radiative transition rates.

The coupling between excited levels and the groundstate of the next ionisation stage (called subsystem) is very intense compared to the coupling between subsystems. This implies that the "bottle neck" for excitation-deexcitation between subsystems is found in the transition from first excited level to ground level of a system. This is caused by the huge energy gap between the first excited states and the groundstate.

Due to this "bottle neck" the coupling between subsystems can be described by the excitation-deexcitation rates between the first excited level and the groundlevel of one system. Of course one must pay attention to peculiarities in the level system of the element to be considered.

Subsequently excitation and deexcitation in the subsystems 1 and 2 of Magnesium is treated.

The radiative losses in subsystems 1 and 2 can be described by an average effective transition probability, which also accounts for absorption. Note however that even a 1000 ppm solution does not show an extreme absorption of the resonance lines. Corrections will be very small (< 40%). Regarding the qualitative rature of the present model, this absorption shows no significant influence.

The relevant electron excitation deexcitation rates, ionisation rates and recombination reates are calculated in Appendix D. A graphical presentation of the rate coefficients as a function of temperature is provided there.

Figure 3.2.3a) and b) and tables 3.2.1a) and b) present all relevant rate coefficients for $\hat{T}_e$ = 0,56 eV and $n_e = 2.10^{20}$ m^{-3}. Various values of the rate coefficients are compared in Appendix D. The approach of Drawin [35] will be used here for optically allowed transitions, except for the recombination rate. This will be approximated by a collisional radiative recombination rate α_{CR} calculated by Bates for a pure hydrogen plasma.

The rate coefficients of Vriens [41] will be used for optically disallowed transitions. (For a discussion on this subject see appendix D).

Finally fig. 3.2.4 supplies all the information on the transition rates between subsystems we used.

In the subsequent text the following notation is used:

a) upper index or indices: indicate quantities which must be treated in connection with subsystems (eq. k^{21} collisional deexcitation rate between subsystems 1 and 2).
b) lower index or indices indicate quantities which must be treated in connection with separate levels of systems (eq, C^1_{01} collisional excitation rate between level 0 and 1 of system 1, C^0_{01} the same for system 0.
c) k_c is used for the charge exchange transition rate.

Collisional excitation and deexcitation between subsystems 0 and 1.

(i) Excitation.

For the excitation rate k^{01} between subsystems 0 and 1 one can write:

$$k^{01} = \sum_{q=1}^{n} C_{0q} + S_{0+} \qquad (3.2.8)$$

where C_{oq} electron excitation rate between ground level and excited level q

S_{o+} electron ionisation rate from the groundlevel
Summation over all excited levels 1-M, M an arbitrarily high level.

With a view at figure 3.2.3a) and table 3.2.1a) it seems the main term in eq. (3.2.8) is C_{01} (for designation of the levels see fig. 3.2.2-3).
The rate coefficient C_{01} is much smaller in the approach of Drawin because this transition is optically disallowed. It is doubtfull whether this approach is correct. In this particular case we use the Vriens rate coefficient (see Appendix C). Then $C_{01} \gg C_{02}$ and, in a good approximation one can state

$$k^{01} \approx C^{o}_{01} \tag{3.2.9}$$

(ii) Deexcitation.

For the total deexcitation rate between subsystems 0 and 1 one can write

$$k^{10} = \sum_{q=1}^{M} F_{qo} + \alpha_{+o} \tag{3.2.10}$$

where F_{qo} the deexcitation rate between level q and the groundstate

α_{+o} the recombination rate to the groundstate.

Since $\alpha_{+o} < \alpha_{CR}$, where α_{CR} the collisional radiative recombination rate to all levels and $\alpha_{CR} < F_{10}$, in a good approximation (see fig. 3.2.3a)

$$K^{10} = F_{10} \tag{3.2.11}$$

Collisional excitation and deexcitation between subsystems 1 and 2.

The same considerations as applying to the transitions between subsystems 0 and 1 are valid.
One finds easily (see fig. 3.2.3b))

i) Excitation: $K^{12} = C^1_{01}$ (3.2.12)

ii) Deexcitation: $K^{21} = F^1_{10}$ (3.2.13)

Note that in the Mg II system the rate coefficients C^1_{12} and F^1_{21} are smaller than C^1_{10} and F^1_{01}. Yet the net rate coefficient is determined by C^1_{01} and F^1_{10} because of the strong coupling between levels 2 and 3. An extra excitation channel from level 1 to 2 is provided via level 3. The same reasoning is valid for the reverse processes.

Transition probabilities A^{10} and A^{20}.

For transitions resulting from various levels of subsystems 1 and 2 one may use an average transition probability A as defined in [21].

$$A = \sum_i \frac{\sum_j g_j A_{ji}}{\sum_j g_j} \qquad (3.2.14)$$

where $\sum_j$ denotes a sum over the upper levels of a transition
$\sum_i$ denotes a sum over the lower levels of a transition
g_j the statistical weight of the upper level of the transition
A_{ji} the transition probability from level j to level i.

Since the main contribution result from the resonance transition from the first excited level (in the Mg I system: the first excited level in the singlet system), the average transition probabilities are equal to these main contributions. Thus:

$$A^{10} = A^0_{20} = 4.95 * 10^8 \ 1/s$$
$$A^{21} = A^0_{10} = 2.67 * 10^8 \ 1/s \qquad (3.2.15)$$

Where A^{i}_{qp} the transition probability for radiative decay $q \rightarrow p$ in system i.

A^{ij} the transition probability for radiative decay from subsystem i to subsystem j.

These probabilities have to be corrected for line absorption. Introducing the effective transition probability $A_{eff} = A.\Lambda$, where Λ is the escape factor as introduced in 3.2.1 (iv) one obtains:

$$A^{10}_{eff} = 3.1 * 10^{8}\ 1/s \qquad (3.2.16)$$

$$A^{21}_{eff} = 1.7 * 10^{8}\ 1/s \qquad (3.2.17)$$

3.3. Rate equations for the subsystems from the analyte

Once the main contributions to radiative and collisional population and depopulation processes are determined it is possible to set up the rate equations for subsystems 0 to 2. One can obtain a set of two equations. Known parameters are of course the electron density n_e, the total concentration of analyte atoms (summed over all levels) and, the electron temperature T_e.

The only thing we want to know is the ratio of the population densities in the subsystems 1 and 2. Then only one equation together with some general assumptions on the behaviour of the population density in subsystem 1 is needed to provide a relation between those two population densities.

The rate equation for subsystem 2 is:

$$\frac{dn^{(2)}}{dt} = k_c n_{Ar^+} n^{(0)} - k_c^{REV} n^{(2)} n_{Ar_0} - k^{21} n_e n^{(2)} + k^{12} n_e n^{(1)} - A^{21}_{eff} n^{(2)} \qquad (3.3.1)$$

where $n_{Ar^+} = n_e$ Argon ion density

$n^{(i)}$ Subsystem (i) density

n_{Ar_0} Argon neutral groundlevel density

K^{ij}	Collisional transition rate $i \rightarrow j$
A^{ij}_{eff}	Effective transition probability $i \rightarrow j$
k_c, k_c^{rev}	Rate coefficient for the charge transfer process and for the reverse charge transfer process respectively

We shall neglect the reverse charge exchange process with respect to the charge exchange process, one demands (see eq. (3.3.2)):

$$k_c n^{(0)} n_e \ll n^{(2)} A^{21}_{eff} \qquad (3.3.2)$$

If we assume $\frac{n^{(0)}}{n^{(2)}} \approx \frac{n^{(0)}_{SaHa}}{n^{(2)}_{SaHa}} \approx R^{02} = 10^3$ (see Fig. 3.4.1)

$n_e \approx 2.10^{20}$ and A^{21}_{eff} and k_c as derived in preceeding sections: $A^{21}_{eff} \approx 1.7 * 10^8$ 1/s and $k_c \approx 4 * 10^{-15}$ m^3/s one finds: $k_c n^{(0)} n_e = 5 n^{(2)} A^{21}_{eff}$. According to the discussion in section 3.2.1 then still, roughly speaking one fifth of the original reactions remains unbalanced. One can ofcourse correct for this partial balancing by substituting $k_c = \alpha k_c$ with $\alpha = 1/5$. This is not carried through in this calculations because the uncertainty in charge transfer exceeds this factor α.

If one introduces reduced densities

$$b^{(i)} = \frac{n^{(i)}}{n^{(i)}_s} \qquad (3.3.3)$$

where $n^{(i)}_s$, the Saha population of subsystem i, is determined by:

$$\frac{n^{(i)}_s}{n^{(i-1)}_s} = \frac{1}{n_e} S(T_e, 0) \qquad (3.3.4)$$

$$n^{(1)} + n^{(2)} + n^{(3)} = n^{(1)}_s + n^{(2)}_s + n^{(3)}_s = n_t \qquad (3.3.5)$$

where n_t is the total density of analyte atoms.

We will apply the principle of detailed balancing
Then eq. (3.3.1) reduces to (we choose $b^{(0)} = 1$)

$$\frac{1}{n_s^{(2)}} \frac{dn^{(2)}}{dt} = (-k^{21} n_e - A_{eff}^{21}) b^{(2)} + k^{12} n_e b^{(1)} \frac{n_s^{(1)}}{n_s^{(2)}} + k_c n_e \frac{n_s^{(0)}}{n_s^{(1)}} \qquad (3.3.6)$$

The right hand side of this equation can be rewritten as follows (see also section 2.2.3)

$$\frac{1}{n^{(2)}_{SHHA}} \frac{dn^{(2)}}{dt} = \frac{1}{n^{(2)}_{SHHA}} \left(\frac{\delta n^{(2)}}{\delta t} + div(\underline{v} \cdot n^{(2)}) + div(\underline{w}^{(2)} n^{(2)}) \right)$$

$$= \frac{1}{n^{(2)}_{SHHA}} \left(\frac{\delta n^{(2)}}{\delta t} + \underline{v} \cdot grad\, n^{(2)} + n^{(2)} div\, \underline{v} + div(n^{(2)} \cdot \underline{w}^{(2)}) \right) \qquad (3.3.7)$$

where $\underline{v}$ the lineair velocity of the carrier gas
$\underline{w}^{(2)}$ the diffusion velocity of analytes in subsystem 2

If we make the following assumptions:

i) Diffusion can be neglected.

$$\frac{1}{n^{(2)}_{SHHA}} div\, \underline{w}^{(2)} n^{(2)} \ll k^{21} n_e + A^{21}_{eff}. \qquad (3.3.8)$$

ii) Electron density and temperature are uniform.

iii) $\underline{v} = (0,0,v_z)$. The carrier gas stream velocity only has a velocity in the axial (z) direction.

iv) Stationarity applies ($\frac{\delta}{\delta t} = 0$).

Then we can rewrite eq. 3.3.7 to

$$\frac{1}{n^{(2)}_{SHHA}} \frac{dn^{(2)}}{dt} = \frac{1}{n^{(2)}_{SHHA}} \cdot \underline{v} \cdot grad\, n^{(2)} \approx v_z \frac{\delta b^{(2)}}{\delta z} \qquad (3.3.9)$$

And the final rate equation one obtains is:

$$v_z \frac{\delta b^{(2)}}{\delta z} = (-k^{21} n_e - A^{21}_{eff}) b^{(2)} + k^{12} n_e b^{(1)} \frac{n^{(1)}_{SHHA}}{n^{(2)}_{SHHA}} + k_c n_e \frac{n^{(0)}_{SHHA}}{n^{(2)}_{SHHA}}. \qquad (3.3.10)$$

When this equation is solved under the assumption $\frac{\delta b^{(1)}}{\delta z} \ll \frac{\delta b^{(2)}}{\delta z}$ the overpopulation of subsystem 2 can be expressed in the overpopulation of subsystem 1 ($b^{(1)}$) with z as a parameter. The assumption $\frac{\delta b^{(1)}}{\delta z} \ll \frac{\delta b^{(2)}}{\delta z}$ can be considered to be valid because analyte ion lines ("hard" lines [13]) peak very sharply as a function of observation height and analyte atom lines ("soft" lines [13]) only vary relatively slowly with increasing observation height [58]. Moreover, the coefficient of $b^{(1)}$ is much smaller then the coefficient of $b^{(2)}$ (factor 10 at KTe = 0,56 eV and $n_e = 2.10^{20}$ $1/m^3$). So one can conclude that the variations in $b^{(1)}$ do not influence the value of $b^{(2)}$ in a serious manner.

3.4. The time independent solution of the rate equation

Solution of the equation

If the coefficients in eq. (3.3.10) are constant. (This is of course the case as n_e, T_e are constant). Then, after a certain time, or at a certain height the time independent solution of eq. 3.3.10 is obtained. One can find this solution by setting $\delta/\delta z$ equal to zero. One finds for the overpopulation of the second subsystem with respect to the Sahapopulation:

$$b^{(2)} = \frac{k^{12} n_e R^{12} b^{(1)} + k_c n_e R^{02}}{k^{21} n_e + A^{21}_{eff}} \qquad (3.4.1)$$

where $R^{ij} = \frac{n^{(i)}_{SAHA}}{n^{(j)}_{SAHA}}$

The quantities R^{ij} and the various terms in this equation are presented in figures 3.4.1 and 3.4.2.

Interpretation of the results

The quantity which is frequently measured is the relative overpopulation of subsystem 2 with respect to subsystem 1 (α). Thus $\alpha = b^{(2)}/b^{(1)}$. Unfortunately our model does not predict

a value of $b^{(1)}$. However one can find the maximum possible value of this parameter

$$b^{(1)}_{MAX} = \frac{n^{(1)}_{max}}{n^{(1)}_{SAHA}} = \frac{n_t}{n^{(1)}_{SAHA}} = \frac{1}{R^{10}} + 1 \qquad (3.4.2)$$

This quantity is shown in figure 3.4.2. If $b^{(1)}_{max}$ reaches the value 1 all analyte atoms are ionised.
For the further interpretation of figure 3.4.2 we distinct between 3 regions.

i) $\hat{T}_e < 0{,}55$ eV, low temperature region.

To a good approximation eq. 3.4.1 can be rewritten to read:

$$b^{(2)} = \frac{k_c n_e R^{02}}{A^{21}_{eff}} \qquad (3.4.3)$$

In this case the major population process is charge transfer. The major depopulation-process of subsystem 2 is radiative decay. Note that even with very high $b^{(1)}_{max}$ values the term for collisional excitation remains well below the term for charge transfer. In this region extremely high values for $b^{(2)}/b^{(1)}$ are obtained ($b^{(1)}/b^{(2)} \approx 3.10^5$). It is possible that our model fails in this low temperature regions. Probably assumption (i), that each subsystem is in saha equilibrium, is violated.

ii) $T_e > 0{,}55$ eV, $T_e < 0{,}65$, equilibrium temperature region.

Both charge transferprocesses and electron excitation populate subsystem 2. The major depopulation process remains radiative decay. So eq. 3.4.1 has to be applied. In this region the maximum $b^{(1)}$ value equals 1. However, for higher temperatures ($\hat{T}_e > 0{,}6$ eV) an underpopulation $b^{(1)} < 1$ may occur. This may result in the **dashed** curve (not calculated!) For further treatment we will assume that subsystem 0 is in LTE with subsystem 1, so $b^{(1)} = 1$. The full treatment of this problem would require another balance equation for subsystem 1. For this temperature range $\alpha = b^{(2)}/b^{(1)}$ takes

values from 100 to $\frac{1}{2}$. This agrees with measurements [13, 14, 19]. One can also conclude from fig. 3.4.2 that $b^{(2)}$ decreases very rapidly with increasing temperature. This could explain the scattering of results of various authors.

iii) $KT_e > 0{,}65$ eV. High temperature region.

The major population process has become collisional excitation, the major depopulation process remains radiative decay.

At this temperature subsystem 2 is underpopulated with respect to the sahapopulation, and with respect to the population of subsystem 1 if subsystems 1 and 0 in LTE.

This situation could prevail in, or just above the load coil. Temperatures of such magnitude are found there

3.5. The time dependent solution

Before the steady state is reached the equilibrium between charge transfer, electron excitation processes and radiative decay processes has to be established. This phenomena can be described by the time - or place - dependent solution of eq. (3.3.10).

One finds with the assumption $b^{(1)}=1$ for the overpopulation $b^{(2)}$:

$$b^{(2)} = \left(k^{12} n_e R^{12} + k_c n_e R^{02}\right)\left(1 - \exp\left[\frac{-z\left(k^{21} n_e + A^{21}_{eff}\right)}{v_z}\right]\right) \tag{3.5.1}$$

Since $A^{21}_{eff} \gg k^{21} n_e$ and $A^{21}_{eff} \approx 1{,}7.10^8$ 1/s equilibrium is settled very fast. If we substitute V_z = 7m/s, one calculates that after a length $z_o = 10^{-7}$ m, this equilibrium is settled within 10% of its final values.

This result has very drastic consequences for the description of the excitation of the analyte. An implication is that, as

equilibrium is settled so fast, the over or under population of excited levels must be explained only from the local temperature and electron density in the plasma.

A first, only approximate solution can be obtained by assuming that the overpopulation changes only slightly over the length z_o. At every height the time independent solution describes the population of excited states.

A better approach is off course to integrate eq. (3.3.10) numerically with $\delta b^{(1)}/\delta z \neq 0$. This of course would require another time resolved equation, which results from the balance equation for sublevel 1.

3.6. Conclusions

This section lists the most important conclusions which can be drawn from the previous sections.

i) Charge transfer reaction rates can be large compared to collisional transition rates (see fig. 3.4.2 and table 3.2.1b).

ii) In the temperature range $0{,}55 < \hat{T}_e < 0{,}65$ overpopulations of subsystem 2 with respect to the overpopulations of subsystem 1 of 0,5 - 100 can be explained. This is in accordance with literature.

iii) A complete, accurate, calculation of such overpopulation factors would require detailed knowledge on the population of subsystem 1. This can be obtained by solving another rate equation for this subsystem. However calculations on this subject are in progress, it seems at least some approximations in e.g. rate coefficients, or the neglecting of some processes are not valid.
A solution is obtained which could describe overpopulations in the steady state $\alpha = b^{(2)}/b^{(1)}$ up to a factor 2. This does not agree with experimental results.

iv) Presumably the model is not valid in the very low temperature region ($\hat{T}_e < 0{,}5$ eV). Abnormal high overpopulations are obtained in this region.

v) The latter could be due to the fact, that the LTE assumption in each subsystem is violated.

vi) Equilibrium between the most important processes charge transfer-radiative decay is settled very fast. The determining factor is the transition probability for radiative decay. Equilibrium is settled within lengths of the order 10^{-7} m.

vii) The last conclusion implies that any over population of subsystem 2 can be explained from the local temperature and electron density.

viii) For the high temperature region ($\hat{T}_e > 0{,}65$ eV) which one would expect in or just above the load coil underpopulations $b^{(2)}$ of the order 10^{-2} are expected.

ix) As Lovett [15] did in his calculations, we neglected diffusion. The validity of this assumption is not proven in this paper and may be very doubtfull. Diffusion however, requires very accurate knowledge of radial density gradients of analyte species and a rather elaborate treatment. There is ample evidence of the importance of diffusion (see e.g. section 6.2) of both analyte neutrals and ions.

4. Instrumental set up.

4.1. Plasma generator.[+]

The plasma generator is a commercial unit supplied by Philips. Calibration of flow meters and power are assumed to be accurate enough and reproducable. For present work however, only reproducability is essential as will become evident. The torch is supplied with the generator and is described in reference [40]. Important data are listed in table 4.1.1.

The ICP system, optical system and detection system (see section 4.2 and 4.3) are optimized with the use of the Mn II 2576.10 Å line. Maximum signal to background ratio is used as the criterion. The conditions found by this single element optimisation using a hardline [13, 58] are close to the optimum compromise conditions for simultaneous multielement analyses [40]. This line is measured in the second order with the use of an UG 5 filter. Optimum conditions are listed in table 4.1.1. All measurements in this paper are performed with this particular parameter setting of gas flows and power.

4.2. Optical system.

4.2.1. Monochromator.

The monochromator is a Jarrell Ash Ebert monochromator with 500 mm focal length (type 82000) and an aperture of f/9,6. The slit assembly was revised, to permit different settings of entrance and exit slit widths.

A grating blazed at 7000 Å and with 1160 grooves/mm is used in the measurements.

The full width at half maximum (FWHM) of the apparatus profile of the monochromator is measured for the Hg line 3654.8 Å in the second order, emitted from a low pressure mercury discharge lamp which was mounted in the axis of the loadcoil of the generator. The FWHM of this line is assumed to be much smaller than the width of the apparatus profile. Results are showed in Fig. 4.2.1. It is found that for d_u and $d_i < 10$ um a gaussian profile fitted reasonably to the experimental data. For d_u or $d_i > 10$ um trapezium ($d_i \neq d_u$) or triangular ($d_i = d_u$) shaped profiles fitted accurately. (This is exactly the convolution of the two rectangular slit functions). Top width (a) and slope (b) of the trapezium or triangular shaped profiles are given in Fig. 4.2.1.
Note that this width changes with the wavelength setting on the monochromator. Therefore we shall always measure the FWHM of the actual line to obtain the correct FWHM (eq. 5.1.8) for each transition to be measured.

4.2.1. Entrance optics.

Since we want to obtain detailed spatial information of the object (the discharge) one chooses for imaging the object in the plane of the entrance slit of the monochromator [5, 63].

The optical system is sketched in Fig. 4.2.2. Diafragma 1 is an aperture stop limiting the aperture of the system to f/10. Diafragma 2 is a field diafragm stopping all the non-relevant parts of the discharge image. The "90° rotating mirror system" rotates the image of the discharge so,that its vertical axis is eventually projected horizontally on the entrance slit. One of

the mirrors and the first lens in the optical system is adjustable in height with a steppermotor. The optical axis of the optical system can thus be scanned over full height of the discharge ($\approx$ 60 mm). An intermediate image of the discharge is formed at diafragm 2 and this image is focussed on the entrance slit. The demagnification of the optical system is measured to be 0,34 $\pm$ 0,02. The dimensions of the entrance slit (d_i x h_i) determine the area of the discharge observed by the monochromator.

In these measurements the entrance slit width was fixed at 20 μm and the entrance slit height at 0,640 $\pm$ 0,005 mm. Accordingly a discharge zone 60 μm in height and 1,9 $\pm$ 0,1 mm in width is observed. The latter value was chosen since it is close to the inner diameter of the carrier gas tube. The reproducability of the slit adjustments is better then 3% (with the measured intensity as a criterion). The height of the optical axis is absolute adjustable within 0,02 mm with the aid of a computer controlled stepper motor.

To eliminate the emission of the discharge in the second order and reduce stray light, filters have been used for the following wavelength areas:

$4000 < \lambda < 6000$	Blue green filter BG 38 Spindler und Hoyer, and common glas (not optically qualified).
$6000 < \lambda < 8400$	Red filter 3G1 Spindler und Hoyer, and common glas (not optically qualified).
$2000 < \lambda < 3500$	no filters have been used. Transitions with this wavelengths were measured in the second order.

4.2.3. Absolute intensity calibration.

We use a tungsten ribbon lamp [46] as a calibration standard. Standard intensities are obtained from de Vos [46]. Emission temperature is derived from the calibration table. Since we use the strip in a horizontal position due to a lack of space in the plasma chamber of the generator and the strip is vertically calibrated, a correction on the vertical emission temperature T_v is determined. Temperature appeares to be a factor 0,9952 $\pm$ 0,0004 lower in horizontal position at T_v = 1675 K. Current is measured with an accuracy of 0,1% by measuring the voltage over a "fresh" calibrated resistance.

Another not absolutely calibrated tungsten lamp is mounted in the plasma chamber at a distance of approximately 12 cm behind the coil axis on the optical axis. This "diffuse" light source is used as a secondary standard for quick everyday calibrations at other slit widths. After a calibration with this secondary standard the intensity of the absolutely calibrated tungsten ribbon lamp is measured with the new calibration data. In the range 4000 Å $< \lambda <$ 8400 Å this secondary calibration reproduces the correct intensities within 10%, even with other slit widths of the monochromator.
The entire calibration procedure is carried out with both filter sets used (see section 4.2.2.).

Since systematic errors in current measurement ("fresh" calibrated!) and calibration errors of the first tungsten ribbon lamp are expected to be small we take this 10% as an overall accuracy of the calibration data.

4.2.4. Detection system.

A lens (Fig. 4.2.1) is attached to the exit slit of the monochromator in the photo multiplier housing. This lens is used to ensure a more homogeneous illumination of the photocathode of the photomultiplier. This proves to be very usefull, since skewed monochromator profiles (see section 4.2.1) became

symmetrical after this measure.

The photo multiplier used is an EMI 9558QB operated at 1000 V anode voltage and a load resistance of 1 MΩ .

Phase sensitivity detection is used. The image at diafragma 2 is chopped with a frequency of 256 Hz. The Lock in amplifier is a Princeton Applied research HRB. The time constant is set to 100 ms for intensity measurements with the aid of the micro-computer so as to sample statistically correct data.

4.3. Measurement and read out.

An Apple II computer is used to control and measure the following items

i) height adjustment of the observation zone
ii) wavelength setting of the monochromator
iii) intensity measurements.

This paper does not describe the complete software which is developed. A users manual for the different basic PASCAL procedures is supplied in appendix E.

These standard procedures are inserted in the system library with the names Unit CONTROL and Unit MISCIO. Adjustment or measurement of one of the above parameters requires the linking of both units into the host program.

5. Measurements.

5.1. The determination of the levelpopulation of an upper level of a radiative transition in an ICP with a measurement of the lateral intensity of the emitted radiation.

The place dependent population $N_m(\underline{r})$ of an excited level m of the analyte or argon system dictates the emissivity of the plasma for transitions with m as upper level, together with the radiative transition probability of the transition in question. The relation between emissivity, transition probability and level population is [1] :

$$\varepsilon(\omega, \underline{r}) = \frac{\hbar\omega}{4\pi} L(\omega) A_{mn} N_m(\underline{r}) \qquad (5.1.1)$$

or $$\varepsilon(\lambda, \underline{r}) = \frac{hc}{4\pi\lambda} L(\lambda) A_{mn} N_m(\underline{r})$$

where $L(\omega)$, $L(\lambda)$ the normalized ($\int L d\lambda = \int L d\omega = 1$) emission profile of the line transition per unit of angular frequency and per unit of wavelength interval respectively.

$N_m(\underline{r})$ the density of the upper level of the transition at position $\underline{r}$.

A_{mn} the transition probability for radiative decay from excited state m to excited state n.

$\varepsilon(\omega, \underline{r})$, $(\lambda, \underline{r})$ the emissivity of the plasma at position $\underline{r}$, and angular frequency ω or wavelength λ respectively.

This relation can be integrated over the entire line profile in order to obtain the total emission from the upper level m:

$$\int_{\lambda_0-\delta\lambda}^{\lambda_0+\delta\lambda} \varepsilon(\lambda, \underline{r})\, d\lambda = \varepsilon_{\lambda_0}(\underline{r}) = \frac{hc}{4\pi\lambda_0} A_{mn} N_m(\underline{r}) \qquad (5.1.2)$$

where λ_0 the wavelength of the center of the line.

$\delta\lambda$ determines a sufficiently large wavelength interval.

$\varepsilon_{\lambda_0}(\underline{r})$ The total emissivity of the plasma for line radiation with central wavelength λ_0.

The quantity $\varepsilon_{\lambda_0}(\underline{r})$ is not directly measurable because the

discharge has finite dimensions. The quantity which can be measured more or less directly is the lateral intensity $I(\lambda,\underline{b})$ (see fig. 5.1.1), that is the intensity of the radiation at wavelength λ at position $\underline{b}$, integrated over a line of sight, per unit wavelength, solid angle and area of radiating surface.

If the plasma behaves as an optically thin cylindrical discharge (see appendix A), the relation between the emissivity $\varepsilon(\lambda,\underline{r})$ and intensity $I(\lambda,\underline{b})$ becomes:

$$I(\lambda,\underline{b}) = 2\int_{y}^{R_p} \frac{\varepsilon(\lambda,r)\, r\, dr}{(r^2-y^2)^{1/2}} = 2\int_{0}^{(R_p^2-y^2)^{1/2}} \varepsilon(\lambda,r)\, dx \qquad (5.1.3)$$

for meaning of symbols see Fig. 5.1.1.
The integration must be performed over a "line of sight" (the optical axis through the discharge).

The intensity $I(\lambda,\underline{b})$ is measured with a monochromator with a normalized apparatus profile $H(\lambda)$. Convolution of (5.1.3) with this monochromator profile yields:

$$\begin{aligned} P(\lambda,\underline{b}) &= \int_{-\infty}^{\infty} I(\lambda',\underline{b})\, H(\lambda'-\lambda)\, d\lambda' \\ &= 2\int_{-\infty}^{\infty} d\lambda' \int_{0}^{(R_p^2-y^2)^{1/2}} \varepsilon_{\lambda_0}(\underline{r}).\, L(\lambda').\, H(\lambda'-\lambda)\, dx \\ &= 2\int_{-\infty}^{\infty} d\lambda' L(\lambda')\, H(\lambda'-\lambda) \int_{0}^{(R_p^2-y^2)^{1/2}} \varepsilon_{\lambda_0}(\underline{r}),\, dx \end{aligned} \qquad (5.1.4)$$

where $P(\lambda,\underline{b})$ is the response of the monochromator at a wavelength setting λ, at the lateral coordinate $\underline{b}$.

Now we shall assume that the monochromator profile is much wider than the line profile, so in a good approximation

$$L(\lambda) = \delta(\lambda-\lambda_0) \qquad (5.1.5)$$

Substituting (5.1.5) in (5.1.4) yields:

$$P(\lambda,\underline{b}) = H(\lambda_0-\lambda).\, 2.\int_{0}^{(R_p^2-y^2)^{1/2}} \varepsilon_{\lambda_0}(\underline{r})\, dx \qquad (5.1.6)$$

If we measure the peak intensity of the measured convoluted profile one finds ($\lambda = \lambda_0$)

$$P(\lambda_0, \underline{b}) = I(\underline{b}) = H(0) \cdot 2 \cdot \int_0^{(R_p^2 - y^2)^{1/2}} \varepsilon_{\lambda_0}(\underline{z})\, dx \qquad (5.1.7)$$

where H(o) is the "peak height" of the (normalized!) monochromator profile.

(For a rectangular or trapezium profile one finds $H(o) = 1/\Delta\lambda_{FWHM}$).

$I(\underline{b})$ the measured intensity at the center of the line.

If we furthermore assume the plasma to behave like a more or less homogeneous emitting cylindrical body with r_{eff} as radius, and we observe the discharge through the axis of the cylinder, we obtain for the average emissivity $\bar{\varepsilon}_{\lambda_0}(z)$

$$I(\lambda_0, z) = 2\, H(0)\, r_{eff}\, \bar{\varepsilon}_{\lambda_0}(z) \qquad (5.1.8)$$

Substituting equation (5.1.2) we finally obtain

$$I(\lambda_0, z) = 2\, H(0)\, r_{eff} \frac{hc}{4\pi\lambda_0} A_{mn}\, \bar{N}_m(z) \qquad (5.1.9)$$

The relation between measured intensity at the center of the line ($I(\lambda_0, z)$) and the density (averaged over the eff. radius) of the upper state of the transition is given by this relation.

Note, however that with eq. (5.1.7) as a starting point, a better method will be to perform an Abel inversion [1] to obtain the full radial emission profile $\varepsilon_{\lambda_0}(\underline{r})$. This is a very elaborate procedure because detailed knowledge of the lateral intensity distribution is required. Future research is envisaged to perform detailed measurements of the lateral intensity with the aid of a photodiode array mounted in the image plane of the exit slit of the monochromator (see section 6.3 and ref. [38, 43-45, 14].

Determination of the effective emission radius.

As argon emission presumably results from the hot annulus of the discharge, and analyte emission from the relatively cold channel, the approach to determine the effective radius differs

for analyte and argon. Therefore both effective radii will be consecutively considered

i) Argon emission.

If we assume that the plasma behaves like a homogeneous cylindrical discharge with a radius that varies with height we can obtain the effective emission radius as a function of the height above the load coil by measuring the diameter of the luminous part of the discharge. This can easily be performed by photographing the discharge.

Fig. 5.1.3 gives the resulting effective radius as a function of the height above the load-coil. Note that the relative error increases rapidly with increasing height.
Especially at heights of 25 mm the measurement of the effective radius is hampered by an additional systematic uncertainty. At this point the cold outer gasflow mixes with the hot central gases of the discharge. This results in a weak radiating "plume". The effect of this "plume" on the measurements cannot be determined without a full Abel inversion of the lateral intensity.

ii) Analyte emission.

Various authors [14, 16, 45] report radial emission profiles of analytes introduced in an inductively coupled plasma.

Kornblum and de Galan [16] report for calcium a practically constant channel diameter of 2.5 mm with a diameter of the orifice of the carrier tube of 1.3 mm in the region between 7,5 and 30 mm above the loadcoil.

Blades and Horlick [45] report complete emission maps of Magnesium in an ICP using a 1,5 mm tip diameter. From their work it can be concluded that for heights $>$ 10 mm the channel diameter equals 2 mm. For heights $<$ 10 mm off axis maxima in the emission profiles occur. The width of these off axis maxima together equals 2 mm. This phenomenon occurs for both ionic and atomic Mg spectral lines.

Recently Furuta and Horlick [14] measured radial emission profiles using the same 1.5 mm tip diameter. They obtained similar results.

From the data in these three literature sources we can conclude the channel diameter to be approximately 1.5 times the diameter of the orifice of the carrier tube. As the torch we used has a carrier tube diameter of 1.8 mm. The effective radius for the analyte equals 2.7 mm. The uncertainty in this quantity is approximately 25% accounting for deviations in the axial direction, and accidental deviations in gasflows, torch etc.

Absorption

i) Argon transitions.

The optical depth of the 4p-4s transitions (see table A1) approaches unity and thus a correction for absorption on the measured intensity is necessary. Two different approaches can be used (see appendix A). However one of these approaches is a very rough approximation in the center of the line and the other approach strictly speaking is not valid, both methods yield the same result. Because of the simple treatment in [5] we used this approach to correct the line intensities. With the values of n_e, T_e as used in appendix A ($n_e = 5.10^{20}$ 1/m^3, $\hat{T}_e$ = 0,56 eV) one calculates a correction factor $1/\Lambda = 1,4$.

Unfortunately this factor is rather uncertain because it contains uncertain properties as the population density of the 4s level and the effective radius of the discharge. Fortunately we can safely assume that the 4s level is under populated with respect to the saha population (see section 6.1.2). This under population could be up to as much as a factor 10. So we assume for the correction factor:

$$1/\Lambda = \frac{1 + 1,4}{2} \approx 1.2$$

If one finds huge under populations ($>$100) of the 4s level no correction is necessary.
Note that a better, but much more elaborate approach is possible by recalculating the optical depth with estimated 4s densities, and electron densities and temperatures calculated from measurements. At every height a different correction is obtained in this way.

5.2. The determination of the electron density of a lateral intensity profile of the H_β line.

Determination of the electron density from the starkwidth.

According to Griem [1] the stark broadening of the H_β line can be expressed in the electron density n_e with the aid of the semi empirical relation

$$n_e = C(n_e, T_e)\, \Delta\lambda_{FWHM}^{3/2}$$

where $C(n_e, T_e)$ is a coefficient given by Griem [1].

At T = 7000 K and $n_e \simeq 10^{21}$ m^{-3} this coefficient is approximately:

$$C = 3.82 * 10^{20}\ m^{-3}\ \text{Å}^{-\frac{3}{2}}$$

With the first estimate obtained with this value an adapted value of C can be determined [1] and subsequently a new value of n_e can be calculated. After two iterations usually variations in n_e can be neglected and the final value is reached. In our case this final value differs less than 10% from the first value.

Determination of the stark width of the H_β line from a measured intensity profile.

With the monochromator we used (see section 4.2.1) at slit widths of 6 μm a halfwidth of the apparatus profile of about 0,75 Å is obtained. This apparatus profile can be approximated by a Gaussian profile.
The doppler width of the H_β line at T = 7500 K amounts up to 0,3 Å.

The total gauss width of the measured profile equals the quadratic sum of those two, viz. $\Delta\lambda_g$ = 0,8 Å.
Since the Lorentz broadened part of the line will be of the order 1-3 Å strictly speaking a deconvolution is necessary. In this paper a simple "deconvolution" is obtained by comparing the normalized profile with a set of standard Voigt profiles obtained from Ref. [47]. Visually the measured profile is then fitted to one of the standard Voigt profiles, thereby assigning special "weight"

to the Lorentz determined wings of the line.
The uncertainty in such a determination is rather small if sufficient standard Voigt profiles are available. The profiles that do not fit determine the boundaries of the uncertainty area in the starkwidth to be determined.
A better approach is of course to perform a least square approximation (also with an extra weight on the Lorentz wings).

The difference between lateral (measured) and radial line profiles.

Safely it can be assumed that the electron density which is obtained from the above method equals or is close to the electron density in the channel of the discharge. Arguments in favour of this assumption are:

i) The major part of H_β emission is present if aerosol is injected into the discharge. Thus the analyte channel provides virtually all H_β emission.

ii) The sum of several Voigt profiles again is a Voigt profile. Since we assigned special weight to the Lorentz wings in the fitting procedure, the widest profiles will be weighted more heavily then the narrower profiles.
Thus the determined electron density will be closer to the maximum electron density in a section of the plasma than to the average value. Since the electron density appears to be close to the maximum value in the analyte channel [12, 16, 18, 59] this value is determined from lateral H_β profiles.

5.3. Measurements on the argon system.

We want to establish whether it is permitted to assume PLTE in the ICP and, if not, what deviations do occur. For this, we predominantly want to determine whether the plasma is ionizing or recombining and what maximum limits for certain overpopulations can be expected.

Our main aim is to characterize the discharge and we do not expect to obtain an accurate fit to the models described in chapter 2. As is argued in section 2.1 the main parameter for characterisation is the electron density. To determine this density the stark width of the H_β line is measured as a function of the height above the load coil. One observation between the two turns of the load coil can also be carried out. The electron density is determined from the stark width as described in section 5.2.
For further characterisation four absolute level densities are determined from absolute line intensity measurements as described in section 5.1. These absolute line intensity measurements are also carried out with an accurate height resolution.
The upper levels of the transitions to be measured are chosen in such a way that a reasonable spreading in energy is obtained.
The criteria for line choice are:

i) no neighbouring interferent lines.
ii) high signal to noise ratio [48] .
iii) accurate data on transition probabilities.
(data taken from Wiese [49]).
iv) A small line width (also in connection with i) compared to the FWHM of the apparatus profile.

Items i) ii) and iv) are tested.
The FWHM of the monochromator is set at ≈ 2 Å with a trapezium shaped profile (see section 4.2.1) (slits: 20 μm entrance, 80 μm exit). If no detectable addition of the line profile to the apparatus profile is present (iv) can be assumed to be fulfilled.
A background correction is carried out if necessary. The background is assumed to be equal to the mean value of the background at the high and low wavelength side of the line. If possible, background is measured at 5 Å from the center of the line.

Table 5.3.1 lists various relevant properties of the four transitions used.

Possibly errors are made since we do not carry out an Abel inversion. Since it is argued that the determined electron density is the density in the channel and the absolute level densities will be the hot annulus densities agreement between those values may be dissatisfactory. In this preliminary investigation this will cause no serious problems.

5.4. Measurements in the analyte system.

A first aim of these measurements is to determine overpopulations of the analyte ion or neutral system with respect to the calculated Saha populations. Furthermore we want to check the validity of PLTE for the ion and neutral atom system.

Both of these aims will serve to check the excitation model of the analyte by charge transfer as described in chapter 3. Results will be expected to be qualitative rather than quantitative in this stage of the investigation.

Of course many measurements on many different analytes have to be performed to establish the general validity of the model. In this investigation we chose Mg as a first analyte to be measured for the following reasons:

(i) The relatively simple level system of Mg. This faciliates model calculations.

(ii) The presence of two ion levels with an excitation energy (ionisation energy + excitation energy in the ion system!) nearly equal to the ionisation energy of argon. This will promote the charge transfer reaction as proposed in chapter 3.

(iii) Overpopulations of excited ionic states with respect to exited neutral atom states have been measured by e.g. Boumans et al. [19] and more recently by Furuta et al. [14] .

Unfortunately the absolute intensity calibration of the optical system only covers wavelengths in the visible range. Only a few Mg ion and atom levels emit visible spectral lines with a reasonable strength at a reasonable analyte concentration.

Fortunately the wavelengths of e.g. the resonance transitions in ion and atom systems agree very close to each other. This relative intensities can be measured rather easy for this transitions. If one assumes the Mg neutral atom system to be in pLTE (which will be shown to be the case indeed) the absolute density of the ion level can be calculated if the density of the neutral atom level is calculated from pLTE considerations. Using this approach two level densities in the ion system are determined.

It will appear that most Mg spectral lines in the visible range require a solution as strong as 500 ppm, while the reasonance lines only require a 1 ppm solution.

A check for the linearity of the emission intensity with concentration is made in every case where a strong solution has been used. Only at concentrations of approximately 5000 ppm appreciable deviations of linearity have been found.

In section 6 it has been calculated that a 10000 ppm solution would yield a doubling of the electron density if all Mg is ionized as predicted by the Saha operation. It will be checked whether this is correct in reality, by measuring the stark width of the H_β line with and without a 10000 ppm Mg solution introduced in the discharge.

Table 5.4.1 lists important properties of the transitions and their upper levels to be measured.

We will neglect absorption of Mg line radiation in the determination of the Mg level densities. This is considered to be correct (see section 3.2 and appendix A).

The Abel error in the analyte measurements will be much smaller compared to the error in the argon measurements because both electron density and absolute level densities are determined in the channel.

6. Interpretation and discussion of the results; conclusions.

6.1. The Argon system.

6.1.1. Results and discussions.

The results will be treated according to the graphical presentation in Figures 6.1.1 - 6.1.7.

(i) The electron density as a function of the height above the loadcoil (Fig. 6.1.1).

As one would expect,the electron density gradually decreases with increasing height. In the load coil however, the electron density seems to be constant. This is, with only one data point measured in the load coil a very tentative conclusion.

(ii) The various excitation temperatures as a function of the height above the loadcoil (Fig. 6.1.2).

With a view at this plot it is clear that a simple two line temperature measurement with argon as thermometric species is extremely ticklish. Depending on the spectral lines used, deviations upto 0.2 eV can be obtained.

The temperatures c) and d) seem to coincide reasonably. This implies that at least for this levels and presumably all levels with an excitation energy above the excitation energy of the 4d level, PLTE is justified. However, the measured temperature differs appreciably from the calculated LTE temperature (see section 1.1). Even if over or under populations of the groundlevel up to a factor of 10 are assumed, no agreement between these temperatures is obtained.

Just in the region where the normally used ICP AES observation zones are located temperatures b) c) and d) agree within the experimental error. This means all levels down to 4p are in Saha equilibrium.

(iii) The underpopulation of the 4p level with respect to the levels 4d, 5d and 7d (Fig. 6.1.3).

This underpopulation is calculated with respect to the best fit of the straight boltzmann line to the levels 4d - 7d.

Of course the underpopulation approaches unity in the region

15 mm $<$ h $<$ 22 mm, where the temperatures coincide (see section (ii)). With increasing height (h $>$ 22 mm), starting from this region the under population of the 4p level increases very rapidly. This is in agreement with the Fujimoto model as the electron density decreases with increasing height (see Fig. 2.3.3b). With decreasing height (h $<$ 15 mm) the under population practically remains constant. Note the sudden increase of the under population at h = 9 mm.

(iv) The under population of the groundlevel with respect to the Saha population (Fig. 6.1.4).

This under population is calculated with T_{4d5d7d} (see (ii)) and n_e (see (i)) substituted in the modified Saha equation (eq. 1.1.2) under the assumption $T_o = T_e$.

In the region 10 $<$ h $<$ 25 under population of the groundlevel with a factor 10^3 occurs. For higher regions this under population rapidly increases. For lower regions the underpopulation appears to be constant at 10^5 - 10^6. In contradiction with the results of the four level model an under population of the groundstate is found. This may be caused by an underestimation of the convection term. If one recalculates v_c with the area between outer and intermediate tube determining the convection velocity this would yield $v_c \approx 17$ m/s and $\delta b_o \simeq -1$ indicating large under populations.

Note the apparent "discontinuity" for 5 $<$ h $<$ 9 mm

(v) Calculated versus measured electron density (Fig. 6.1.5).

The calculated electron density is obtained from the Saha equation with $T_e = T_{4d5d7d}$ (see (ii)) and an estimate of the intersection-point of the axis $E = E^+$ and the best fit to the levels 4d 5d and 7d.

In the region 10 $<$ h $<$ 20 agreement is obtained between the measured and calculated density.

In higher regions this ratio of measured to calculated density passes a minimum and then rapidly increases. In lower regions the measured n_e exceeds the calculated n_e by a factor 6.

This errors could be due to the fact that no radial resolution is obtained. First the value of r_{eff} is rather uncertain for heights of 25 mm, where the cold outer gasstream mixes with the hot annular

gasses, and second, the electron density is determined in the channel while absolute leveldensities are determined in the hot annulus. Especially in or just above the loadcoil appreciable differences between those two quantities may occur.

Note the sudden jump in the curve at $5 < h < 9$ mm (see also (iv)). At this height just the rim of the outertube is located. A correction in the effective radius is unprobable because this would yield $r_{eff} \approx 1$ mm. This is not correct for this heights. Furthermore no error in the optical system or the refractive behaviour of the quartz tube can explain this behaviour, because the plots in Fig. 6.1.7 show no discontinuity.

The plots of Fig. 6.1.2 - 4 may give a link to explain this phenomena. A slight, but significant minimum in excitation temperature is present. One may conclude from this fact, that a change in plasma conditions must be the cause of this discontinuity. This change in conditions may be caused by the lack of confinement of the discharge in the outer tube (see section 6.2). Thus cold air may diffuse into the discharge. A solid explanation for this "jump" cannot be given with this preliminary data, so only the cause has been indicated. Presumably Abel inverted measurements would provide the solution.

(vi) The population density as a function of the effective quantum number (Fig. 6.1.6).

Since the 4p level is underpopulated with respect to higher levels, and temperatures disagree (see (ii)) one may assume this level to be in the saturation phase (see section 1.3). To check this Fig. 6.1. is provided. The lines represent Boltzmann distribution with $T_e = T_{4d5d7d}$ and distributions according to section 1.3 (saturation phase).

It is clear that the slope of the level density curves for the 4p level fits better to a p^{-6} dependence then to the Boltzmann distribution. This level thus finds itself predominantly in the Saturation phase.

Note for h = 17 ($n_e \approx 10^{20}$ m^{-3}) no appreciable difference between the saturation phase distribution and the Boltzmann distribution exists (see also Fig. 2.3.3b). The exact agreement of those two distributions is obtained when

$$k_{T_e} = \frac{E^+ - E_i}{\frac{1}{2} p} \qquad (6.1.1)$$

For the 4p level this would be at approximately 0.8 eV. Or if $\hat{T}_e$ = 0,5 eV agreement would be obtained for p = 3,0 viz. just between the levels 4p and 4d.
This is the reason why it is very difficult for the 4p level for some heights in an ICP to determine whether it is in saturation or in PLTE, and accordingly, why many temperature determinations basically are erroneous, however agreement may be satisfactory.

A check on the validity of the Boltzmann distribution must be made in the regime of this electron density (10^{20} m^{-3}) and electron temperatures (0,5 eV).

(vii) Excited level densities integrated over a line of sight as a function of height (Fig. 6.1.7).

For every level population, at h = 25 a small peculiarity is present.
No physical explanation for this sharp discontinuity is present. This height is practically the height at which the tail of the hot annulus of the discharge is situated. Cold outer (argon) gas is mixed with the hot annulus gasses. This could provide a possible explanation for this rather peculiar behaviour.

6.1.2. Conclusions

The foregoing section leads to the following conclusions.

(i) It is reasonable to split the discharge in three regions distinguished by their different population density behaviour.

a) The confined region, h < 7.
In this region the discharge is still situated in the outer quartz confinement tube..
A practically constant under population of 4p and ground level is present. This indicates a recombining plasma with an inflow of argon ions and an outflow of groundstate atoms from a volume

element of the discharge. The 4p level can be shown to be in saturation. No agreement between calculated (from absolute leveldensities) and measured (from Starkwidths) electron density is obtained. This is due to the lack of radial resolution in both intensity and stark width measurements. The first electron density is determined in the hot annulus of the discharge while the second electron density is determined in the channel of the discharge. Radial electron density measurements indicate upto a factor 2-3 difference in the electron densities [12, 16, 59].

b) The unconfined region $7 < h < 15$.
Since the plasma is no longer bound by the quartz tube cold air may penetrate in the outer zones and/or the discharge may expand more or less freely. This results in a number of transitions shown e.g. in figures 6.1.2-6.1.6.
The most pronounced transitions to be seen are:
1) The ratio of the measured electron density to the Saha density calculated from the levels 4d,5d,7d approaches unity.
2) under population of the 4p level decreases from 3 to unity.
3) under population of the ground level increases from 10^{+6} to approximately 10^{+3}.
4) excitation temperature decreases, passes a minimum and then increases.

In this area the 4p level remains in saturation, but as temperature increases gradually the 4p saturation population density will coincide better with the Boltzmann density. So the under population of the 4p level decreases.

The under population of the groundlevel decreases for similar reasons.

This has very drastic consequences for the explanation of the under population of these levels. Presumably no change in mechanism, but just a change in electron temperature causes the underpopulations to decrease because the calculated Saha populations decrease.

c) The pLTE region: $15 < h < 22$.
In this region the observation zone of the ICP as an AES source is situated.
A small over population of the 4p level occurs.
The groundlevel is underpopulated by a factor 10^3-10^4. At least all excited levels with an excitation energy above the energy of the 4p level are in pLTE. The concept as described in section 1.1 is justified but one has to assume a much higher under population for the groundstate. As upper and lower limits we propose

$$10^{-2} < b_o < 10^{-4}$$

For $h > 22$ mm temperature decreases rapidly. Since we are rather uncertain about the effective radius in this area we cannot predict any sensible behaviour of population densities.

(ii) Generally it is justified in an ICP to characterize the discharge by an electron density and the density of e.g. the 4d level.

(iii) Throughout the whole discharge all levels with an excitation energy higher than the excitation energy of the 4d level are in pLTE.
This leads to the conclusion that the temperature T_{4d5d7d} equals the real electrontemperature to a fair approximation.

(iv) The under population of the groundlevel seems to have no correlation with variations in the electron density. Thus the groundlevel density, and the groundstate ion density are completely decoupled. Then those densities are only ruled by diffusion and convection, thus reducing the problem to advanced gaseous dynamics with two different species. The excited level density is coupled to the argon ion density either by the Saha equation or (especially for the 4p and 4s level) by the recombining plasma model in the saturation phase (see section 1.3).

(v) It is a major necessity to perform future measurements with an Abel inversion application, because of the very high radial temperature gradients in the discharge.

(vi) To exclude any influence from the upper boundary of the quartz outer tube it may be usefull in future investigations to use a torch with an extended tube, of which it is probably easier to get to the bottom of physical behaviour of the discharge.

6.2. The analyte system

6.2.1. Results and discussion

The results of the measurements for every height are plotted in Boltzmann diagrams similar to fig. 6.2.1., which refers to h = 14.
From fig. 6.2.1. and the Boltzmann diagrams for other heights (not shown) it becomes clear that

(i) The neutral atom ground state is over populated with respect to neutral atom excited levels.

(ii) At first sight ionic excited levels seem to be over populated with respect to the neutral excited levels (see iii).

(iii) Ionic excited level densities together with the ion ground level density yield a straight line in the Boltzmann diagram. The slope is different from the straight line which is obtained from the neutral atom excited level densities.

(iv) For h > 21 the resonance level $3^2P_{1/2}$ in the ion system seems a factor 5 under populated with respect to the ion ground level and the other ion excited levels (not shown in this work). With a view to the peculiarities observed in the argon system level densities for this heights we assume that this has the same causes as mentioned in section 6.1 viz. mixing of the colder outer gas stream with the hot annulus gases. Moreover, as the $3^2P_{1/2}$ level density misfits any continuous curve between ion ground level densitv and the other two ionic excited levels for this heights, we do not pay any special attention to this problem.

We shall now discuss the results of (i) to (iii).

(i) The total analyte atom density can be calculated from:

$$n_t = \frac{\eta N_A Q c}{M_{ng} F_c \chi} = 5.10^{16}.c \frac{m^{-3}}{ppm} \qquad (6.2.1.)$$

where N avogadro number $6.0*10^{23}$ 1/mol
Q pumping rate ($\approx$ 1 ml/min)
c concentration of analyte in the solutions (ppm)
M_{Mg} Molecular weight of Mg (24 gr/mol)
F_c carrier gas flow ($\approx$ 1 l/min)
χ Expansion coefficient. To a first approximation $\chi \approx T_g/G_a$ where T_a the initial carrier gas temperature and T_g the final carrier gas temperature. So $\chi \simeq 3000/300 \simeq 10$
η nebulizer efficiency ($\approx$ 0,02).

It is checked by measurement of the electron density (see 5.4) that this number equals the neutral ground state density. A solution of 10000 ppm is nebulized in the discharge. No significant change in electron density is observed, thus the ionisation degree ξ of Mg has to fulfill the following condition:

$$\xi \leq \Delta_2 n_e \frac{n_e}{n_t} \qquad (6.2.1.)$$

where $\Delta_2 n_e$ the relative accuracy of the electron density measurement.

With $n_e = 5.10^{20}$ m^{-3} and $\Delta_2 n_e = 7.5\%$ one obtains $\xi < 7{,}5\%$.
This shows that, in contradiction to the prediction from the Saha equation with the measured temperatures (Te $\approx$ 0,45 eV) only a minor part of the initial Mg atoms is ionized. This deviation from LTE is probably due to inhomogenities in the discharge. Especially at the boundaries of the analyte channel one is not too sure about temperature. Diffusion effects will also play an important rôle in this region of the discharge.
Thus it appears that the MgI ground state is over populated with respect to excited states.

Fig. 6.2.2. shows the over population b_o of the ground state with respect to the Saha extrapolation of the measured atomic excited levels as a function of h (see also Fig. 6.2.1.). Relative and absolute errors are shown. The relative error results from the extrapolation and the statistical scattering of the measured level densities. The absolute error results from

the systematic error in the density measurements and the uncertainty in the factor χ (eq. 6.2.1). Fig. 6.2.2. shows a steady increasing over population of the neutral ground state with increasing height.

Note that axial variations in the analyte concentration have not been taken into account. Presumably the analyte concentration decreases with increasing height and the slope of the curve in Fig. 6.2.2. would thus decrease. It is unlikely that this deviation of the initial density would exceed a factor of 10, so still an ascending curve is obtained. But, the determined ground state density is an average value. In the centre of the channel this concentration may be very different from the concentration at the channel boundaries. Thus at the channel boundaries LTE may exist in the MgI system.

(ii) The ratio $\alpha = b^{(2)}/b^{(1)}$ is defined according to section 3.3 viz. the over population of a fictitious level just below the ionisation limit of MgII with respect to the over population of a fictitious level just below the MgI ionisation limit (for clarification see also Fig. 6.2.1). Fig. 6.2.3 shows this over population as a function of the height above the load coil. In the ICP observation zone ($h \gtrsim 15$ mm) indeed apparent over populations are measured upto a factor 10^3 as is confirmed by many authors [14,19,58]. The cause of this over population will be considered in (iii).

(iii) From the Boltzmann diagrams (e.g. Fig. 6.2.1) it appears that analyte excitation can be described very adequately by two different temperatures (see Fig. 6.2.4).

1) a temperature T_{exc}^{MgI} which describes the equilibrium between atomic excited states and the ion ground level. This temperature appears to be in fair agreement with the argon excitation temperature (see section 6.1.1) and thus the equilibrium is governed by the same excitation mechanism (electron excitation-deexcitation).

   As is the case in the argon system, the ion ground level should be in equilibrium with excited states near the ionisation limit and may be calculated by the Saha equation.

2) a temperature T_{exc}^{MgII} which describes the equilibrium between ionic excited states and surprisingly, the ion ground state (calculated with the temperature T_{exc}^{MgI} and the atom level densities). This implies that the MgII system is in LTE but with a temperature which differs appreciably from the MgI excitation temperature.

This means that another equilibrium mechanism or other plasma-conditions (n_e, T_e) must account for the excitation of analyte ions. It seems not accidental that the ion ground level densities calculated from the MgI level densities and the MgII level densities coincide since this appears to be the case for every height and thus in a fairly large temperature range (see Fig. 6.2.4).

The different ion excitation temperature can be only explained by a different electron temperature. But this means in turn that ions are created and observed in another spatial position in the discharge where a higher electron temperature prevails. In addition in this region no significant MgI density can be present, otherwise $T_{exc}^{MgI} = T_{exc}^{MgII}$.

Complete ionisation of Mg analyte atoms is indicated by the Saha equation, however, this ionisation process is limited by the rate coefficients C_{01}^{1} or C_{01}^{0} (see section 3.22) which are much smaller than the direct charge transfer rate coefficient k_c. This indicates that charge transfer is the most dominant excitation mechanism in the analyte ion excitation region. (Penning ionisation is already considered to be unimportant in chapter 1.)

The fact that ions and atoms are created and observed at different spatial positions is confirmed by very recent radial emission profile measurements performed by Furuta and Horlick [14]. They mention areas of major "non LTE behaviour" to be the boundary of the analyte channel.

Furthermore as the ion ground level is in equilibrium with both ion excited states and neutral excited states (but with a different equilibrium temperature) the population of neutral excited states must be mainly a result from the deexcitation of ion excited states.

Thus only one logical solution remains for the analyte excitation mechanism.

Near the hotter annulus of the discharge, at the boundaries of the analyte channel, creation of analyte ions is possible in a direct way by charge transfer processes. Equilibrium then is settled very fast between ion excited states and the ground state by electron collisions. This requires the collisional equilibrium time to be shorter than the charge transfer characteristic time. The electron temperature in this region still is very high (T_e= 6000 - 8000 k) thus resulting in the relatively low slope in the Boltzmann plot. These created analyte ions will diffuse into the central region of the analyte channel where recombination processes create neutral excited states. This requires the characteristic diffusion time of ions to be shorter than the recombination time. Then, thermal equilibrium is settled very fast by electron collisions between excited states. This requires the collision time to be shorter than the recombination time. Since electron temperatures in this central region are much smaller (3000-6000 k) this results in the steeper Boltzmann plot.

With increasing height the "hot ion gas" will diffuse more and more in the "cold atom gas" and a final equilibrium will be reached with a "mean" electron temperature.

We measured an over population of the neutral ground state. In a recombining plasma this would require the diffusion time to be much shorter than the collisional equilibration time between levels 0 and 1 in the neutral system. With rough estimates of these characteristic times one concludes the gradient length to be of the order 10^{-4} m. This is very unlikely to be the case and accordingly the apparent over population must be a result from inhomogenities in the neutral atom distribution over a section of the analyte channel (see discussion under (i)).

Spatially resolved measurements, especially in radial direction will solve this problem.

The final key for understanding ICP analyte excitation mechanism is situated in the radial density profiles of the various species.

6.2.2. Conclusions

(i) The over population of analyte ion excited states with respect to atom excited states is due to different electron temperatures governing the equilibrium between a) ion ground level and excited atom levels, and b) ion ground level and ion excited states.

(ii) This in turn can only be explained by the fact that ions are created and observed in hotter regions of the discharge compared to atoms.

(iii) Furthermore it has been shown that analyte excitation must take place directly from the ground state by a charge transfer process, and population of excited atom states is a consequence of recombination processes from the ion levels.

(iv) Collisional excitation-deexcitation equilibrates levels of ion and atom and these processes are fast compared to any non LTE process (e.g. not detailed balanced charge transfer and diffusion of ground state ions).

(v) Recombination processes, however, must be slow compared to diffusion so as to let the different ionisation stages to be described by different temperatures.

(vi) Therefore neglecting diffusion for analyte ion ground states is basically not correct because this is the major cause of the "high temperature" population of analyte ion excited states.

(vii) The calculationsof Lovett [15] dit not account for any diffusion. These calculations resulted in only very small over populations of excited ion states for magnesium. This once again shows the minor deviations from LTE conditions in an ICP. Equilibrium is predominantly governed by electron collisions. Deviations between different ionisation stages are primarily caused by diffusion.

(viii) Our calculations on the charge transfer model (see section 3) did not account for diffusion. In contrast with Lovetts calculations, charge transfer is taken into account. Only

this charge transfer is enough to explain over populations of ion excited states upto orders of magnitude. Owing to the strong spatial inhomogenities no safe conclusion about the validity of the model can be drawn. It is very likely that, in a spatially very limited area (the ion excitation area), the model would describe the analyte excitation correctly. Therefore radially resolved measurements with an accurate Abel inversion technique are indispensable.

(ix) Soft and hard line behaviour [13,58] can be explained from the spatial area where the upper levels of the transition in question are created. This could also explain the different spatial behaviour and power dependence of soft and hard lines.

(x) The different behaviour of e.g. elements as Cd in the soft-hard line concept can be explained from the particular structure of the energy level diagram (e.g. the possibility of charge transfer in the ion system and the energy gap between first excited levels and ground levels for ion and atom system). Soft ion lines might be produced by elements that do not exhibit charge transfer reactions. Then the only possible excitation channel is provided by electron collisions resulting in a LTE population density distribution.

6.3. Future investigations

i) To exclude the influence of the quartz outer tube upper boundary a torch with an extended outertube must be used in future.

ii) Abel inverted measurements are indispensable.

iii) The radial resolution of these measurements should be better than 0.1 mm. The ion excitation area could be a very thin boundary layer between "hot" annulus and "cold" channel.

iv) These measurements could be easily set up with the use of a computer controlled photo diode array measurement system [14,43-45].

v) Accurate absolute intensity calibration is necessary in a very wide wavelength range (2000-8000 Å), to determine both argon and analyte excited level densities.

vi) A very useful set of data would be the spatial map of analyte ground state (ion and atom) densities. This requires e.g. absolute absorption measurements.

Acknowledgements

The encouragement and day-to-day supervision of Dr. P.W.J.M. Boumans is highly appreciated.

The enthousiasm of, and valuable discussions with Prof.Dr.Ir. D.C. Schram and Dr.Ir. B. v.d. Sijde (University of Technology, Physics Dept., Eindhoven) surely improved the quality of the performed research and the present report.

The permission of Dr. P.W.J.M. Boumans to let me adopt some parts of his Nat.Lab. Technical Note (132/82) in the general introduction of this report is appreciated.

At last I would like to thank Prof.Dr.Ir. D.C. Schram for arranging the possibility and Dr. W.F. Knippenberg for offering the opportunity to perform my graduate work in the Spectrochemical Department of Philips' Research Laboratories.

Appendix A.

Absorption of line radiation in plasma's

We define the effective absorption coefficient (according to Griem [1] as the difference between absorption and induced emission:

$$k(\omega) = \frac{2\pi}{c}\hbar\omega\left[-B_{mn}N_m + B_{nm}N_n\right].L(\omega) \qquad (A1)$$

where $L(\omega)$ is the normalized emission (or absorption) profile
N_n, N_m densities of lower and upper excited states
B_{nm}, B_{mn} the Einstein coefficients for resp. absorption and induced emission.

Application of the Einstein relations:

$$B_{nm} = g_m/g_n\, B_{mn} \qquad (A2)$$

$$A_{mn} = \frac{2\hbar\omega^3}{\pi c^3} B_{nm}$$

yields for equation (A1)

$$k(\omega) = \frac{\pi^2c^2}{\omega^2} A_{mn}\left[N_n - g_n/g_m\, N_m\right] L(\omega) \qquad (A3)$$

$$= \frac{\pi^2c^2}{\omega^2} A_{mn}\left[1 - g_n/g_m\, \frac{N_m}{N_n}\right] N_n L(\omega)$$

In the case of TE between levels m and n one may apply the Boltzmann relation to relate the densities of upper and lower excited states:

$$\frac{N_m}{N_n} = \frac{g_m}{g_n} \exp\left[-\frac{E_m - E_n}{kT}\right] \qquad (A4)$$

This yields for equation (3):

$$k(\omega) = \frac{\pi^2c^2}{\omega^2} A_{mn}\left[1 - \exp\left(\frac{-\hbar\omega}{kT_e}\right)\right] N_n L(\omega) \qquad (A5)$$

For convenience we rewrite this form with λ instead of ω as a variable

$$k(\lambda) = \frac{\lambda^4}{8\pi c} A_{mn} N_n \left[1 - \exp\left(-\frac{hc}{\lambda kT}\right)\right] L(\lambda) \qquad \text{(A6)}$$

Where $L(\lambda)$ is the normalized line profile in units per wavelength interval.

Assuming a completely Gaussian broadened line then the line profile can be written as:

$$L_g(\lambda) = \frac{1}{\sigma_\lambda \sqrt{\pi}} \exp\left[-\frac{(\lambda-\lambda_0)^2}{\sigma_\lambda^2}\right] \qquad \text{(A7)}$$

where λ_0 the central wavelength of the transition
σ_λ the 1/e width of the line profile,
$\sigma_\lambda = \frac{\Delta\lambda_{FWHM}}{2\sqrt{\ln 2}}$, where $\Delta\lambda_{FWHM}$ is the full width at half maximum.

Substituting this in equation (A6) yields for the center of the line profile ($\lambda = \lambda_0$)

$$k_g(\lambda_0) = \frac{\lambda_0^4}{\Delta\lambda_{FWHM}} \frac{2\sqrt{\ln 2}}{8\pi c} A_{mn} N_n \left[1 - \exp\left(\frac{-hc}{\lambda_0 kT}\right)\right] \qquad \text{(A8)}$$

If a completely Lorentz broadened line is the case the line profile reads:

$$L_l(\lambda) = \frac{\Delta\lambda_{FWHM}}{\pi} \frac{1}{(\lambda-\lambda_0)^2 + \left(\frac{\Delta\lambda_{FWHM}}{2}\right)^2} \qquad \text{(A9)}$$

Substituting this profile in eq. (A6) yields for $\lambda = \lambda_0$:

$$k_l(\lambda_0) = \frac{\lambda_0^4}{\Delta\lambda_{FWHM}} \frac{1}{2\pi^2 c} A_{mn} N_n \left[1 - \exp\left(\frac{-hc}{\lambda kT_e}\right)\right] \qquad \text{(A10)}$$

Combination of eqs. (A8) and (A10) yields:

$$k_L(\lambda_0) = \frac{2}{a} k_g(\lambda_0) \qquad \text{(A11)}$$

where a is the Voigt parameter of the line profile;

$$a = \sqrt{\ln 2}\ \frac{\Delta\lambda_l}{\Delta\lambda_g} \qquad \text{(A12)}$$

In the above text indices g are used for parameters for Gaussian broadened lines while indices l are used for Lorentz broadened lines.

Generally the absorption factor will be a function of the position $\underline{x}$ in the plasma.

Now one can define the optical depth of the plasma as:

$$\tau = \int k(\lambda_0, \underline{x})\, dx \qquad \text{(A13)}$$

where the integration has been performed over a line of sight through the plasma.

If we can approximate the plasma as a homogeneous layer of depth d then the optical depth is

$$\tau = k(\lambda_0) \cdot d \qquad \text{(A14)}$$

For a homogeneous cylindrical discharge one usually takes: $\tau = k(\lambda_0) \cdot R$. If the optical depth is small enough (say $\tau \ll 1$) then the radiation will not be absorbed significantly in the plasma. If the optical depth approaches or exceeds unity one has to correct the results from intensity measurements.

Calculations of the optical depth of the discharge for argon transitions.

One needs to know at least a reasonable estimate of the optical depth because of two reasons

i) to determine whether a correction on the measured intensity is needed (section 5.1).

ii) One needs to know the escape factor of the discharge to correct the transition probabilities in the collisional radiative model (section 2.2).

Once the optical depth is known the escape factor Λ can be determined from either reference 21 (in a good approximation if a Voigt profile is present), or (eq. A15) (see below) if a rough estimate in the center of the line is desired. For the correction factor $1/\Lambda$ one writes

$$1/\Lambda = \frac{\tau}{1 - \exp(-\tau)} \qquad (A15)$$

The optical depth for the relevant argon transitions is calculated for a complete Lorentzian and a complete Gaussian profile. In the discharge LTE is assumed. Excited level densities are calculated according to eq. 2.0.1. Ground level densities are calculated according to eq. 2.0.3.
Table A.1 lists the optical depths of some argon transition, together with some other relevant properties.

Appendix B

Line broadening

Lorentz and Gauss profiles of spectral lines are needed if one calculates e.g. escape factors, optical depths and absorption factors. Furthermore an intensity measurement must yield the correct total intensity of the transition. To avoid an elaborate integration one chooses the halfwidth of the monochromator profile large compared to the line width (see section 5.1.1). If this is not completely the case a correction has to be applied.
Table B.1 lists the correction factor if a complete Lorentz profile is assumed for the transition and a rectangular monochromator profile. In our measurements linewidths are always a factor 10 smaller than the monochromator halfwidth, thus corrections are smaller than 6%. In comparison with the error of the absolute intensity measurement ($\approx$ 10%) this error can be neglected.

It is not our aim to give an elaborate treatment on the line broadening mechanisms of spectral lines. Numerous clarifying treatments exist [1, 22. 51-53] . Because of its simplicity we chose the approach of Griem [1,22].

The line broadening due to thermal (doppler) and collisional (Stark, resonance, v.d. Waals) broadening is been calculated for various argon lines. Doppler broadening will result in a Gaussian line shape, while collisional broadening results in a Lorentzian line shape. Table B.2 lists numerically both broadening mechanisms for an electron temperature $\hat{T}_e$ = 0,58 eV and an electron density $n_e = 2.10^{20}$ m^{-3} in an argon LTE plasma. Note that the Lorentz line width is proportional to n_e.

The linewidth of analyte spectral lines can also be calculated according to Griem. One finds for e.g. the 4f-3d transition in the MgII system, at $n_e = 2.10^{20}$ m^{-3} and T_e = 0,5 eV for the Doppler ($\Delta\lambda_g$) and Lorentz ($\Delta\lambda_l$) width

$\Delta\lambda_g = 0{,}05$ Å
$\Delta\lambda_l = 0{,}03$ Å.

Since this is the transition with the largest stark width [1] all linewidths can safely be neglected with respect to the monochromator profile width ($\approx$ 2 Å).

Appendix C. Rate coefficients in the ArI system.

The application of the four level model described in section 2.2 requires accurate knowledge of rate coefficients for electron excitation and deexcitation, radiative recombination and effective transition probabilities. Furthermore we need to know the statistical weights and effective energy of the levels in the simplified Argon 4 level system. We will follow the approach of Rosado [21] applying the expressions for lower electron temperatures, except for the collision cross sections between excited states where we will use semi empirical expressions from Vriens [41].

(i) The effective energy

The effective energy of a level q can be written as:

$$E_q = \frac{\sum_i g_i E_i}{\sum_i g_i} \qquad (C.1)$$

where $\sum_i$ is a summation over all sublevels in a group

g_j, E_j the statistical weight and energy respectively of a sublevel in a group

$g_q = \sum_i g_j$ is the statistical weight of the level q.

Table C.1 lists effective energies, statistical weights and nomenclature of the levels in the simplified Ar system.

(ii) Transition probabilities

For optically thin transitions the transition probability between levels can be averaged over the various transitions between sublevels.

$$A_{qp} = \sum_i \frac{\sum_j g_j A_{ji}}{\sum_j g_j} \qquad (C.2)$$

where $\sum_i$ denotes a summation over the upper states of a transition
$\sum_j$ a summation over the lower states of a transition
A_{ji} the transition propability between sublevel j of group q and sublevel i of group.

If the transition is optically thick (e.g. resonance lines and, in a minor way, the 4p-4s transition) a more correct procedure is to include trapping coefficients (see appendix A) and average $A_{ji}\,\Lambda_{ji}$ over the transitions considered viz.

$$A_{qp}\,\Lambda_{qp} = \sum_i \frac{\sum_j g_j A_{ji}\,\Lambda_{ji}}{\sum_j g_j} \qquad (C.3)$$

For the transition between levels 1 and 0 (4s group and ground state) this formula is used. The optical depth of resonance lines is calculated in appendix (A).
One can also define an effective wavelength by averaging the wavelengths from transitions between sublevels

$$\lambda = \frac{\sum_i [g_i \sum_j g_j \lambda_{ji} A_{ji}]}{\sum_j g_j \sum_i g_i} \qquad (C.4)$$

Table C.2 lists the transition probabilities calculated with the above formula's together with effective wavelengths and optical depths.

(iii)Electron excitation, deexcitation and ionisation

Excitation-deexcitation and ionisation between excited states.

The hydrogenic approach can be used here. Two semi empirical approaches are on hand. The elaborate treatments of Vriens [41] and of Drawin [35].
As the values of Vriens yield better agreement with experimental reality [54], especially for optically disallowed transitions, we will use his approach.
Generally the coefficients of Drawin are lower with a factor 5-20 compared to those of Vriens. Rosado [21] uses values of Drawin [35].

Excitation-deexcitation and ionisation from or to the ground state.

For this rate coefficients the hydrogenic approach is expected to lose its validity. We will use the linear approach as in [21]. A lineair increase of the collision cross section after a threshold energy E_T is assumed. The slope of this curve and the threshold energy are found empirically and are listed in [21]. Integration of this collision cross section over a Maxwellian velocity distribution yields the rate coefficient for electron excitation from the ground state. The rate coefficient for the reverse process can be obtained from the principle of detailed balancing. The rate coefficient for electron ionisation from the ground state will be calculated from Vriens [41].

iv. Radiative recombination

We will again use different approaches for recombination to the ground state and to excited states. For the rate coefficient for radiative recombination to the ground state we use the approach followed by Rosado [21]. For radiative recombination to the ground state radiation trapping may be of importance. The results of Rosado [21] are extrapolated to obtain the escape factor for recombination radiation to the ground state at lower temperatures. For a better approach one refers to Hermann [55]. One finds for the escape factor $\Lambda_{+1}^{(2)} \approx 0.1$.

Radiative recombination to excited states will be approximated by a hydrogen approach [21].

In Fig. C.1.a-d the rate coefficients for various processes are shown. In Fig. C.2 some rate coefficients calculated from Drawin [35] Vriens [41] and for ground state transitions, the lineair approach [21] are compared with each other. For convenience with the treatment of the argon four level model, the R coefficients are shown as a function of temperature in Fig. C.3.a-c.

Appendix D.

Rate coefficients in the Mg system

In order to perform practical calculations on the rate equations for the excitation in the analyte system one needs to know the rate coefficients for electron ionisation, electron excitation and deexcitation and collisional radiative recombination between levels in the analyte ion and atom system.

Since we consider Magnesium as analyte in this report we will calculate rate coefficients between the first levels of MgI and MgII. We will assume that for higher excited levels (e.g. the 4th level in MgI and II) electron excitation and deexcitation is much higher then transition rates from or to lower lying levels, thus restricting the number of levels to be considered.

Three approaches are on hand. Drawin [35] and Vriens [41] give semi-empirical formulas in a hydrogen approach. Lovett [15] uses formulas suited for rate coefficients in highly ionized systems.

It is demonstrated that rate coefficients obtained from the Vriens and Drawin formulas show a fare agreement, with the rate coefficients of Vriens tending to exceed those of Drawin by a factor 2.

Only if the transition for electron excitation or deexcitation in question is optically disallowed agreement is rather unsatisfactory. In contrast to Vriens, Drawin distincts between the optically allowed and disallowed case. Since we believe that optically forbidden transitions will not outline themselves in electron excitation-deexcitation with respect to other transitions (e.g. C_{01} in the MgI system)[54] , we used Vriens rate coefficients for this transitions: All rate coefficients for optically allowed transitions are taken from Drawin [35]. The reason for this is a practical one. Drawins rate coefficients where first known to the author. No serious influence on the predictions of the excitation model have to be expected in the, rather qualitative, treatment described in this report.

The rate coefficients used by Lovett show no agreement with the rate coefficients obtained from Vriens or Drawin. As Lovett uses an approach especially valid for multiply charged ions (i.e. Al^{7+}) these rate coefficients are not used.

Especially in the MgII system the hydrogen approach must show excellent results because of only one electron in the outer shell. Similarity with the hydrogen atom thus is established

For the collisional radiative recombination coefficient we used a hydrogen approach from Bates [42].

The energies and statistical weights of the levels considered are showed in table D.1 for MgI and MgII. In the column "level designation" the indexes used in the designation of the rate coefficient are given.

Fig. D.1-D.7 show the most important rate coefficients as a function of the temperature.

Appendix E.

Apple II software.

The software will be described by a usermanual for the various PASCAL procedures implemented in the system library of the apple II computer in units MISCIO and CONTROL. The use of one of the procedures which are implemented in Unit CONTROL requires the linking of both units MISCIO and CONTROL in the host program because unit CONTROL uses some procedures implemented in unit MISCIO,

i) Unit MISCIO:

```
(*$S+*)

UNIT MISCIO;      INTRINSIC CODE 12 DATA 13;

INTERFACE
  VAR PAPER: INTERACTIVE;
  PROCEDURE NEWLINES (N:INTEGER);
  PROCEDURE HURRAY (N:INTEGER);
  PROCEDURE COMMENT;
  PROCEDURE CHKREAD (VAR X:REAL);

IMPLEMENTATION

BEGIN REWRITE (PAPER, 'PRINTER:') END.
```

After the linking of this unit to the host program the file identifier PAPER is coupled to the printer.

```
PROCEDURE NEWLINES (N:INTEGER);
```

This procedure causes the printer to skip N lines.

```
PROCEDURE HURRAY (N:INTEGER);
```

This procedure is written to humanize computer aided measurements. After success from the measurements it may be nice to call HURRAY (5).

```
PROCEDURE COMMENT;
```

This procedure enables to comment any output to the printer in a line by line data input from the keyboard. The execution of the procedure is terminated by a combination of the keys "." followed by RETURN.

```
Procedure CHKREAD (VAR X:REAL)
```

This procedure allows to read a real number typed at the keyboard. If a mistake is made any character but ".", "E" or RETURN allows to enter the new number.

(ii) UNIT CONTROL

```
UNIT CONTROL; INTRINSIC CODE 14 DATA 15;

INTERFACE
  USES MISCIO, GONIO, APPLESTUFF,
       LABIO, TRANSCEND;
  TYPE ARCON1          = ARRAY  1..4, 1..2  OF REAL;
       ARCON2          = ARAAY  1..2, 1..100  OF REAL;
  VAR DATA             : INTERACTIVE;
  PROCEDURE INITLAMBDA (VAR LLIMIT:ARCON1;VAR LLAST:REAL);
  PROCEDURE SETLAMBDA (LLIMIT:ARCON1; VAR LLAST:REAL; L:REAL;
                       VAR MEAS:BOOLEAN);
  FUNCTION POSITION (Z:REAL): BOOLEAN;
  FUNCTION MOVEDOWN (Z:REAL): BOOLEAN;
  FUNCTION CALIFAC (CALIB:ARCON2; LAMBDA:REAL): REAL;
  FUNCTION MEASINT (VAR SENS:REAL; TIME:REAL; SENSLIM:BOOLEAN;
                    VAR SIGMA:REAL): REAL;
  PROCEDURE INITINT (VAR CALIB:ARCON2);

IMPLEMENTATION
  CONST CORR=-8.7;
        LLOW=3;
        LHIGH=1997;
        LMAX=8440.4;
        NULPUNT=41.06;
        ZMIN=-19;
        INTTIME=0.1;
        ADCTIME=1.67E-3;

BEGIN END.
```

Before CONTROL is linked MISCIO has to be linked already in the host program. Linking CONTROL causes two types to be decleared globally (TYPE ARCON1, ARCON 2) and one file identifier (DATA). This file identifier is not coupled to any actual file. The user is free to do so.

Parameter list:

CORR	Wavelength correction for monochromator (Angstr$\ddot{o}$m) (=real wavelength-counterreading)
LLOW LHIGH	Define an area in which no computer controlled wavelength setting is possible.
LMAX	Maximum wavelength of monochromator range.
NULPUNT	Position of the "zero" switch with respect to the top of the loadcoil (mm)
ZMIN	Minimum height above the load coil (mm)
INTTIME	Integration time Lock In amplifier (seconds)
ADC Time	Integration time of AD converter used with the apple II.

PROCEDURE INITLAMBDA (VAR,LLIMIT:ARCON1; VAR LLAST:REAL);

This procedure initialises the monochromator and goniometer control. Every program written with the intention to use computer controlled monochromator setting must be initialized by INITLAMBDA.

Parameter list

VAR LLIMIT:ARCON1

After excecution of INITLAMBDA this array contains wavelength limits and counter limits of respectively the monochromator and the goniometer control. Between the four indicated wavelength regions computer controlled wavelength setting is possible. This array will be used by the procedure SETLAMBDA.

VAR LLAST:REAL

After excecution LLAST equals the wavelength belonging to the "zero" of the goniometer control, and thus the actual position of the monochromator since the goniometer will be initialized to zero.

PROCEDURE SETLAMBDA (LLIMIT:ARCON1; VAR LLAST:REAL
L:REAL; VAR MEAS:BOOLEAM);

This procedure sets the monochromator at the absolute position L (Angstrom). If the wavelength is out of the monochromator range (SEE INITLAMBDA) a message is given to the user and MEAS gets the value 'FALSE'. If the call is succesfull MEAS gets the value 'TRUE'. After excecution LLAST=L. Before a first call, always a call of INITLAMBDA has to be performed.

Parameter list:	LLIMIT	As in INITLAMBDA
	LLAST	As in INITLAMBDA.
	L:REAL	Wavelength to go for (Angstrom)
	VAR MEAS:BOOLEAN	Indicates succesfull ('TRUE') or unsuccesfull ('FALSE') wavelength setting.

FUNCTION POSITION (Z:REAL):BOOLEAN;

This function sets the optical axis of the mirror and lens system at an absolute height z above the load coil. If z is out of the controllable range POSITION gets the value 'FALSE'. Otherwise POSITION remains 'TRUE'.
parameter list: Z:REAL absolute position of optical axis above the loadcoil (ZMIN Z (NULPUNT)

FUNCTION MOVEDOWN (Z:REAL): BOOLEAN

This function displaces the optical axis down over a distance Z.
If an uncontrollable region is entered MOVEDOWN gets the value 'FALSE' otherwise MOVEDOWN remains 'TRUE'

PARAMETER LIST: Z:REAL distance to move down (mm).

FUNCTION CALIFAC-(CALIB:ARCON2); LANBDA: REAL): REAL

This function determines the calibration factor at a certain wavelength by lineair interpolation between the closest values in the first column of the array CALIB and assigns the corresponding calibration factor to CALIFAC. CALIB contains in the first columns the calibration wavelengths and in the second column the calibration factors. The maximum length of the array is
100x2 elements. The last elements and elements not used for calibration must be zero.

```
FUNCTION MEASINT (VAR SENS:REAL; TIME:REAL; SENS LIM:BOOLEAN;
                  VAR SIGMA-REAL):REAL;
```

This function measures the output of the lock-in amplifier (=INPUT ADC(0), SLOT 4).

The internal time constant is 0.1 s. This is equal to the sampling time.
Samples are taken during a time TIME ($\gg$ 0,1 s!!). These samples are statistically averaged and the standard deviation of this series of samples is assigned to SIGMA.
If the sensitivity SENS is given in mV, MEASINT gets the value of the output of the lock in in mV.
The ADC delivers a 10 bits/number (0-1024) to the computer.
If SENSLIM = 'TRUE' then a message is given to the user if the output voltage of the lock in exceeds 0,9^{x}full scale value or is less then 0,1xfull scale value. An opportunity to correct the sensitivity is given by the computer. If senslim = 'FALSE' no correction is possible. If over flow occurs MEASINT and SIGMA get the value -1.

PROCEDURE INITINT (VAR CALIB:ARCON2);

This procedure initialises the absolute intensity measurements by creating an array CALIB as used in CALIFAC . If absolute intensity measurements are required, a first call of INITINT is necessary before any call of CALIFAC. Input data for INITINT consists of a file on disk with the following structure.

wave lengths	standard radiance	output lock in	standard deviation	] 10 lines for comment.
-	-	-	-	
-	-	-	-	
-	-	-	-	
-	-	-	-	
0	0	0	0	

The name of the file will be asked by the computer.
A maximum of 99 datapoints can be used.

References

1. H.R. Griem, "Plasmaspectroscopy", Mc Graw Hill Book Company, New York (1964).
2. A.A. Kruithof en B. v.d. Sijde, "Evenwichten in plasmas", Internal Report University of Technology,Eindhoven, nr.: VDF/NT75-3 (1975).
3. B. v.d. Sijde, "Thermisch en Locaal thermisch evenwicht", Internal Report, University of Technology,Eindhoven, nr.: VDF/NT78-13.
4. D.C. Schram and C.J. Timmermans, "Plasmafysica". Internal Report, University of Technology, Eindhoven, nr.: VDF/NT79-10.
5. R. Huddlestone & S.L. Leonard, (editors), "Plasma diagnostic techniques", New York, (1965).
6. G.V. Marr, "Plasmaspectroscopy", Elsevier Publishing Company Amsterdam, (1968).
7. T. Fujimoto, J. Phys. Soc. Japan 47, 265 (1979).
8. T. Fujimoto, J. Phys. Japan 47, 273 (1979).
9. T. Fujimoto, J. Phys. Soc. Japan 49, 1561 (1980).
10. T. Fujimoto, J. Phys. Soc. Japan 49, 1569 (1980).
11. J.J.A.M. v.d. Mullen, B. v.d. Sijde, D.C. Schram, Phys. Lett. 79A 51 (1980).
12. J. Jarosz, J.M. Mermet, and J.P. Robin, Spectrochim. Acta 33B, 55 (1978).
13. P.W.J.M. Boumans, Spectrochim. Acta 37B, 75 (1982).
14. N. Furuta and G. Horlick, Spectrochim. Acta 37B, 53 (1982).
15. R.J. Lovett, "A rate model of ICP analyte spectra", to be published.
16. G.R. Kornblum and L. de Galan, Spectrochim. Acta 32B, 71 (1977).
17. R.M. Barnes, CRC Crit. Rev. Anal. Chem. 7, 203 (1978).
18. D.J. Kalnicky, V.A. Fassel, and R.N. Kniseley, Appl. Spectrosc. 31, 137 (1977).
19. P.W.J.M. Boumans and F.J. de Boer, Spectrochim. Acta 32B, 365 (1977).
20. P.W.J.M. Boumans and F.J. de Boer, Spectrochim. Acta 31B, 355 (1981).
21. R.J. Rosado, "An Investigation of Nonequilibrium Effects in Thermal Argon Plasma", Thesis University of Technology, Eindhoven, (1980).

22. H.R. Griem, "Spectral line broadening by plasmas", Academic Press, New York, (1974).
23. J.M. Mermet, Spectrochim. Acta 30B, 383 (1975).
24. V.M. Goldfarb, Proc. of Int. Winterconf. on Spectrochem. Analyses, San Juan, Puerto Rico, (1980).
25. E.W. Mc Daniel,"Collision Phenomena in Ionized gases", Wiley and sons Inc., New York, (1964).
26. A.C.G. Mitchell and M.W. Zemansky,"Resonance radiation and excited atoms",Cambridge university press, New York, (1971).
27. V.A. Kartazaev and Yu.A. Folmachev, Opt. Spectrosc. 45, 620, (1978).
28. R. Johnson and M.T. Leu, Phys. Rev. 8, 1808, (1973).
29. B.A. Huber, J. Phys. B. 13, 809, (1980).
30. E. Graham iv, M.A. Biondi and R. Johnson, Phys. Rev. A 13, 965 (1976).
31. A.R. Turner Smith, J.M. Green and C.E. Webb, J. Phys. B 6, 114, (1973).
32. J.M. Green, G.J. Collins and C.E. Webb, J. Phys. B 6, 1545, (1973).
33. H.S.W. Massey, Rep. Progr. Phys. 12, 248, (1949).
34. J.B. Hasted, "Physics of atomic collisions", Butterworths London, (1971).
35. H.W. Drawin, Euratom Report, (1967), EUR CEA FC 383.
36. R.C. Miller and R.J. Ayen, Journal of Applied Physics 40, 5260, (1969).
37. H. Kawaguchi, T. Ito, S. Rubi and A. Mizuike, Anal. Chem. 52, 2440 (1980).
38. R.M. Barnes and R.G. Schleicher, Spectrochim. Acta 30B, 109, (1975).
39. R.M. Barnes and S. Hikdel, Appl. Phys. 47, 3929, (1975).
40. P.W.J.M. Boumans and M.Ch. Lux-Steiner, Spectrochim. Acta 37B, 97 (1981).
41. L. Vriens and A.H.M. Smeets, Phys. Rev. A22, 940 (1980).
42. D.R. Bates, A.E. Kingston, R.W.P. McWhirte, Proc. Roy. Soc. (London) A267, 297 (1962).
43. G. Horlick, Appl. Spectrosc. 30, 113, (1976).

44. T.E. Edmonds and G. Horlick, Appl. Spectrosc. 31, 536 (1977).
45. M.W. Blades and G. Horlick, Appl. Spectrosc. 34, 696, (1980).
46. P.W.J.M. Boumans and F.J. de Boer, ICP information newsletter 3, 228, (1977).
47. J.T. Davies and J.M. Vaughan, Astrophys. Journal 137, 1302, (1963).
48. P.W.J.M. Boumans, F.J. de Boer, Spectrochim. Acta 30B, 309 (1973).
49. W.L. Wiese, "Transition probabilities", Nat. Bureau of Standards, (U.S.), (1963).
50. S. Bashkin and J.A. Stoner jr., "Atomic energy levels and grotrian diagrams", North Holland Publishing Company, Amsterdam, (1975).
51. I.I. Sobelmann, Introduction to the theory of atomic spectra Pergamon Press, Oxford, (1972).
52. H. Margeneau and M. Lewis, Rev. of Mod. Physics 31, vol.3, 569, (1959).
53. G. Traving, "Line broadening and lineshift" in: "Plasmadiagnostics". ed. W. Lochte-Holtgreven, North Holland Publ. Comp., Amsterdam, (1968).
54. B. v.d. Sijde, Private Communication, August 1982.
55. W. Hermann, Z. fur Physik 216, 33, (2968).
56. I.J.M.M. Raaijmakers and P.W.J.M. Boumans, Internal Report, Philips Research Laboratories, nr. 132/82, (1982).
57. J.M. Mermet, C.R. Acad. Soc. Ser. B281, 273 (1975).
58. M.W. Blades and G. Horlick, Spectrochim. Acta 36B, 861 (1981).
59. J.M. Mermet, Spectrochim. Acta 30B, 383 (1975).
60. H.U. Eckert, Winter Conference on Spectrochemical Analyses, San Juan, Puerto Rico, (1981).
61. P.W.J.M. Boumans, Internal Report, Philips Research Laboratories, nr. 89/82, (1982).
62. R.M. Barnes and R.G. Schleicher, Spectrochim. Acta 30B, 109, (1975).
63. E.L. Groove (Editor), "Analytical spectroscopy series", part 1 Marcel Bakker Inc., New York, (1971).

64. T.B. Reed, J. of Appl. Phys. 32, 821, (1961).
65. P.W.J.M. Boumans and F.J. de Boer, Spectrochim. Acta 27B, 391 (1972).
66. V.A. Fassel, R.N. Kniseley, Anal. Chem. 46, 1110A, (1974).
67. P.W.J.M. Boumans, Fresenius Z. Anal. Chem. 299, 337 (1979).
68. R.H. Scott, V.A. Fassel, R.N. Kniseley, and R.N. Nixon, Anal. Chem. 46, 75 (1974).
69. S. Greenfield, I.Ll. Jones, H.McD. McGeachin, and P.B. Smith, Anal. Chim. Acta 74, 225 (1975).
70. V.A. Fassel, Science 202, 183 (1978).
71. S. Greenfield, H.McD. McGeachin and P.B. Smith, Talanta 23, 1 (1976).
72. P. Tschoepel, "Plasma Excitation in Spectrochemical Analysis", in: Comprehensive Analytical Chemistry (Ed. G. Svehla), Vol. 9, Ch. 3, p. 173. Elsevier, Amsterdam (1979).
73. S. Greenfield, ICP Information Newslett. 1, 3 (1975).
74. V.A. Fassel, ICP Information Newslett. 1, 267 (1976).
75. V.A. Fassel, Anal. Chem. 51, 1290A (1979).
76. G.I. Babat, Vestn. Elektroprom., No. 2, p. 1, No. 3, p. 2 (1942).
77. G.I. Babat, J. Inst. Elect. Eng. 94, 27 (1947).
78. T.B. Reed, J. Appl. Phys. 32, 2534 (1961).
79. T.B. Reed, Int. Sci. Technol. 6, 42 (1962).
80. S. Greenfield, I.Ll. Jones, and C.T. Berry, Analyst 89, 713 (1964).
81. R.H. Wendt and V.A. Fassel, Anal. Chem. 37, 920 (1965).
82. G.W. Dickinson and V.A. Fassel, Anal. Chem. 41, 1021 (1969).
83. V.A. Fassel, Proc. 16th Coll. Spectr. Int., Heidelberg 1971, Plenary Lectures and reports, p. 63. Adam Hilger, London (1972).
84. R.H. Wendt and V.A. Fassel, Anal. Chem. 38, 337 (1966).
85. S. Greenfield, C.T. Berry, and L.G. Bunch, Spectroscopy with a High Frequency Plasma Torch, Radyne International, Workingham, England (1965).
86. S. Greenfield, I.L.W. Jones, and C.T. Berry, U.S. Patent 3, 467, 471, September 16, 1969.

87. S. Greenfield, I.L.W. Jones, C.T. Berry, and L.G. Bunch, Proc. Soc. Anal. Chem. 2, 111 (1965).
88. S. Greenvield, P.B. Smith, A.E. Breeze, and N.M.D. Chilton, Anal. Chim. Acta 41, 385 (1968).
89. H.C. Hoare and R.A. Mostyn, Anal. Chem. 39, 1153 (1967).
90. D. Truitt and J.W. Robinson, Anal. Chim. Acta 49, 401 (1970); 51, 61 (1970).
91. R.M. Barnes, Emission Spectroscopy. Dowden, Hutchinson & Ross, Stroudsburg, PA (1976).
92. J.C. Souilliart and J. Robin, Analusis 1, 427 (1972), 391 (1972).
93. V.A. Fassel and R.N. Kniseley, Anal. Chem. 46, 1110A, 1155A (1974).
94. P.W.J.M. Boumans and F.J. de Boer, Proc. Anal. Div. Chem. Soc. 12, 140 (1975).
95. C.C. Butler, R.N. Kniseley, and V.A. Fassel, Anal. Chem. 47, 825 (1975).
96. R.N. Kniseley, V.A. Fassel, and C.C. Butler, Clin. Chem. 19, 801 (1973).
97. D.E. Nixon, V.A. Fassel, and R.N. Kniseley, Anal. Chem. 46, 210 (1974).
98. A.L. Davison, J.R. Bethune, and R.M. Ajhar, 24th Pittsburgh Conf. Anal. Chem. and Appl. Spectrosc., Abstr. Paper No. 30 (1973).
99. J.L. Jones, R.L. Dahlquist, J.W. Knoll, and R.H. Hoyt, 24th Pittsburgh Conf. Anal. Chem. Appl. Spectrosc., Abstr. Paper No. 147 (1974).
100. R.M. Barnes, Trends Anal. Chem. (TrAC) 1, 51 (1981).
101. E. Kranz, Proc. 15th Coll. Spectr. Int., Madrid 1969, Vol. 4, p. 95. Iberica, Tarragona, 34-Madrid-7 (1971).
102. E. Kranz, Spectrochim. Acta 27B, 327 (1972).
103. M.E. Britske, J.S. Sukach and L.N. Filimov, Zh. Prikl. Spektrosk. 25, 5 (1976).
104. K.I. Zil'berstein, ICP information Newslett. 5, 508 (1980).
105. F.E. Lichte and S.R. Koirtyohann, ICP Information Newslett. 2, 192 (1976).

106. C.T. Apel, D.V. Duchane, B.A. Palmer, T.M. Bieniewski, H.V. Pena, L.E. Cox, D.L. Gallimore, K. Vincent, M. Lopez, J.V. Kline, and D.W. Steinhaus,"Developments in Plasma Spectrochemical Analysis"(Edited by R.M. Barnes), p. 383. Heyden, London (1981).
107. J. Robin and C. Trassy, C.R. Acad. Sc. (Paris) 281, 345 (1975).
108. L.R.P. Butler, H.G.C. Human, and R.H. Scott, "Electrical Flames", in: Handbook of Spectroscopy (Ed. J.W. RObinson),
109. Annual Reports on Analytical Atomic Spectroscopy, from Vol. 1 (1971). The Society for Analytical Chemistry, London.

Coefficient	unit	value
<u>Collisional</u>		
k_{10}	m^3/s	2.0×10^{-16}
k_{20}	"	1.4×10^{-16}
k_{23}	"	5.0×10^{-12}
k_{12}	"	4.5×10^{-13}
k_{21}	"	2.8×10^{-12}
K_0	"	2.2×10^{-24}
K_1	"	4.5×10^{-13}
K_2	"	7.8×10^{-12}
<u>Radiative</u>		
α	1/s	4.6×10^{6}
β	"	2.6×10^{7}
γ	"	6.2×10^{6}
δ	"	1.6×10^{-2}
$A_{10} \Lambda_{10}$	1/s	1.6×10^{6}
$\Lambda_{0+}^{(2)}$	no unit	0,1 *

* extrapolated value to $\hat{T}_e$ = 0,56 eV [21] .

Table 2.2.1.
Rate coefficients and effective radiation transition probabilities as to be substituted in the rate equations of the CRM proposed by Rosado [21]. The values are calculated in appendix C. Parameters for the discharge are $n_e = 2.10^{20}$ m^{-3} and $\hat{T}_e$ = 0,56 eV. For meaning of symbols refer to the text.

Rate Coefficient	Value (m^3/s)
C_{01}	7.1×10^{-14}
C_{02}	2.8×10^{-17}
C_{12}	1.8×10^{-14}
C_{23}	5.9×10^{-15}
C_{03}	3.0×10^{-20}
F_{10}	1.1×10^{-10}
F_{20}	2.2×10^{-14}
F_{21}	1.3×10^{-12}
F_{32}	2.4×10^{-14}
F_{30}	9.3×10^{-17}
S_0^+	2.2×10^{-20}
S_1^+	7.3×10^{-18}
α_{CR}	1.1×10^{-17}

Rate Coefficient	Value (m^3/s)
C_{01}	3.3×10^{-17}
C_{12}	7.1×10^{-18}
C_{02}	8.5×10^{-23}
C_{13}	2.8×10^{-17}
C_{23}	1.8×10^{-13}
F_{10}	1.9×10^{-14}
F_{21}	4.5×10^{-15}
F_{10}	4.4×10^{-16}
F_{31}	4.6×10^{-14}
F_{32}	5.0×10^{-14}
S_{0+}	6.3×10^{-25}
S_{1+}	3.1×10^{-23}
α_{CR}	1.1×10^{-17}
K_C	4×10^{-15}

Table 3.2.1.

a) Rate coefficients in the Mg neutral system.

C_{ij} collisional excitation

F_{ji} collisional deexcitation

S_i^+ electron ionisation

α_{CR} collisional radiative recombination

Calculated at $n_e = 2.10^{20}$ m^{-3} and $\hat{T}_e = 0{,}56$ eV. All values are taken from Drawin [35] except α_{CR} which is taken from Bates [42] and C_{01} and F_{10} which are taken from Vriens [41].

b) Same comment as a).

All values calculated from Drawin [35] except α_{CR} which is taken from Bates [42].

Generator: Philips PV 8490.
Nebulizer: Cross flow pneumatic.
Torch : Quartz tubing.

Symbol		unit	value
ϕ_c	orifice diameter of the carrier tube	mm	1.80
h	space between intermediate and outer tube	mm	0.80
R	inner radius of the outer tube	mm	9.00
r	radius tangential inlet	mm	1.5
q	tulip length	mm	12.0

Optimized operating conditions			
F_c	carrier gas	l/min	0.8
F_p	outer gas	l/min	16
F_i	intermediate gas	l/min	0.4 *
P	power	W	950
h	observation height above loadcoil	min	14

* No attention is paid to this parameter while optimizing the operating conditions since it has hardly any influence when aqueous solutions are nebulized [40].

Table 4.1.1.
Important characteristics concerning torch, plasma generator and nebulizer, and optimized operating conditions for the Mn II 2675 Å line.

Transition	E_m(eV)	g_m	λ_0	p	A(10^6 s^{-1})
4p – 4S	13,27	1	7514,65	2,34	43 (± 17%)
4d – 4p	14,71	3	6871,29	3,60	2,9 (± 25%)
5d – 4p	15,11	3	5606,73	5,20	2,29 (± 25%)
7d – 4p	15,45	9	5221,27	6,62	0,48 (± 25%)

E_m = energy upper level [49]
g_m = statistical weight upper level
p = effective quantum number upper level
A = transition probability [49]

Table 5.3.1.
Relevant properties of the four transitions used for the absolute intensity measurements. Data concerning line widths are supplied in appendix B.

wave length (Å)	Mg I/II	upper level: level (+)	upper level: $E_m^{(*)}$ (eV)	upper level: $g_m^{(*)}$	$A_{mn}^{(*)}$ ($10^8 s^{-1}$)	concentration (ppm)	relative or absolute measurement
5183,6	I	4^3S_1	5.11	3	0,575	500	absolute
4351,9	I	6^1D_2	7.19	5	0,21	500	absolute
5528,4	I	4^1D_2	6.59	5	0,14	500	absolute
4481,2	II	$4^2F_{5/2-7/2}$	11.60	14	2,25	500	absolute
2852,1	I	3^1P_1	4,35	3	4,95	1	relative
2802,7	II	$3^2P_{\frac{1}{2}}$	4,42	2	2,66	1	
2779,8	I	3^3P_2	7,18	5	3,92	500	relative
2798,0	II	$3^2D_{5/2}$	8,86	6	4,70	500	

* From ref. [49]
+ See ref. [50] for nomenclature of levels

Table 5.4.1.
Relevant properties of some Mg transitions.

Transition	(Å)	a(*)	$\Delta\lambda_g$(Å)	$\mathcal{T}_1$(+)	$\mathcal{T}_g$(++)	Λ(**) [21]	$1/\Lambda$ (eq. A.14)(+)
4p-4s	7514,65	0,21	$6,9*10^{-2}$	0,72	0,24	0,63	1,4
4d-4p	6871,29	0,64	$6,3*10^{-2}$	$1,3*10^{-3}$	$1,3*10^{-3}$	0,999	1,001
5d-4p	5606,73	1,6	$5,1*10^{-2}$	$2,2*10^{-4}$	$5,5*10^{-4}$	0,999	1,001
7d-4p	5221,27	2,6	$4,8*10^{-2}$	$3,9*10^{-5}$	$1,5*10^{-4}$	0,999	1,001
$4p-3p^6$	1048,0	0,96	$9,5*10^{-3}$	$7,5*10^{2}$	$1,2*10^{3}$	$3,0*10^{-2}$	$7,5*10^{+2}$
	1067,0	0,24	$9,6*10^{-3}$	$1,4*10^{4}$	$5,3*10^{3}$	$1,0*10^{-2}$	$1,4*10^{4}$
$5d \rightarrow 3p^6$	876,06	0,25	$8,0*10^{-3}$	$7,5*10^{4}$	$3,1*10^{4}$	$1,5*10^{-3}$	$7,5*10^{4}$
$3s \rightarrow 3p^6$	866,80	0,29	$7,9*10^{-3}$	$7,5*10^{4}$	$3,4*10^{4}$	$1,5*10^{-3}$	$7,5*10^{4}$
	879,95	0,10	$8,0*10^{-3}$	$6,0*10^{4}$	$9,1*10^{3}$	$1,0*10^{-3}$	$6,0*10^{4}$
	869,75	0,06	$7,9*10^{-3}$	$4,5*10^{4}$	$3,9*10^{3}$	$8,0*10^{-4}$	$4,5*10^{4}$

* $a = \sqrt{\ln 2}\ \Delta\lambda_l / \Delta\lambda_g$, the Voigt parameter
\+ only accounting for the Lorentz part of the line
++ only accounting for the Gaussian part of the line
** valid if $a \gg 100/\mathcal{T}_l$
calculated with R = 7 mm, $\mathcal{T} = k.R$.

Table A.1.
The optical depth of argon transitions in an ICP, calculated at $n_e = 5.10^{20}$ $1/m^3$, $\hat{T}_o = \hat{T}_e = 0,56$ eV.

monochromator width / line width	correction factor *
0	∞
1	1,52
2	1,31
5	1,12
8	1,08
10	1,06

* calculated with the assumption of a pure Lorentz broadened line and a rectangular monochromator profile.

Table B.1.
Correction factor for the measurement of spectral lines which have linewidths approaching the monochromator profile width. For a completely or partial Gaussian broadened line the correction factor will be closer to unity.

parameters are:
temperature (eV) ---------- +.58
electrondensity (m^-3)----------+.20%+21
neutral density p/kT (m^-3) ----------+.11%+25
thermal velocitys (m/s) ions -----+.17%+ 4
electrons -----+.45%+ 6
debye shielding parameter ----------+.27%+ 0

number	transition (jl coupling notation)	wavelength (Angstrom)	total gauss width (Angstrom)	total lorentz width (Angstrom)	tot. gauss width compared to lorentz
start at record 21					
001	3p 0- 3d 3	+876.06	+.00818	+.00056	+14.48497
002	3p 0- 3d'3	+866.80	+.00809	+.00061	+13.17762
003	3p 0- 4s 3	+1066.66	+.00996	+.00064	+15.57830
004	3p 0- 4s'1	+1048.22	+.00979	+.00245	+3.99246
005	3p 0- 5s 3	+879.95	+.00822	+.00025	+32.54551
006	3p 0- 5s'1	+869.75	+.00812	+.00016	+51.49961
024	4s 3= 4p 1	+9122.97	+.08519	+.03254	+2.61813
025	4s 3- 4p 5	+8115.31	+.07578	+.02722	+2.78372
031	4s 3= 4p'1	+6965.43	+.06504	+.02213	+2.93955
032	4s 3= 4p 1	+9657.78	+.09018	+.03637	+2.47931
033	4s 3- 4p'5	+8424.65	+.07867	+.02895	+2.71743
034	4s 3- 4p 3	+8103.69	+.07567	+.02791	+2.71094
035	4s 3= 4p 3	+8006.16	+.07476	+.02735	+2.73346
041	4s'1= 4p 1	+10470.10	+.09777	+.04221	+2.31614
043	4s'1- 4p'3	+7948.18	+.07422	+.02730	+2.71898
044	4s'1= 4p'1	+7724.21	+.07213	+.02694	+2.67730
046	4s'1= 4p 5	+9784.50	+.09137	+.03872	+2.35992
048	4s'1- 4p 3	+9224.50	+.08614	+.03564	+2.41715
050	4s'1- 4p'3	+8408.21	+.07851	+.03059	+2.56660
052	4s'1= 4p'1	+7503.87	+.07007	+.02540	+2.75813
053	4s 3= 5p 1	+4251.18	+.03970	+.01611	+2.46408
054	4s 3- 5p 5	+4200.67	+.03923	+.01615	+2.42890
059	4s 3= 5p'3	+3948.98	+.03687	+.01608	+2.29278
061	4s 3= 5p 5	+4300.10	+.04015	+.01656	+2.42488
062	4s 3- 5p 3	+4272.17	+.03989	+.01660	+2.40283
064	4s 3- 5p 1	+4198.32	+.03920	+.01776	+2.20682
066	4s 3= 5p'3	+4044.42	+.03777	+.01651	+2.28696
068	4s'1= 5p 1	+4522.32	+.04223	+.01766	+2.39093
071	4s'1= 5p'1	+4181.88	+.03905	+.01757	+2.22204
072	4s'1= 5p 1	+4702.32	+.04391	+.01905	+2.30478
076	4s'1- 5p. 1	+4510.73	+.04212	+.02036	+2.06901
080	4s'1- 5p'1	+4259.36	+.03977	+.01914	+2.07752
082	4s 3- 6p 3	+3554.30	+.03319	+.02285	+1.45262
087	4s 3- 6p 1	+3606.52	+.03368	+.02898	+1.16202
092	4s'1- 6p 1	+3834.68	+.03581	+.03255	+1.10011
137	4p 1- 4d 3	+6752.84	+.06306	+.04650	+1.35616
141	4p 5- 4d 7	+7372.12	+.06884	+.05824	+1.18204
162	4p 3- 4d 3	+7891.08	+.07369	+.06343	+1.16165
167	4p 1- 4d 1	+8620.46	+.08050	+.07150	+1.12586
175	4p'3- 4d 3	+8605.78	+.08036	+.07506	+1.07060
181	4p'1- 4d 3	+8761.69	+.08182	+.07761	+1.05418
184	4p 1- 5s 3	+10673.60	+.09967	+.07220	+1.38046
188	4p 5- 5s 3	+12487.60	+.11661	+.09733	+1.19808
196	4p 3- 5s 3	+13825.70	+.12910	+.11904	+1.08452
207	4p'3- 5s'1	+13008.50	+.12147	+.11269	+1.07796
214	4p 1= 5d 1	+5650.70	+.05277	+.06530	+.80802
216	4p 1- 5d 3	+5558.70	+.05191	+.06808	+.76247
219	4p 5- 5d 7	+6032.13	+.05633	+.06360	+.88562
239	4p 3- 5d'5	+5739.52	+.05359	+.08285	+.64689
245	4p 3- 5d 5	+6212.50	+.05801	+.10489	+.55307
255	4p'3- 5d'5	+6105.64	+.05701	+.09328	+.61118
267	4p'1- 5d'3	+6296.87	+.05880	+.09128	+.64417
272	4p 5- 6s 3	+7030.25	+.06565	+.06293	+1.04321
277	4p 3- 6s 3	+7311.72	+.06828	+.06933	+.98483
291	4p'3- 6s'1	+7206.98	+.06730	+.07353	+.91519
302	4p 5= 6d 7	+5495.87	+.05132	+.13188	+.38912
337	4p 5- 7s 3	+5888.58	+.05499	+.07015	+.78385
353	4p'3- 7s'1	+6025.15	+.05626	+.08672	+.64880
375	4p 5- 8s 3	+5421.35	+.05062	+.13755	+.36803
384	4p'3- 8s'1	+5534.49	+.05168	+.17423	+.29662

Table B.2.
Gaussian and Lorentzian parts of some argon line profiles. Not tabulated lines can be approximated by a calculated line in the same transition array [1].
The approach of Griem [1,22] has been used to evaluate the line-widths.
The listed widths are "Full widths at half maximum".

	levels	number	E_{eff} (eV)	g_j
(Ground level)	$3p^6$	1	0	1
	4s	2	11.65	12
	4p	3	13.17	36
	3d+5s	4	14.09	72
(ion ground level)	$2p^5$	+	15.76	6

Table C.1.
Effective energies and statistical weights of the considered levels in the simplified Argon I system.

q-p	λ_{eff}(Å)	A_{eff} 10^8 1/s	Λ	A.Λ 1/s
3-0	880	0,290	10^{-3}	$2,9 \times 10^4$
1-0	1048	1,57	10^{-2}	$1,6 \times 10^6$
	1067		10^{-2}	
2-1	8173	0,36	0,85	$3,1 \times 10^7$
3-2	13430	0,127	1	$1,3 \times 10^7$

Table C.2.
Effective transition probabilities, wavelengths and escape factors for radiative transitions between levels in the simplified Ar system, $n_e = 5.10^{20}$ 1/m^3, $\hat{T}_e$ = 0,56 eV.

level designation	level	energy (eV)	multiplicity	
0	3^1S_0	0	1	Ground state
1	3^3P_{0--2}	2,72	9	
2	3^1P_1	4,35	3	
3	4^3S_1	5,11	3	
4	4^1S_0	5,39	1	
+	$3^2S_{1/2}$	7,64	2	ion ground state

level designation	level	energy (eV)	multiplicity	
0	$3^2S_{1/2}$	0	2	ion ground state
1	$3^2P_{1/2,3/2}$	4,43	6	
2	$4^2S_{1/2}$	8,66	2	
3	$3^2P_{3/2-5/2}$	8,86	10	
4	$4^2P_{1/2,3/2}$	10,0	6	
+	$^1S_0$	15,04	1	doubly charged ion ground state

Table D.1.

a) Relevant quantities of levels in the MgI system.

b) Ditto for the MgII system.

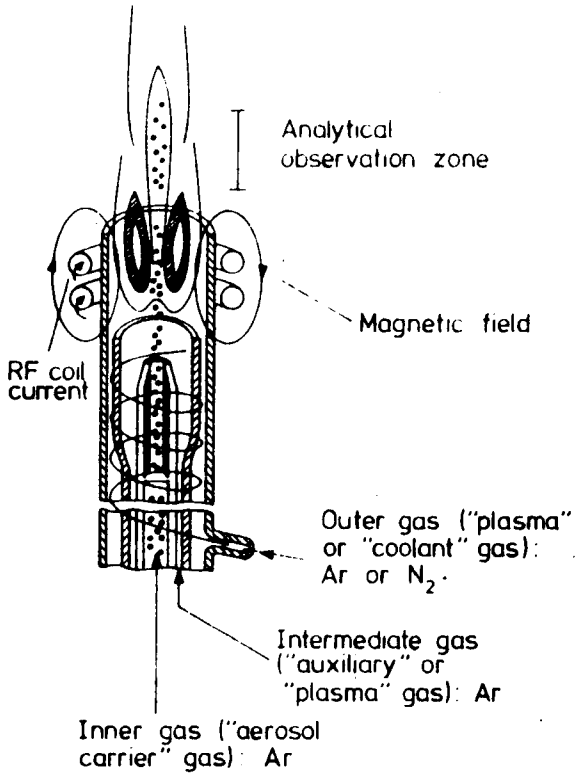

Fig. A.

Schematic drawing of a toroidal ICP. The figure shows three concentric tubes (the "torch") placed in a water-cooled induction coil of an RF generator. The RF current through the coil induces a magnetic field, which, in turn, produces an RF current in the flowing, conducting gas. Two or three gas flows are used. From: Boumans [67].

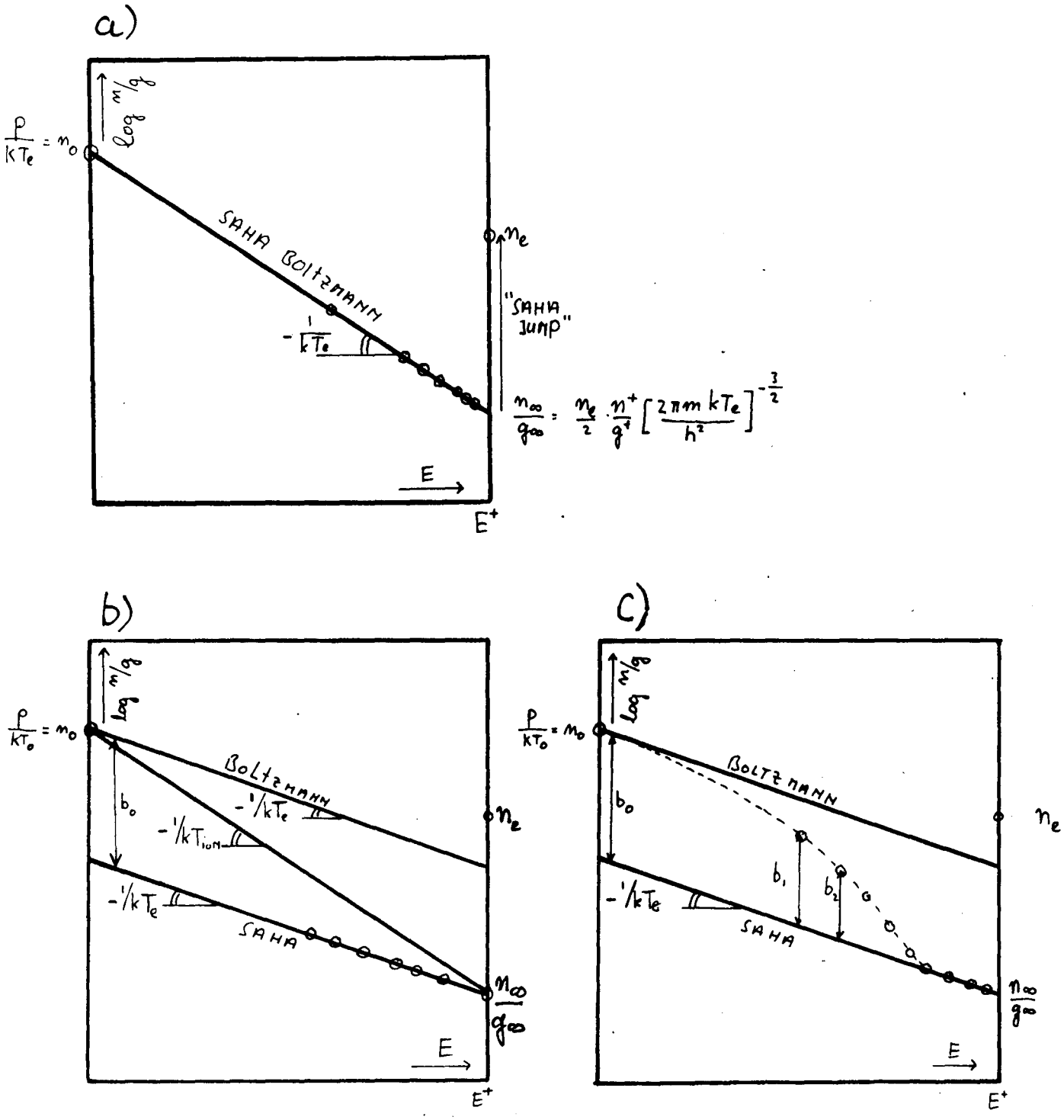

Fig. 2.0.1.

a) Boltzmann plot of an LTE population density in a plasma. For meaning of symbols refer to formula's 2.0.0-2.0.3.

b) Ditto for pLTE, an over population of the ground level is taken as an example (ionizing plasma).

c) Further deviations from pLTE, no easy temperature definition is possible. Many excited levels are under or over populated with respect to the Saha population.

a)

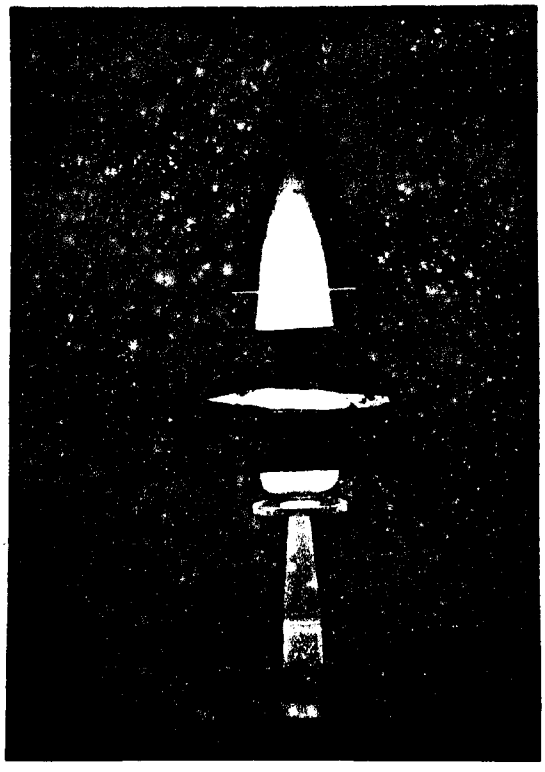

b)

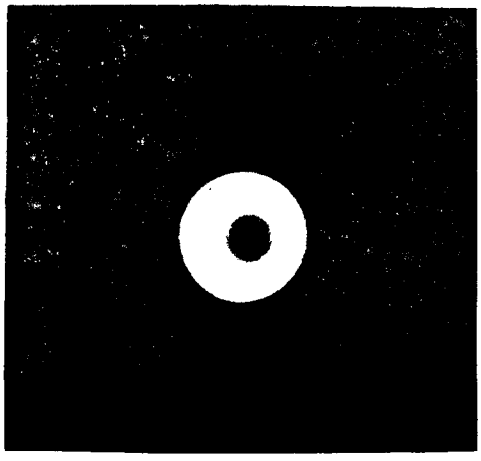

Fig B.

a) Side-on view of a conventional argon ICP.
b) End-on view of an ICP.

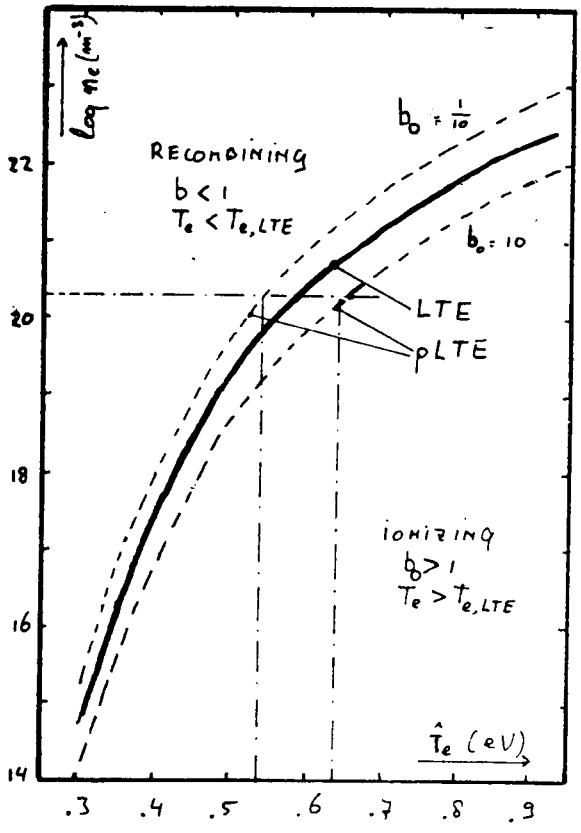

Fig. 2.1.1.
The relation between n_e and T_e for an LTE plasma (solid curve) and a pLTE plasma (factor 10 under or over population of the ground level, dashed curve).

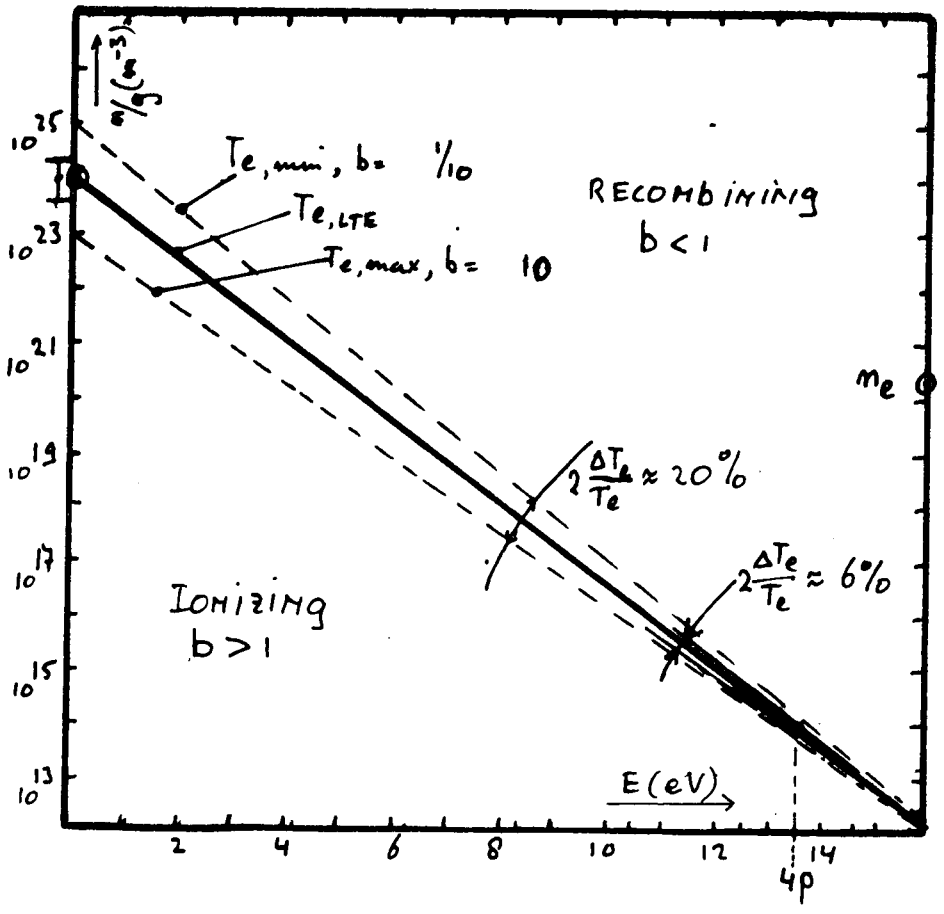

Fig. 2.1.2.
The Boltzmann plot for the population densities of excited states in the pLTE regime. Saha population densities are drawn for the minimum and maximum temperatures, as well as the equilibrium temperature. Note that the variation in n_o resulting from $T_o \neq T_e$ is small compared to the over population b_o (see error bar on the left axis).

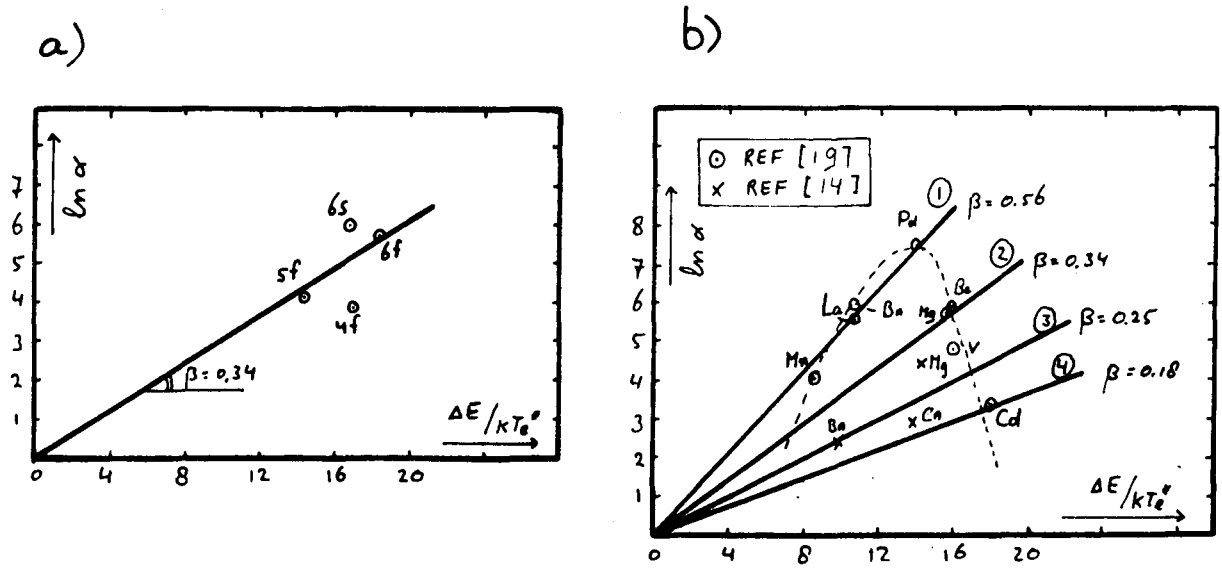

Fig. 2.1.3.

a) Measured [19] relative line intensities divided by calculated LTE relative line intensities in the Mg ion system. The systematic temperature error is given by the slope of the line. Note that at the vertical axis the natural logarithm is plotted.

b) Measured ionic/atomic line intensity ratios divided by LTE ionic/atomic line intensity ratios extracted from Furuta et al. [14] and Boumans et al. [19].

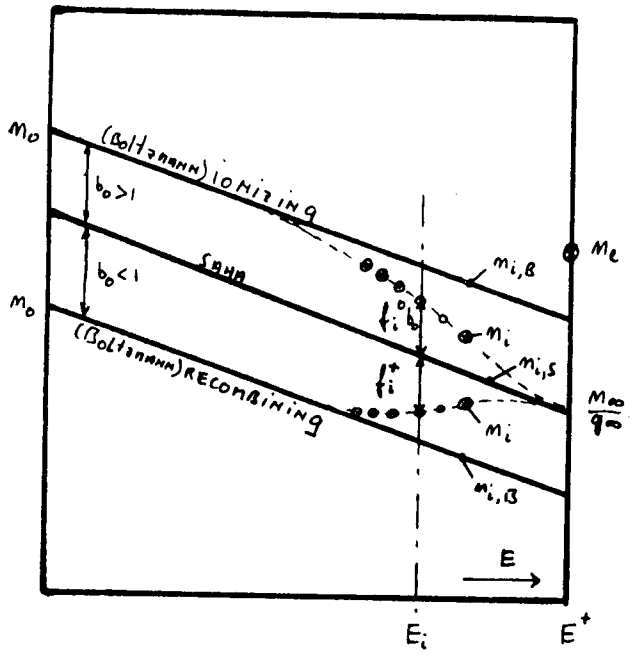

Fig. 2.3.1.
Over population factor with respect to the Boltzmann and Saha equations for an ionizing and a recombining plasma.

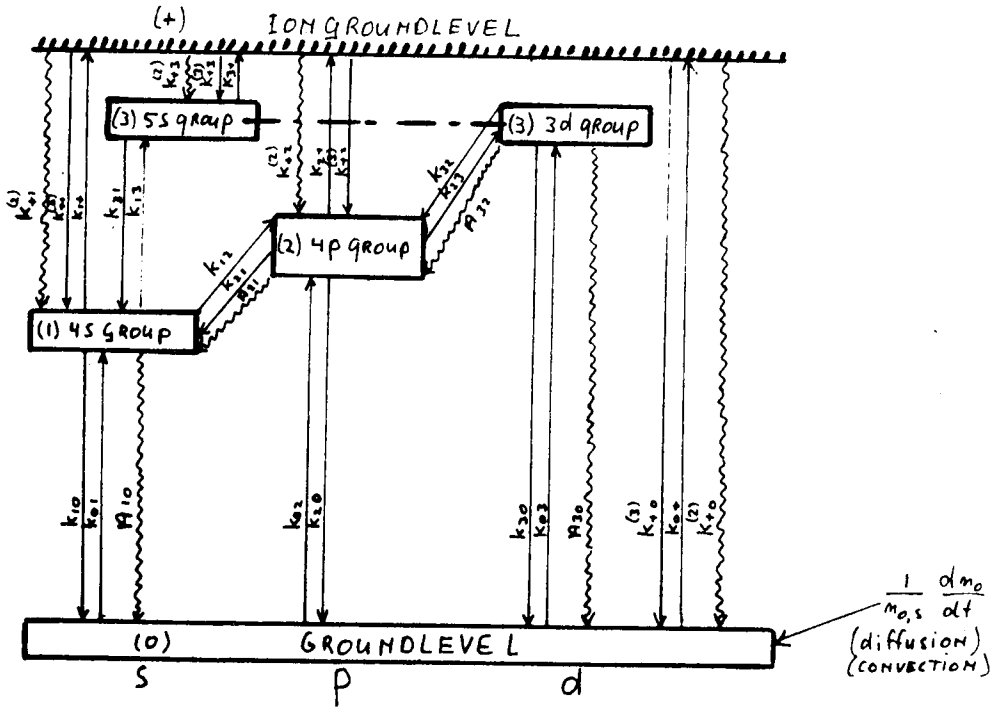

Fig. 2.2.1.
Simplified argon I level diagram showing transitions to be used in the balance equations. Curly arrows indicate radiative transitions. Note that the 3d and 5s group are treated as one effective level.

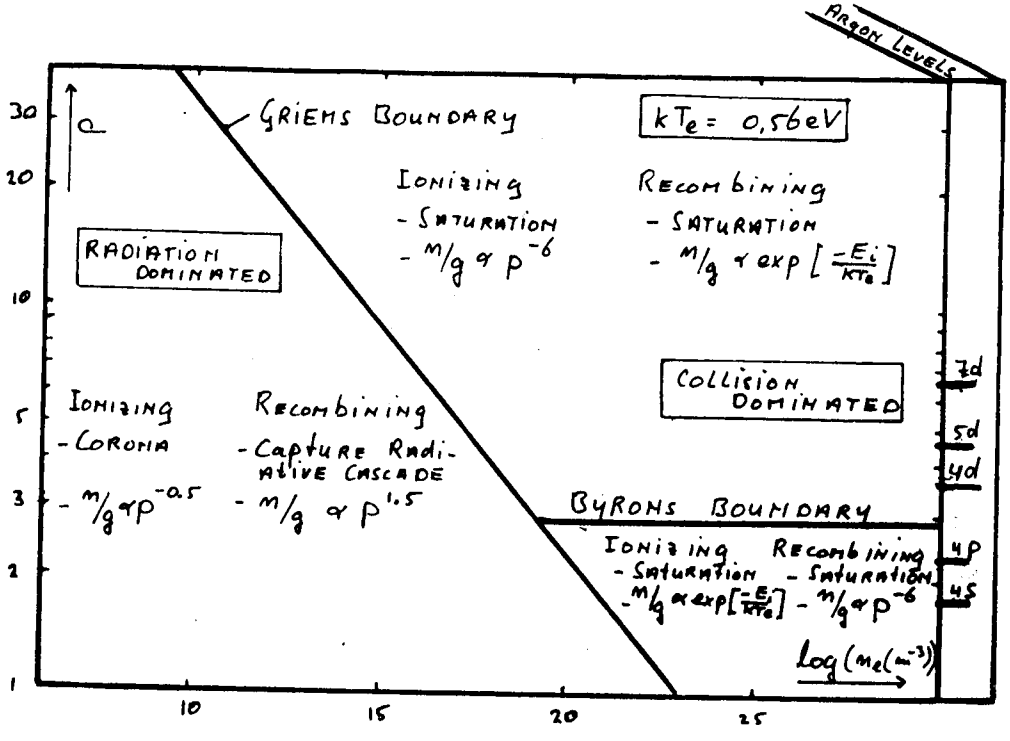

Fig. 2.3.2.
The various regimes of plasma modelling in a n_e-p diagram, p is the effective quantum number defined by $p_i = (E_H/E^+ - E_i)^{\frac{1}{2}}$. The Griem and Byron boundaries are given by eqs. (2.3.8) and (2.3.15) respectively.

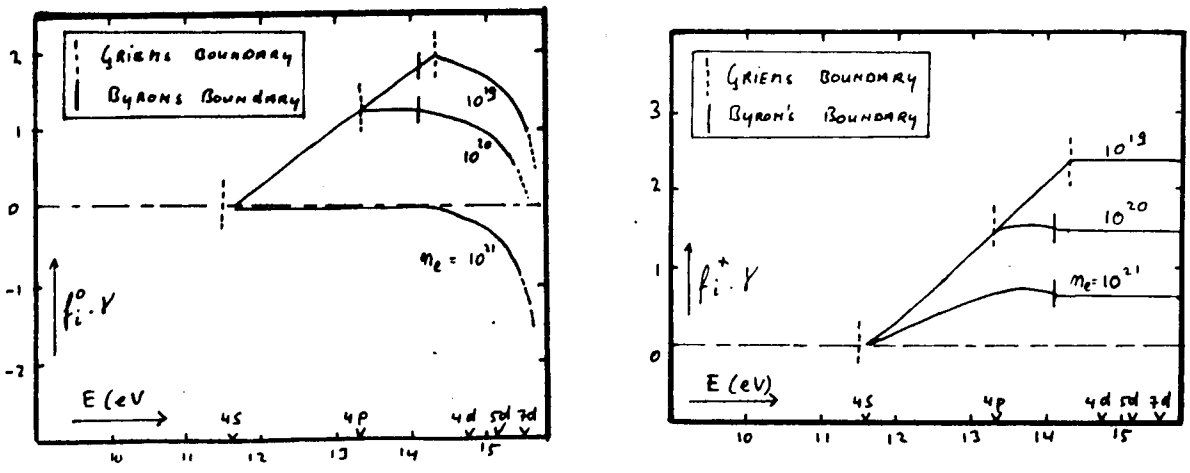

Fig. 2.3.3.
Saha Boltzmann coefficients for a) a purely ionizing plasma and b) a purely recombining plasma. In this figure for the level 4s the Saha Boltzmann coefficients are arbitrarily set to unity. This is necessary since the relation between the population densities of the 4s level and the ground level is not known. γ is an arbitrary constant accounting for this unknown 4s population. Argon levels are indicated along the energy axis.

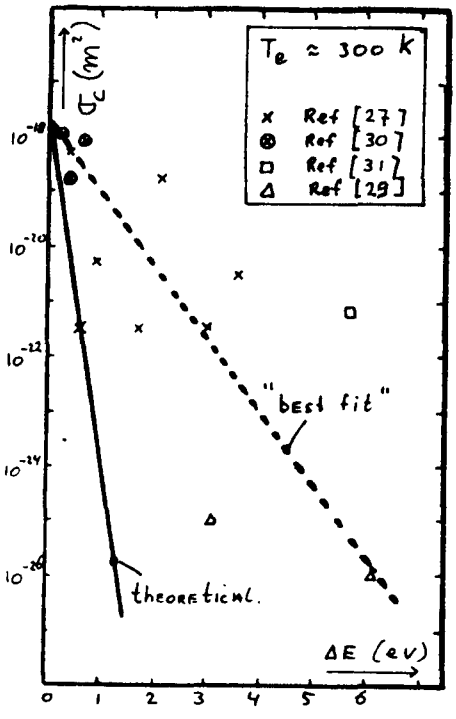

Fig. 3.1.1.
Predicted (eq. 3.1.3) and observed cross sections for non resonant charge transfer. The constant A in eq. 3.1.3 is taken equal to 2.10^{-18} m^2, a rough approximation for the cross sections for resonant charge transfer, uncertainties of two orders of magnitude are possible.

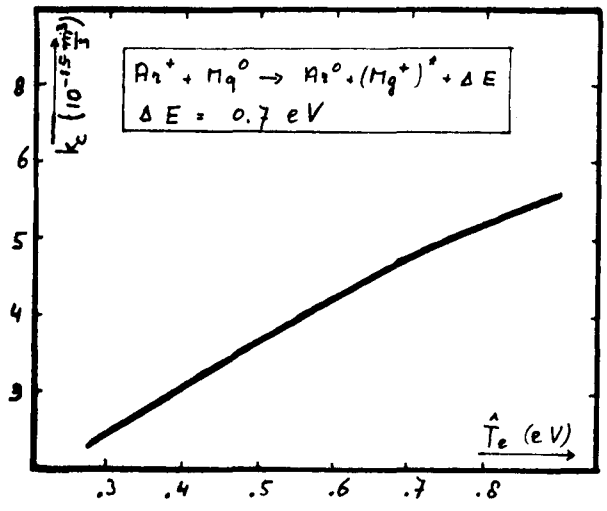

Fig. 3.1.2.
Rate coefficients calculated from eq. (3.3.8, 3.1.10) for charge transfer between argon ions and magnesium atoms. Charge transfer on the levels $3^2P_{5/2,3/2}$ and $4^2S_{1/2}$ is considered. Energy defect is 0,7 eV. The uncertainty in the value of this cross section is a factor 10

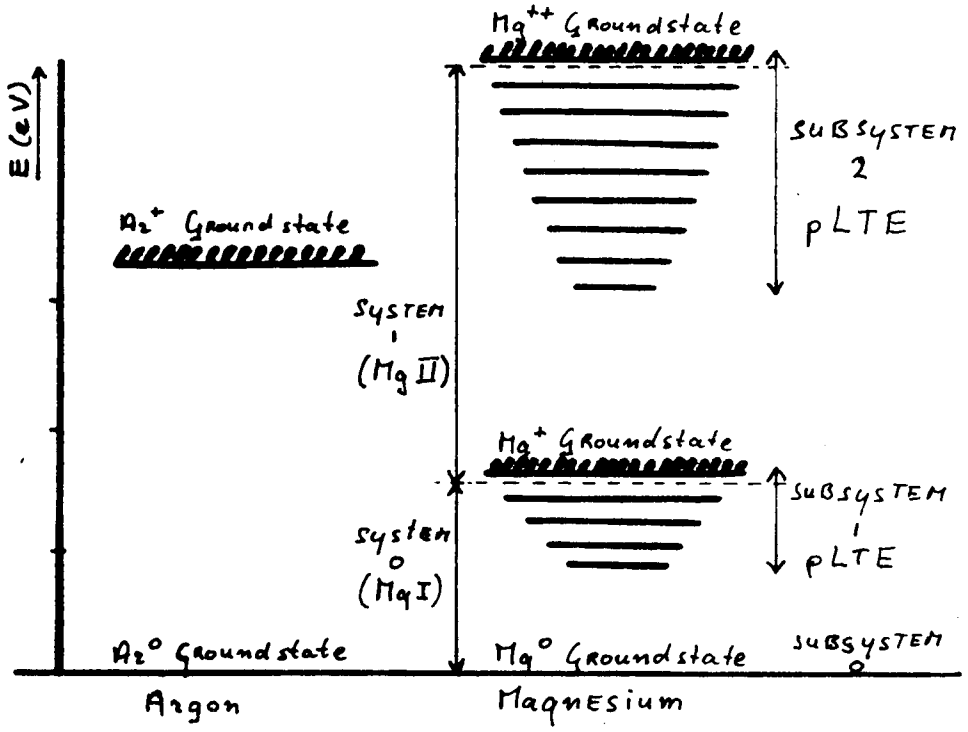

Fig. 3.2.1.
Division of the excited states of Mg in systems and subsystems.

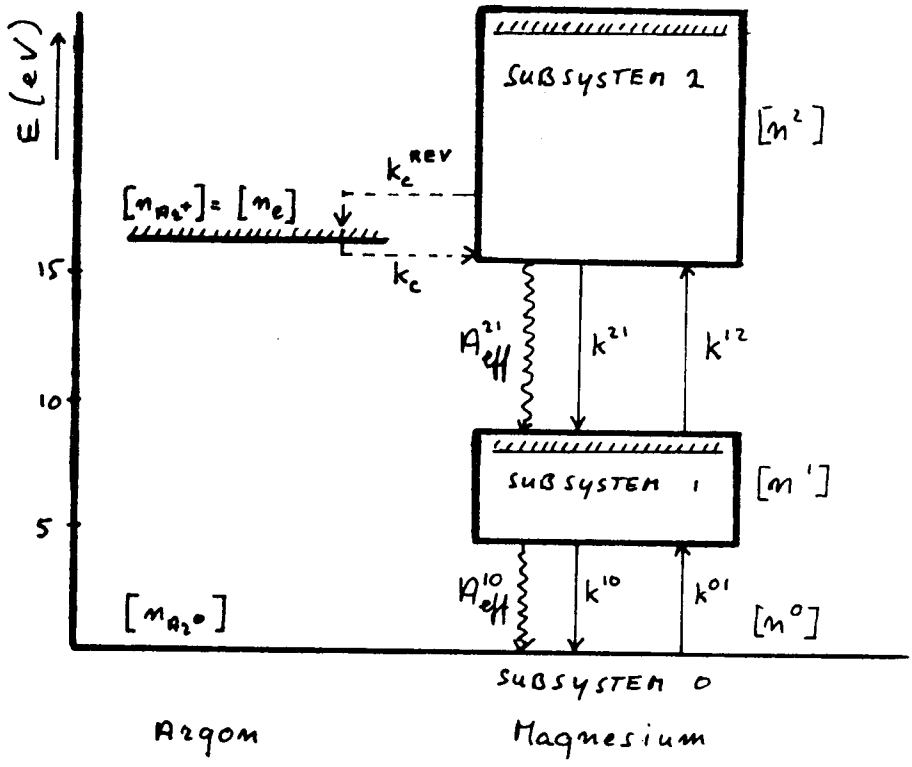

Fig. 3.2.2.
Radiative (curly arrows) collisional (straight arrows) and charge transfer (dashed arrows) transitions between Mg subsystems and Ar I system. The levels in a subsystem (squares) are in pLTE, densities are in square brackets.

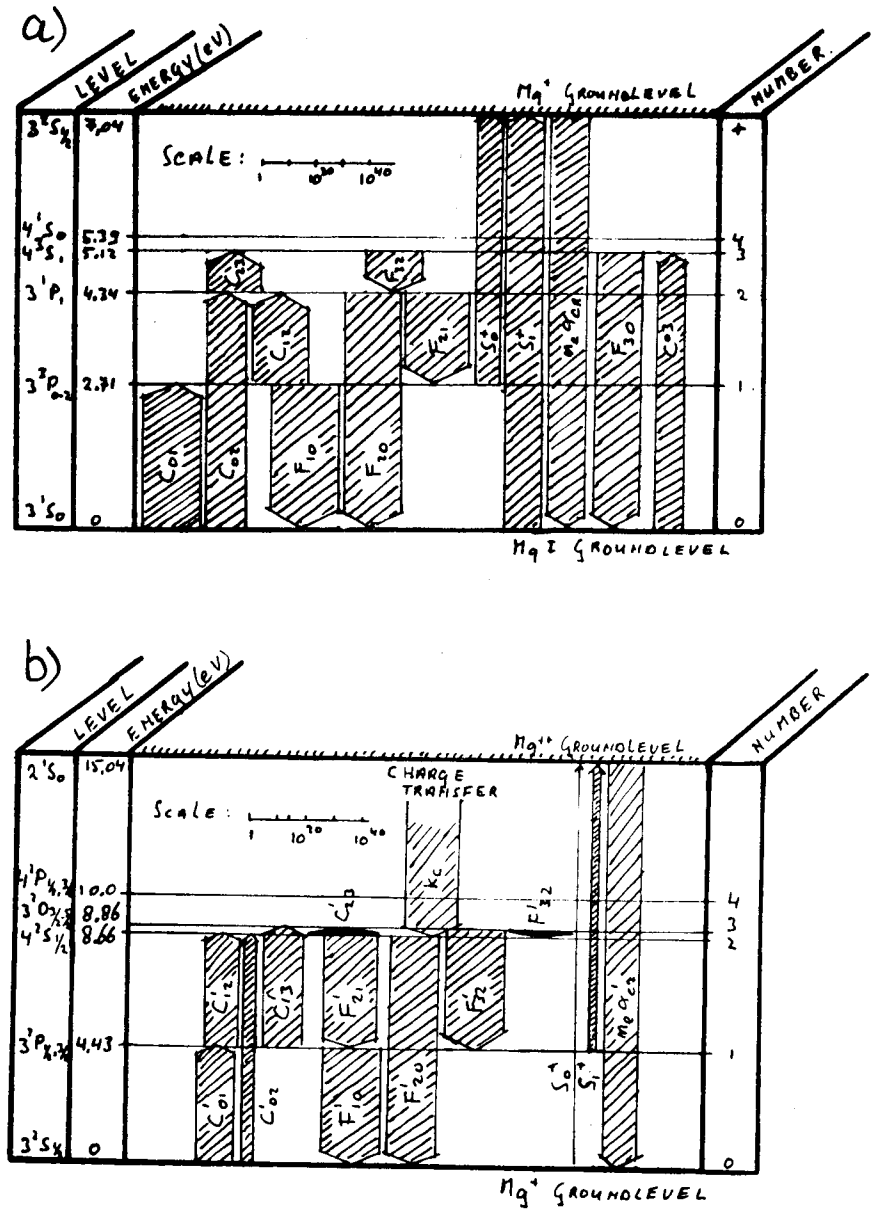

Fig. 3.2.3.
Visualisation of the rate coefficients in the levels of the MgI system (a) and the Mg II system (b). The width of an arrow indicates roughly the magnitude of the transition rate (see scale bars in the figures).

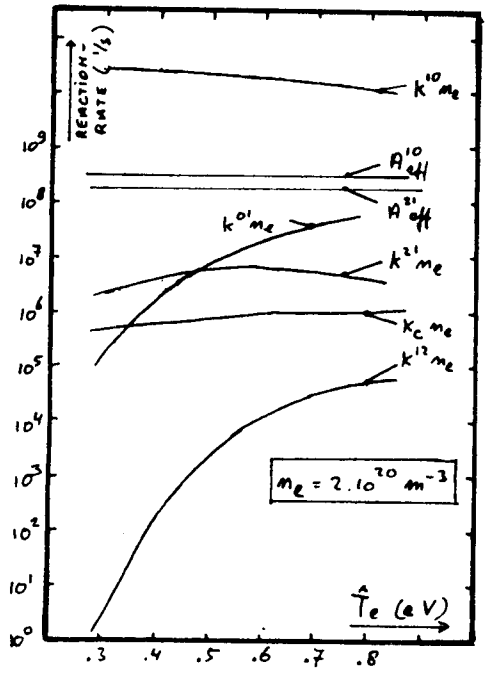

Fig. 3.2.4.
The reaction-rates as we substituted them in the balance equation. Reaction rates are calculated at $n_e = 2.10^{20}$ $1/m^3$ as a function of electron temperature.

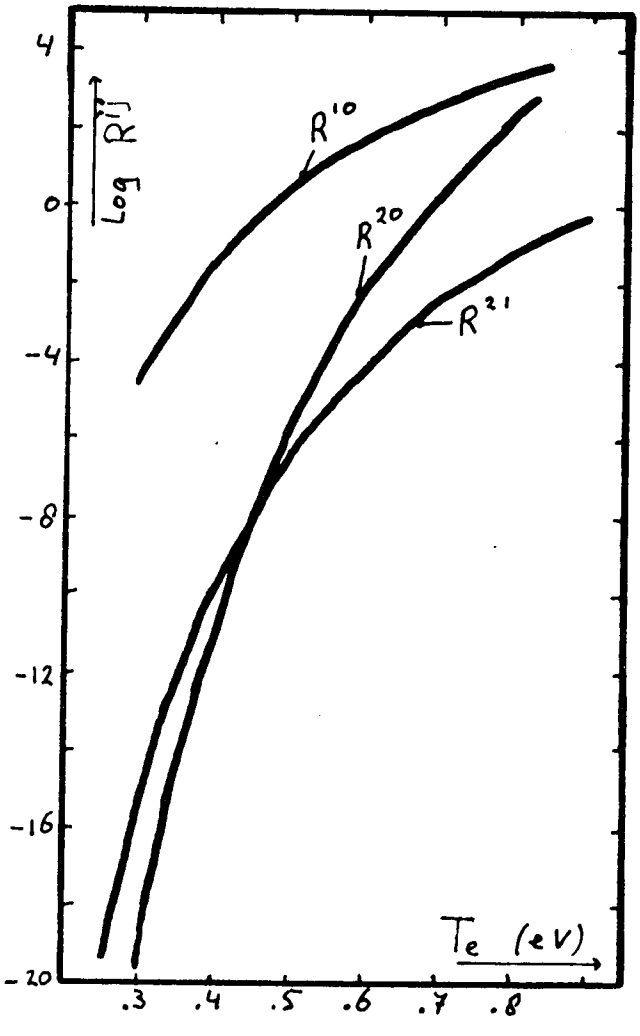

Fig. 3.4.1.
Relative Saha populations R^{ij} of the subsystems 1-2 of Mg. $R^{ij} = n_s{}^i/n_s{}^j$.

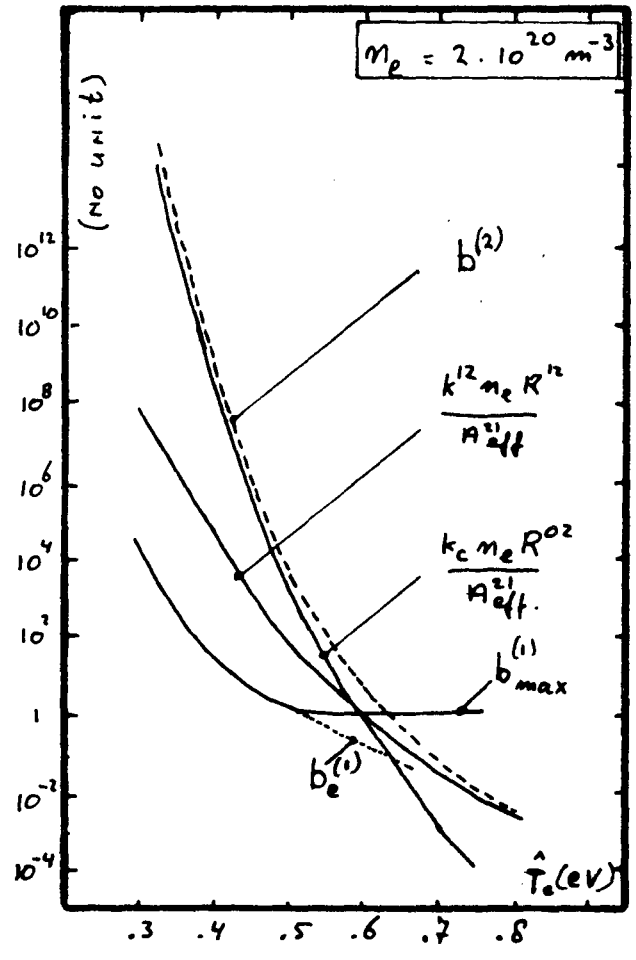

Fig. 3.4.2.
Various terms in the solution of the time independent rate equation. The net over population of the ion system with respect to the atom system is given by the difference between curves $b^{(2)}$ and $b^{(1)}_{max}$. If $\hat{T}_e < 0{,}55$ eV, charge transfer is the dominant population mechanism of subsystem (2). If $\hat{T}_e > 0{,}65$ eV collisional excitation is the dominant population mechanism.
The dotted curve marked $b_e^{(1)}$ is not calculated and represents a possible under population of the atom ground state with respect to the excited level population.

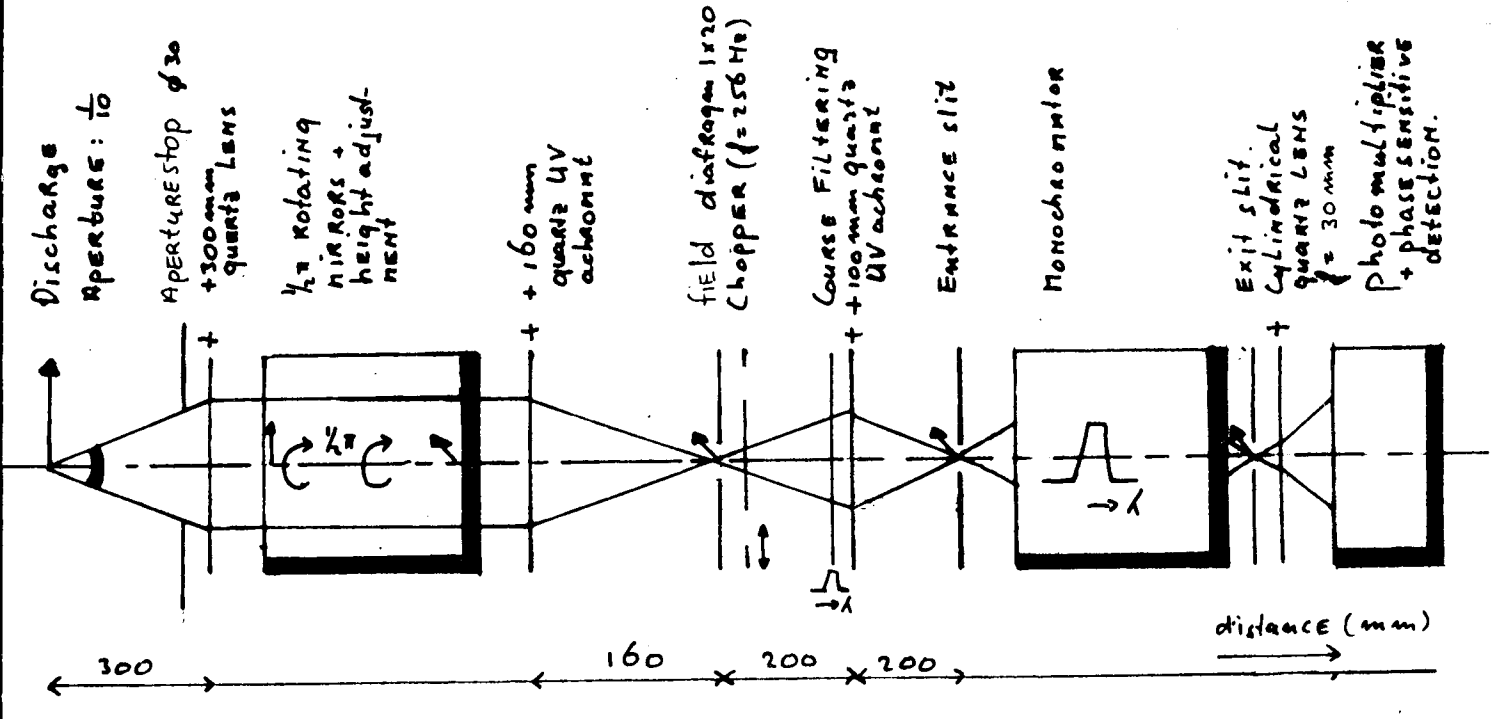

Fig. 4.2.2.
Entrance optics used in the present work.

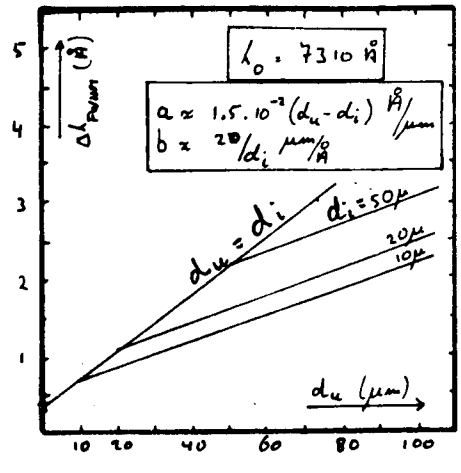

Fig. 4.1.1.
The FWHM of the monochromator profile at 7310 Å as a function of exit and entrance slit widths, the flat top (a) and slope (b) of the trapezium or triangular shaped profile are given by the formulas.

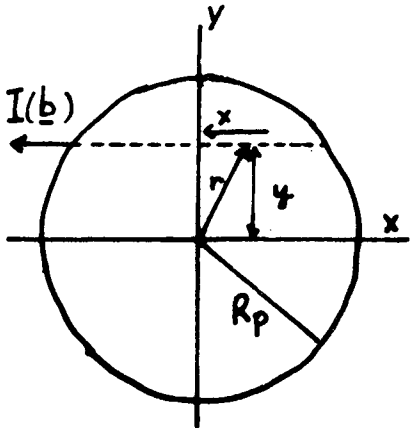

Fig. 5.1.1.
The coordinate system and other relevant properties used for the determination of radial intensity distributions from measured lateral distributions.

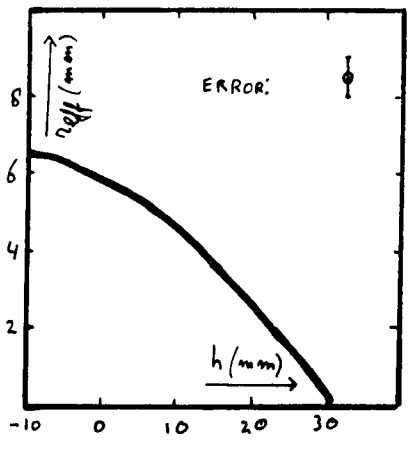

Fig. 5.1.3.
Photographically determined effective emission radius as a function of the height above the load coil.

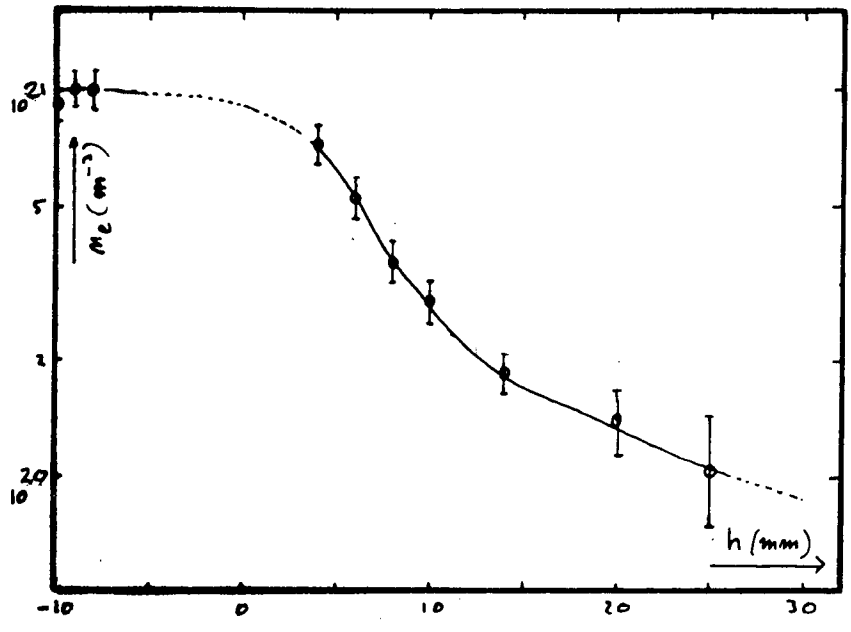

Fig. 6.1.1.
The electron density (n_e) determined from the starkwidth of the H_β transition as a function of the height above the load coil (h).

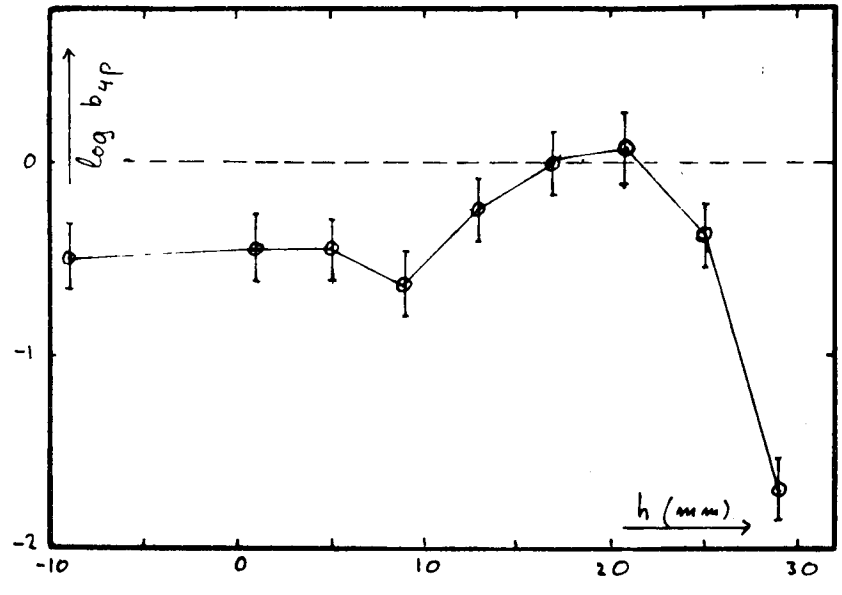

Fig. 6.1.3.
The over population of the 4p level (b_{4p}) with respect to the levels 4d, 5d and 7d. Note the minimum at h = 10 mm. Note that if $b_{4p} < 1$ an under population is the case.

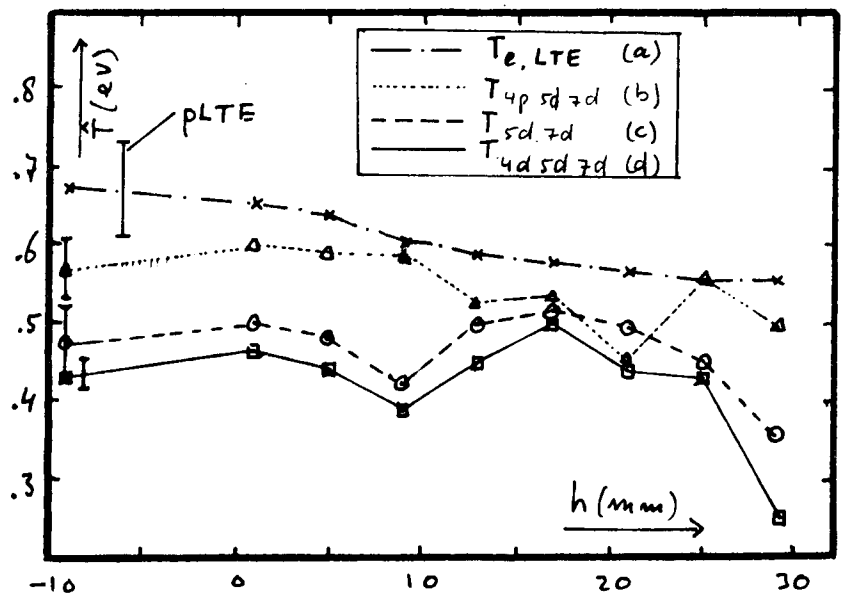

Fig. 6.1.2.
Excitation temperature derived from the argon intensity measurements (T_{pqr}) and from the electron density (T_{eLTE}) (see section 1.1). Note the large difference in the excitation temperatures at some heights, and the slight minimum at h = 10 mm. Error bars are given at the left side of each temperature plot. The error bar marked "pLTE" indicates the temperature clenching as described in section 2.1 with $1/10 < b_o < 10$.

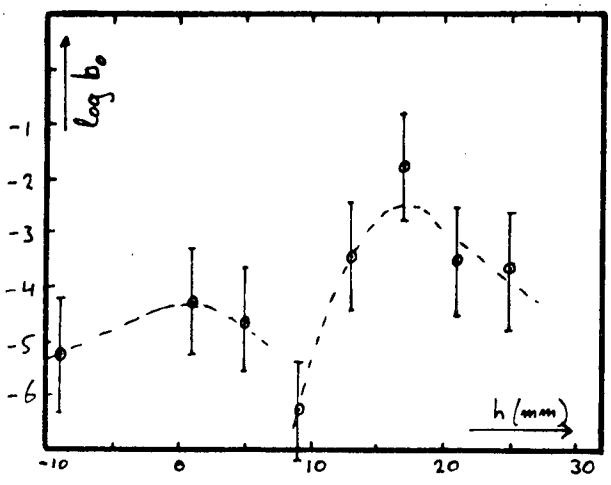

Fig. 6.1.4.
The over population of the ground level (b_o) with respect to the Saha population. Note the apparent discontinuity in the region $5 < h < 9$. This is believed to be due to cold air penetrating the discharge just above the rim of the outer tube.

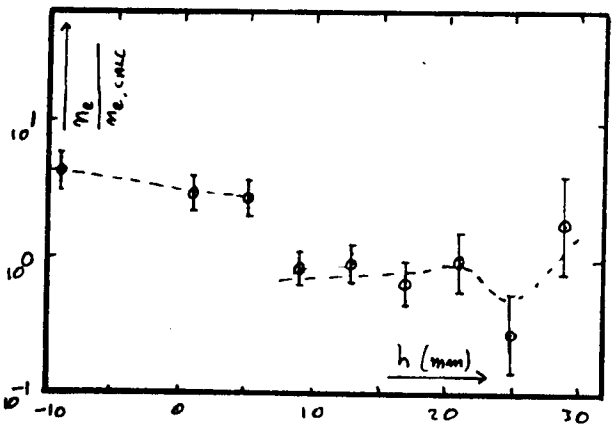

Fig. 6.1.5.
The ratio of measured electron density from Stark widths (n_e) and the electron density determined from the absolute level densities of levels 4d, 5d and 7d ($n_{e,calc}$). Note the discontinuity in the region $5 < h < 9$.

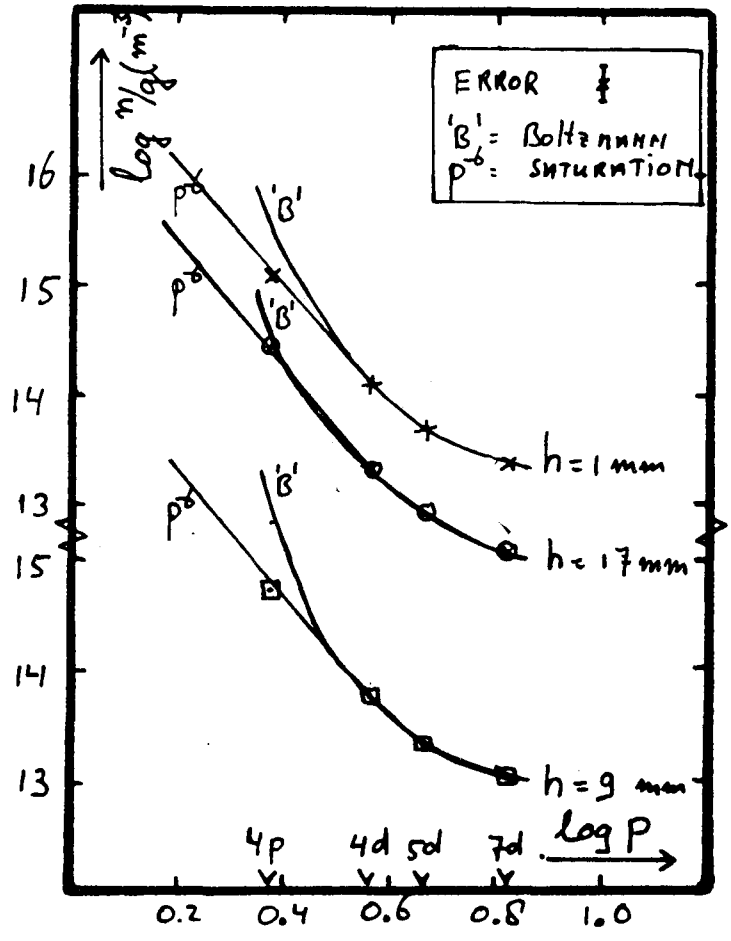

Fig. 6.1.6.
Saturation phase and Boltzmann distributions for various heights in the discharge. Note the very small difference between those two population densities at h = 17 mm.

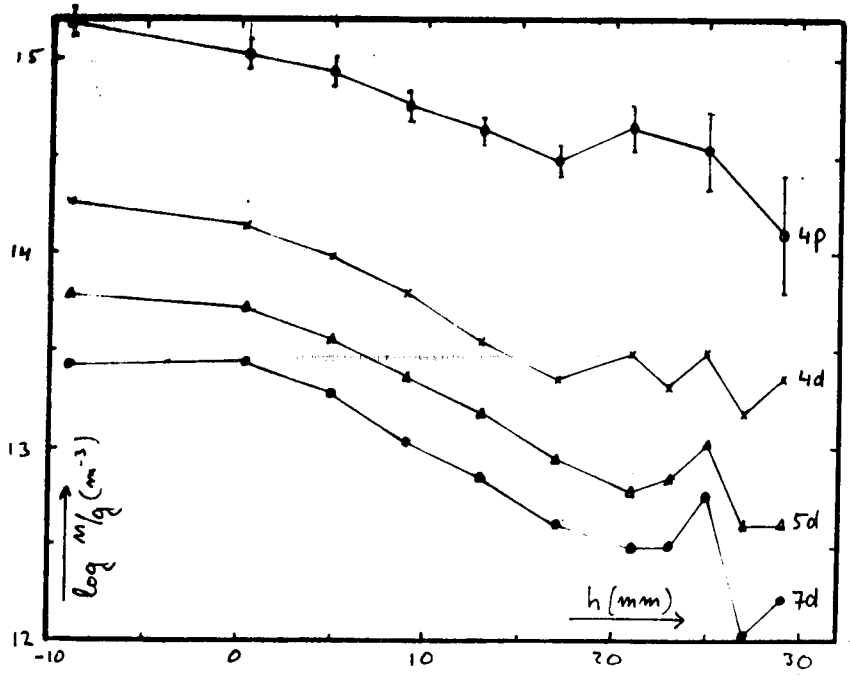

Fig. 6.1.7.
Population densities of the measured levels as a function of the height above the load coil. The rather peculiar behaviour at $h \approx 25$ mm may be due to the mixing of cold outer (argon) gas with the hot annulus gases.

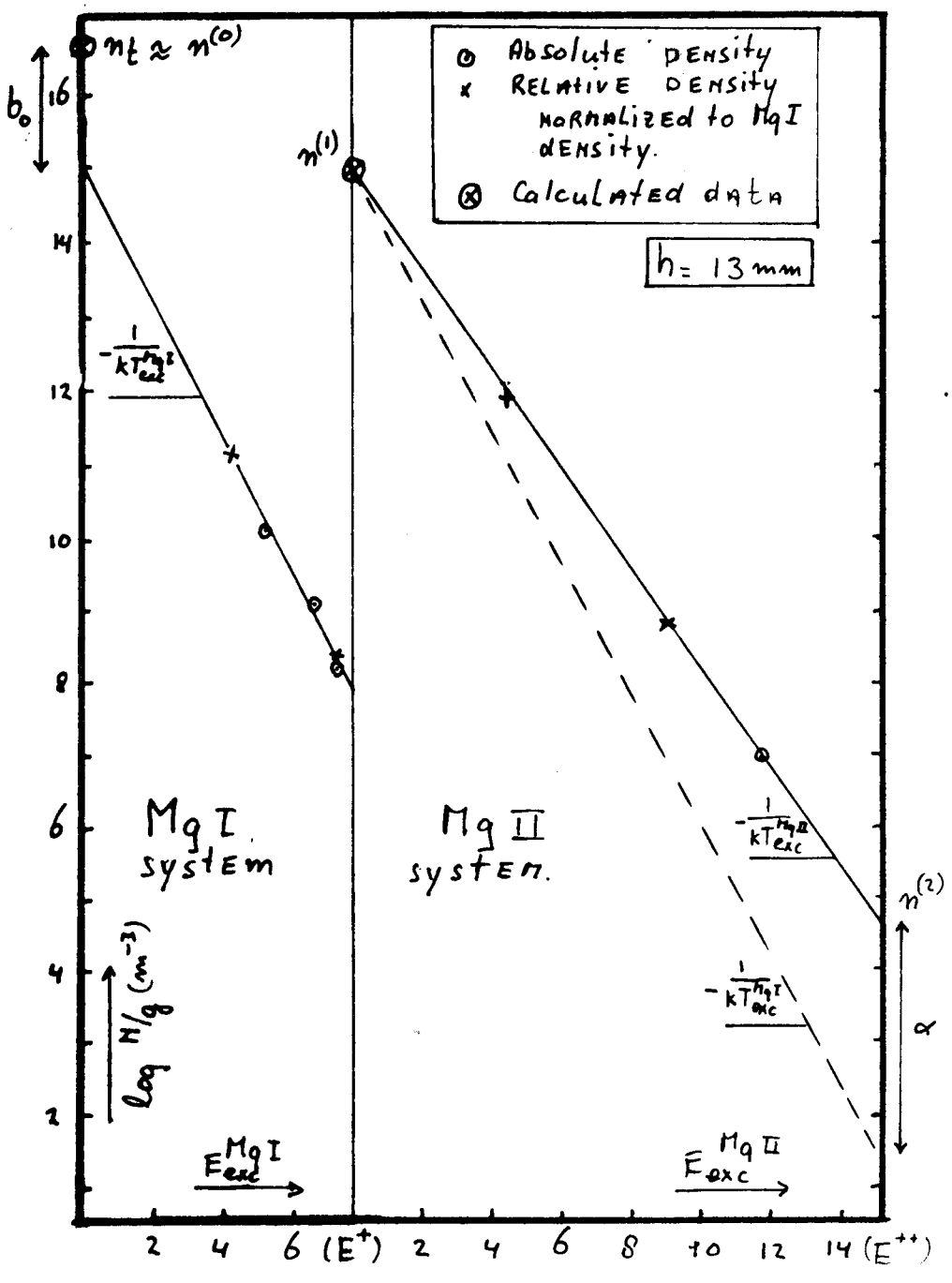

Fig. 6.2.1.
As an example the Boltzmann plot for h = 13 is supplied. Various quantities which can be derived from this plot are indicated. Note the appearing difference between the slope of the straight lines in the I and II system.

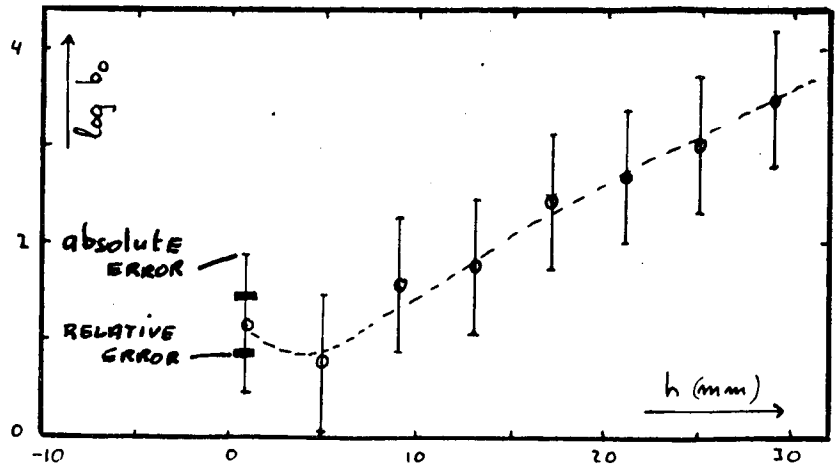

Fig. 6.2.2.
The over population of the Mg neutral ground state. The Mg neutral ground state density is calculated from eq. 6.2.1.

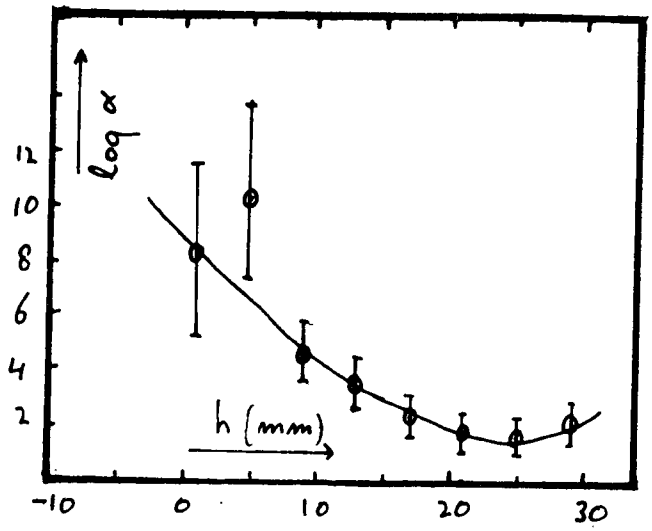

Fig. 6.2.3.
The over population of analyte doubly charge ions with respect to singly charged ions ($b^{(2)}/b^{(1)} = \alpha$) (see also Fig. 6.2.1 for definition).

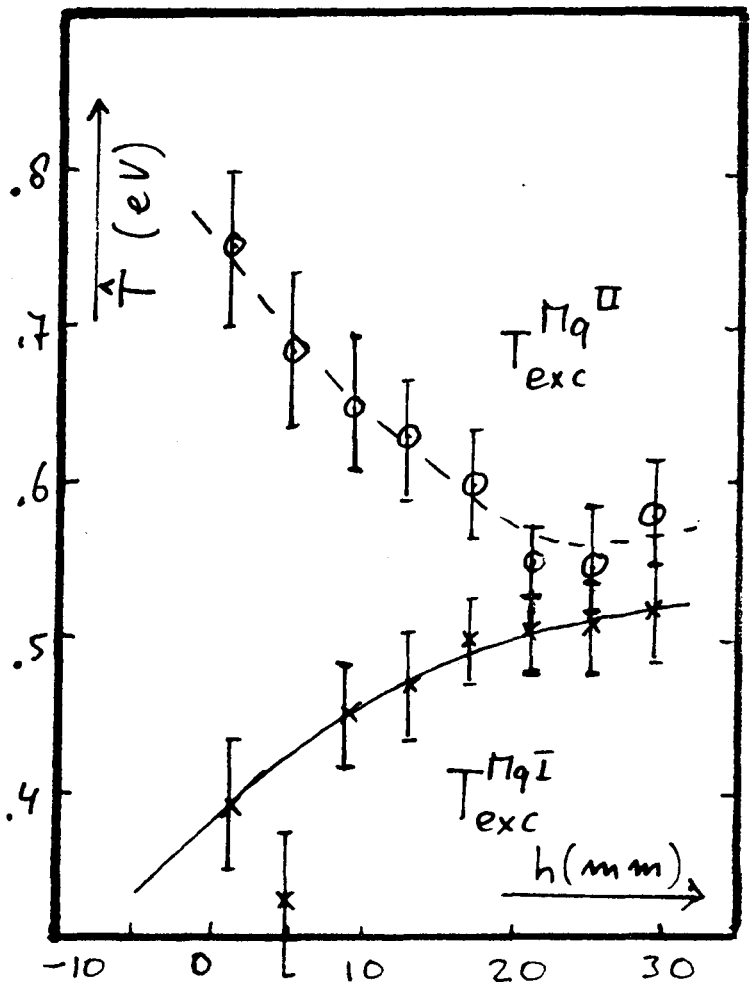

Fig. 6.2.4.
The excitation temperatures of the MgI and MgII systems. Note that the ionisation equilibrium can also be described by the temperature T_{exc}^{MgI} (see Fig. 6.2.1.).

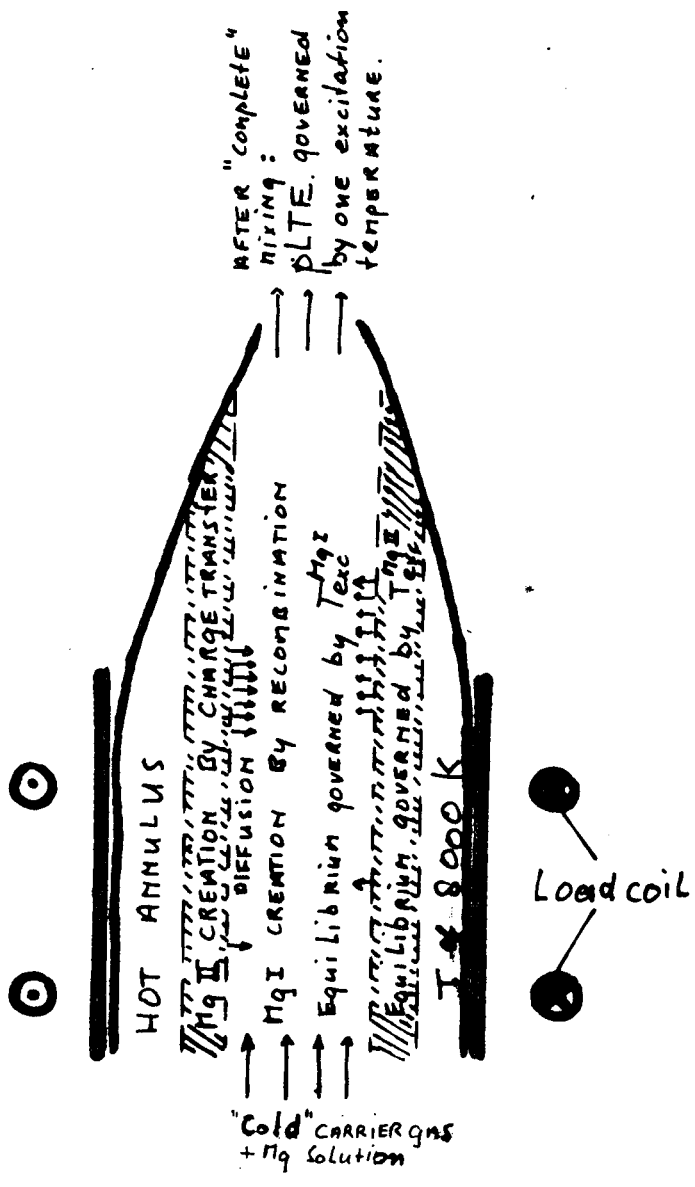

Fig. 6.2.5.
Visualisation of the proposed excitation mechanism in an ICP. Note that the analytically favourable behaviour of an ICP AES source is due to a) spatial inhomogeneities and b) the existence of a charge transfer channel to create Mg ions via direct way. The hatched area is the area with substantial pLTE (and LTE) deviations. This area is also indicated by Furuta et al. [14].

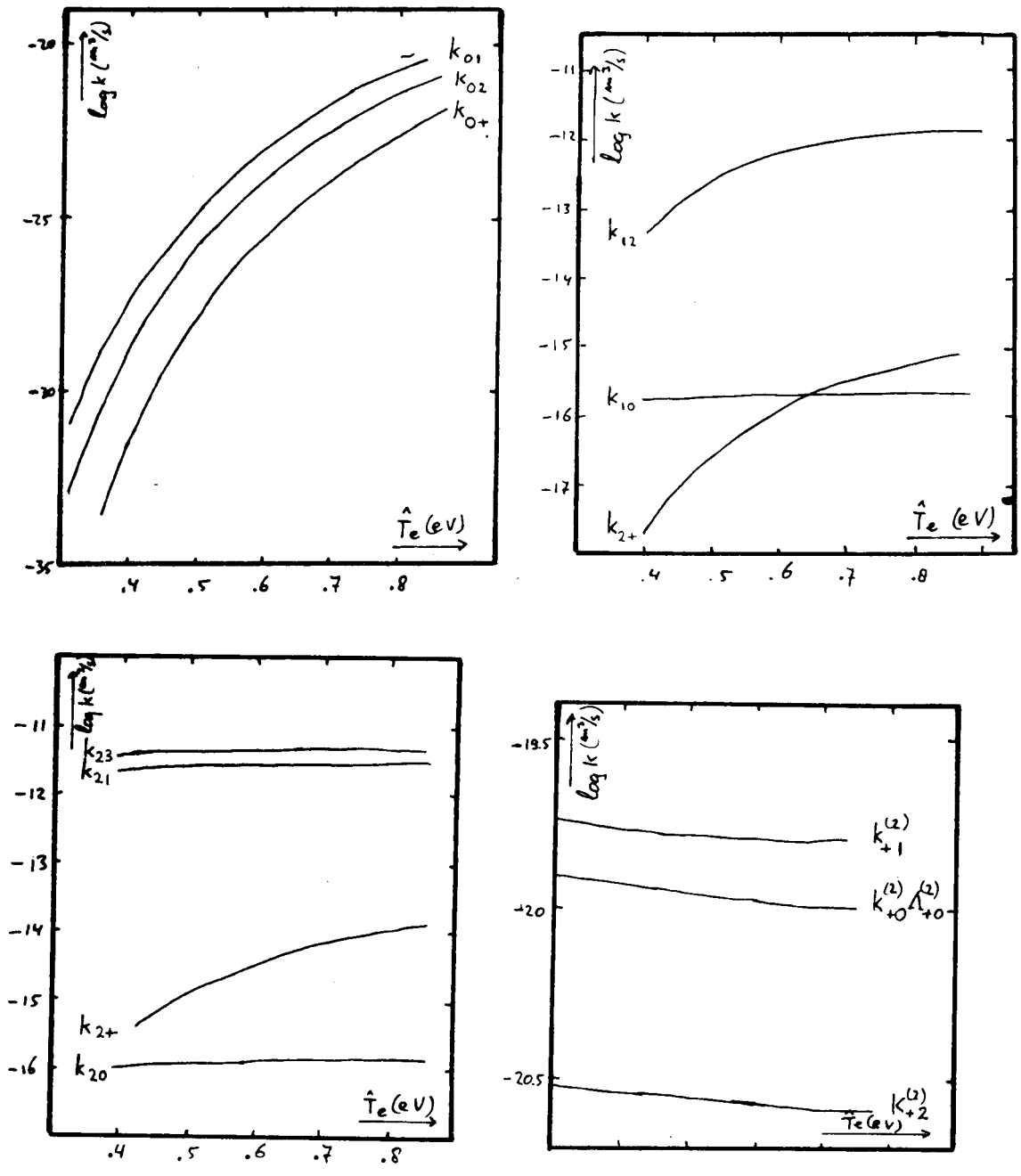

Fig. C.1.
Rate coefficients in the argon neutral system.

a) Transitions from or to the ground state, a linear approximation for the cross section has been used (see text).
b) Transitions from or to the 4s group. The approach of Vriens [41] has been used.
c) Transitions from or to the 4p group, again the Vriens approach is used.
d) Radiative recombination rates. Hydrogenic approaches are used for transitions to excited states. An empirical value is used for the transition to the ground state. In this latter value for recombination radiation trapping is accounted.

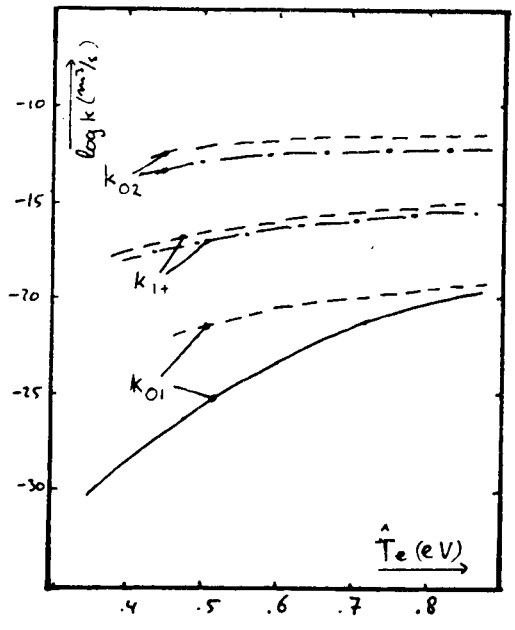

Fig. C.2.
Comparison of various rate coefficients
- lineair approach of the ground state transitions [21]
- Vriens [41] hydrogenic approach
- Drawin [35] hydrogenic approach.

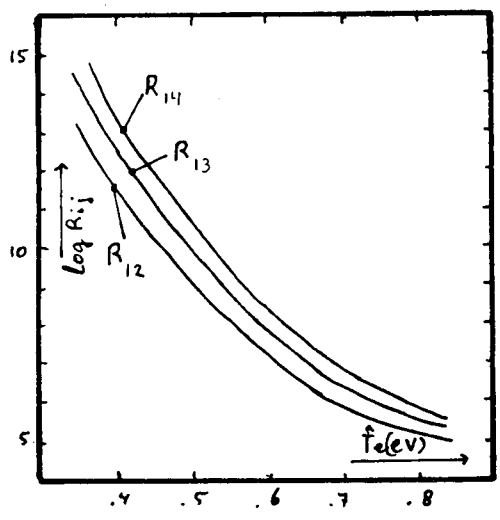

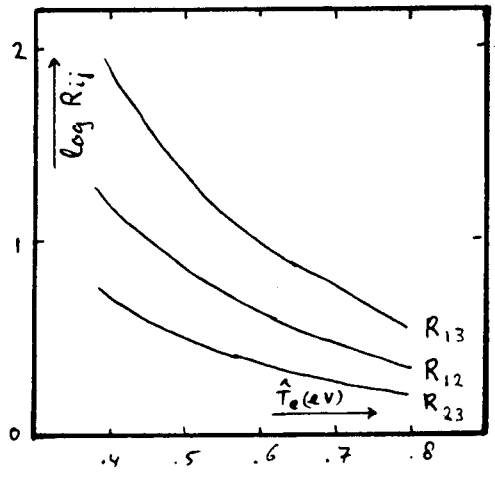

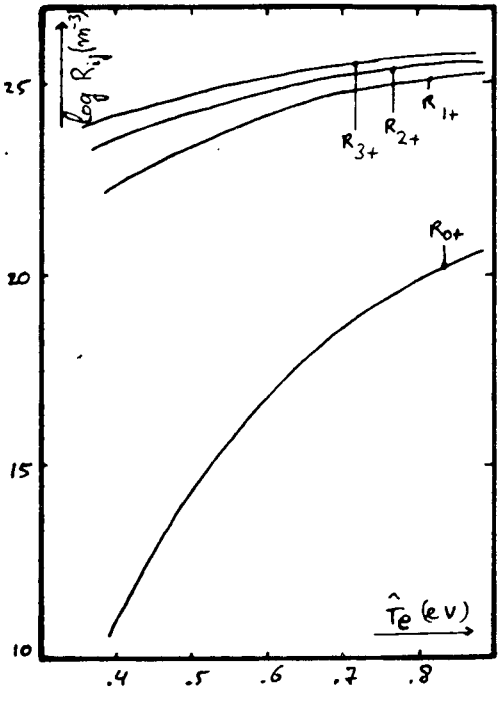

Fig. C.3.
The coefficients R_{ij} (a,b) and R_{i+} (c) as a function of temperature. For definition see text of section 2.2.

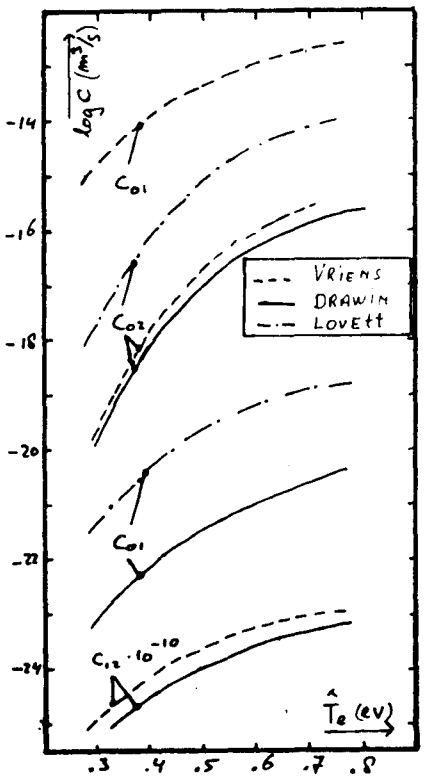

Fig. D.1.
Rate coefficients for electron excitation by electron impact in the MgI system. Note that according to Drawin C_{01} is much smaller than C_{01} according to Vriens. This is caused by the change in multiplicity and the, accordingly very low oscillator strength appearing in the Drawin formulas. Note the scale change for C_{12}.

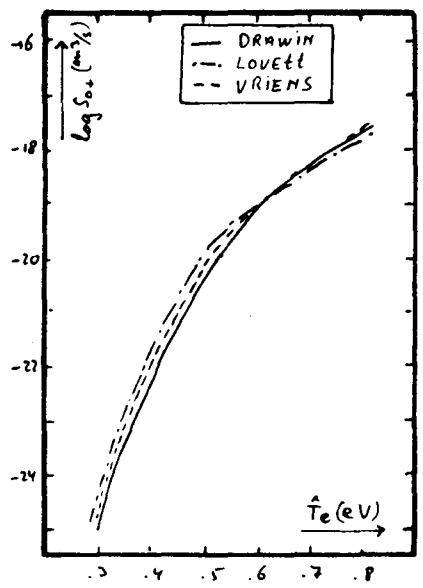

Fig. D.2.
Rate coefficients for electron ionisation in the MgI system.

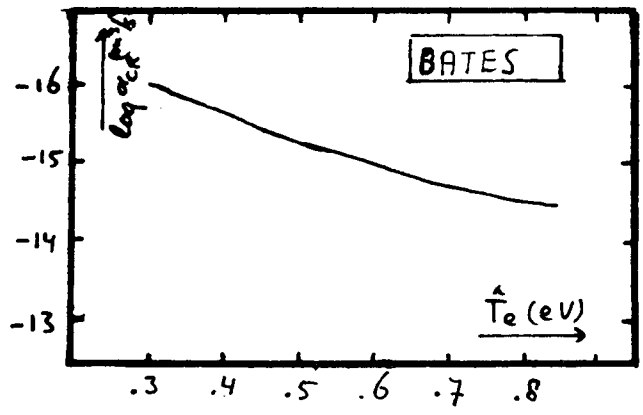

Fig. D.3.
Collisional radiative recombination rate coefficient in the MgI and MgII system according to Bates [42].

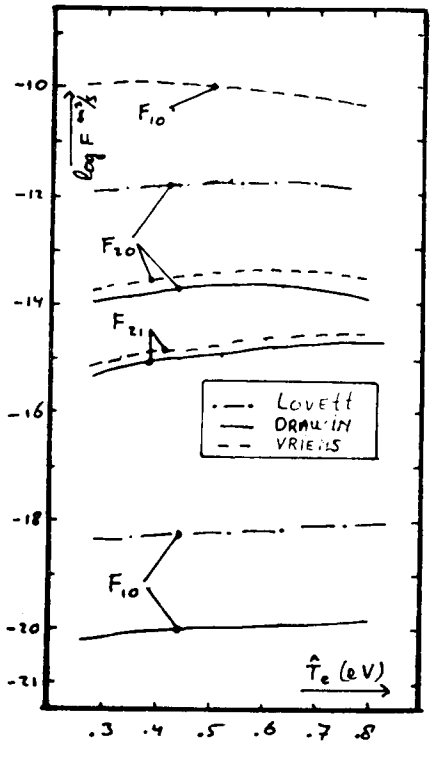

Fig. D.4.
Rate coefficients for electron deexcitation in the MgI system. Obtained by detailed balancing of the rate coefficients of Fig. D.1.

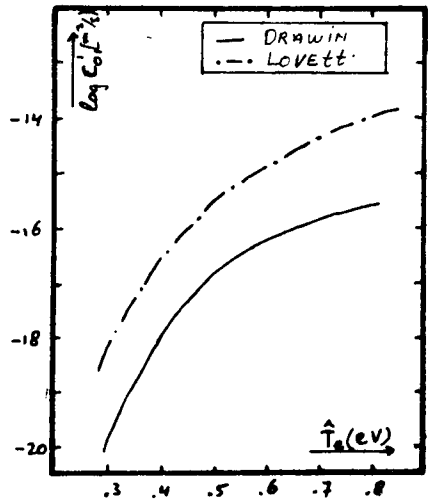

Fig. D.5.
Rate coefficients for electron excitation.
in the MgII system.

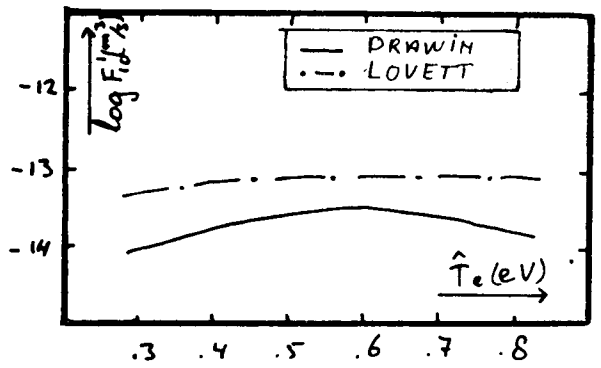

Fig. D.6.
Rate coefficients for electron deexcitation
in the MgII system.

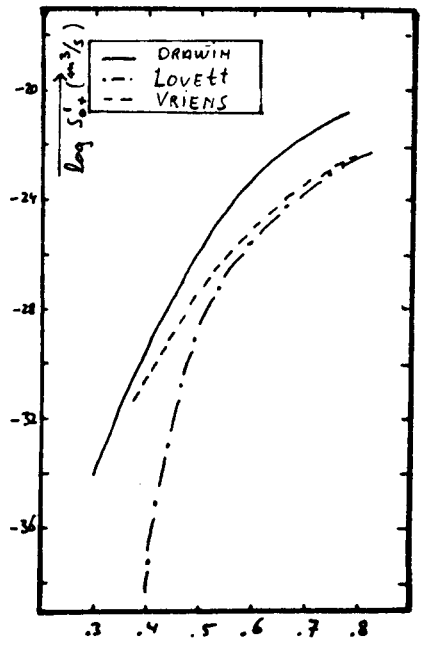

Fig. D.7.
Rate coefficients for electron ionisation in the MgII system.